DISSERTATION

Human Induced Pluripotent Stem Cell-derived Adrenocortical Cell Model Reveals the Pathophysiology of *KCNJ5* Mutation in Primary Aldosteronism

Untersuchung einer *KCNJ5*-Mutation beim Primären Hyperaldosteronismus in einem adrenokortikalen Zellmodell aus humanen induzierten pluripotenten Stammzellen

zur Erlangung des akademischen Grades
Doctor of Philosophy (PhD)

vorgelegt der Medizinischen Fakultät
Charité – Universitätsmedizin Berlin

von

Kieu Nhi Tran Vo

Erstbetreuer*in: Prof. Dr. med Ute Scholl

Datum der Promotion: 30.06.2024

Preface

Partial results of the present work were published in:

Oral presentations:

Tran-Vo N.K., Vallone V.F., Obermayer B., Rauh M., Bachmann S., Beule D., Stachelscheid H., Scholl U.: hiPSC-Derived Adrenocortical Cell Model Reveals the Pathophysiology of *KCNJ5* Mutation in Primary Aldosteronism. 10th German Stem Cell Network Conference, 13.-16. September 2022, Münster, Germany.

Tran-Vo N.K., Vallone V.F., Obermayer B., Rauh M., Bachmann S., Beule D., Stachelscheid H., Scholl U.: hiPSC-Derived Adrenocortical Cell Model Reveals the Pathophysiology of *KCNJ5* Mutation in Primary Aldosteronism. 12th Symposium of the Young Physiologists, 30.-31. March 2023, Kiel, Germany.

Poster presentations:

Tran-Vo N.K., Vallone V.F., Obermayer B., Rauh M., Bachmann S., Beule D., Stachelscheid H., Scholl U.: hiPSC-Derived Adrenocortical Cell Model Reveals the Pathophysiology of *KCNJ5* Mutation in Primary Aldosteronism. 7th Progress in Primary Aldosteronism, 13.-14. October 2022, Munich, Germany.

Table of contents

List of Figures and Tables

List of Figures

List of Supplementary Figure

List of Tables

List of abbreviations

Abbreviation	Name	Abbreviation	Name
AC	Adrenal cortex/adrenocortical	PA	Primary aldosteronism
APA	Aldosterone-producing adenoma	PCR	Polymerase chain reaction
ACTH	Adrenocorticotropic hormone	PM	Paraxial mesoderm
AGP	Adrenogonadal primordium	RAAS	Renin-angiotensin-aldosterone system
ARR	Aldosterone renin ratio	RFLP	Restriction fragment length polymorphism
BCA	Bicinchoninic acid assay	scRNA-seq	Single-cell RNA sequencing
BHA	Bilateral hyperaldosteronism	ssODN	Single-strand oligonucleotide
DAPI	4', 6'-diamidino-2-phenylindole	zF	Zona fasciculata
DCM	Dichloromethane	zG	Zona glomerulosa
DMEM	Dulbecco's Modified Eagle's Medium	zR	Zona reticularis
DNA	Deoxyribonucleic acid		
DZ	Definitive zone		
EGF	Epidermal growth factor		
ELISA	Enzyme linked immunosorbent assay		
ESC	Embryonic stem cell		
FACS	Fluorescence-activated cell sorting		
FGF	Fibroblast growth factor		
FH	Familial hyperaldosteronism		
FZ	Fetal zone		
HDR	Homology-directed repair		
hiPSC	Human induced pluripotent stem cell		
HPA	Hypothalamic-pituitary-adrenal		
hPSC	Human pluripotent stem cell		
IA	Immunoassay		
IM	Intermediate mesoderm		
LC-MS/MS	Liquid chromatography-Mass spectrometry		
LPM	Lateral plate mesoderm		
mRNA	Messenger ribonucleic acid		
MSC	Mesenchymal stem cell		

Units
pg: picogram
ng: nanogram
µg: microgram
pM: picomolar
µM: micromolar
nM: nanomolar
µL: microliter
mL: milliliter
µm: micrometers
°C: Celsius degree
RLU: Relative light unit
%: percentage
g: gram, gravity

Summary

The adrenal cortex is a central site of steroidogenesis. Steroid hormones produced in the adrenal cortex regulate essential processes in the body, including electrolyte and fluid homeostasis, blood pressure, and stress-induced metabolisms. Defects in the structure and function of the adrenal cortex result in inappropriately low or high hormone secretion, leading to a number of diseases, including secondary hypertension due to hyperaldosteronism.

Adrenocortical research has long suffered from a lack of adequate models, which has hampered advances in understanding disease mechanisms and developing therapies for adrenocortical disorders. Adrenocortical animal models and cell lines in many cases do not fully recapitulate the genotype-phenotype association of adrenocortical disorders. Criteria for ideal human-derived adrenocortical disease models include ease of genomic manipulation and adequate hormone production, which are currently unmet.

Here, we developed an improved human induced pluripotent stem cell (hiPSC)-based differentiation system from intermediate mesoderm toward adrenocortical cells. Heterologous forced expression of steroidogenic factor-1 (SF-1) and the addition of adrenal cortex niche factors gave rise to cells that produced a wide range of adrenal steroids, including aldosterone and cortisol, and exhibited typical adrenocortical gene expression profiles. These cells maintained their proliferative capacity during extended cultivation. Using CRISPR/Cas9, we introduced a heterozygous somatic *KCNJ5* mutation found in aldosterone-producing adenomas and familial hyperaldosteronism. Besides elevated aldosterone production, mutant cells showed increased proliferation, a hallmark of tumor development, that was missing in prior models. We conclude that our system is a valid tool for studying the pathophysiology of adrenocortical diseases.

Zusammenfassung

Die Nebennierenrinde ist ein zentraler Ort der Steroidogenese. In der Nebennierenrinde gebildete Steroidhormone regulieren wesentliche Prozesse im Körper, darunter die Elektrolyt- und Flüssigkeitshomöostase, den Blutdruck und den stressbedingten Stoffwechsel. Defekte in der Struktur und Funktion der Nebennierenrinde führen zu einer erhöhten oder erniedrigten Hormonausschüttung, die zu mehreren Erkrankungen, einschließlich sekundärem Bluthochdruck aufgrund eines Hyperaldosteronismus führen kann.

Die Nebennierenrindenforschung leidet jedoch seit langem unter einem Mangel an geeigneten Modellen, was Fortschritte beim Verständnis der Krankheitsmechanismen und bei der Entwicklung von Therapien für Nebennierenrindenerkrankungen erschwert hat. Tiermodelle (Modelle zur Erforschung der Nebennierenrinde) und Zelllinien können die Genotyp-Phänotyp-Assoziation der genetischen Erkrankungen der humanen Nebennierenrinde in vielen Fällen nicht vollständig rekapitulieren. Idealerweise sollten humane Nebennierenrindenmodelle leicht genomisch zu manipulieren sein und eine nahezu physiologische Hormonproduktion aufweisen, Kriterien, die derzeit nicht erfüllt sind.

Wir haben hier ein verbessertes System zur Differenzierung menschlicher induzierter pluripotenter Stammzellen (hiPSC) aus intermediärem Mesoderm in adrenokortikale Zellen entwickelt. Die heterologe Expression des steroidogenen Faktors 1 (SF-1) und Zugabe von Nischenfaktoren der Nebennierenrinde führten zu Zellen, die eine breite Palette von Nebennierensteroiden produzierten, einschließlich Aldosteron und Cortisol, und adrenokortikale Genexpressionsprofile aufwiesen. Diese Zellen behielten ihre Proliferationsfähigkeit auch bei längerer Kultivierung bei. Mithilfe von CRISPR/Cas9 haben wir eine heterozygote somatische *KCNJ5*-Mutation eingeführt, die bei Aldosteron produzierenden Adenomen und familiärem Hyperaldosteronismus vorkommt. Neben einer erhöhten Aldosteronproduktion zeigten die mutierten Zellen eine erhöhte Proliferation, ein Merkmal der Tumorentwicklung, das in früheren Modellen fehlte. Wir schließen daraus, dass unser System ein vielversprechender Ansatz für die Untersuchung der Pathophysiologie von Nebennierenrinden-erkrankungen ist.

1. Introduction:

In this section, an overview of the adrenal cortex development and molecular mechanisms/pathways underlying its development and function will be provided. Moreover, primary aldosteronism (PA), an adrenal cortex disorder, is introduced and I will describe how induced pluripotent stem cells (iPSC)-derived adrenocortical cells can be a model for PA.

1.1. Biology of the adrenal cortex

1.1.1. Adrenal cortex structure and function

The adrenal glands are small, triangular endocrine organs located on top of the kidneys and are vital hormone-producing organs. Each gland is divided into two separate endocrine organs with distinct embryological origins and functions: the inner medulla and the outer adrenal cortex **(Figure 1)**. The inner medulla is derived from the neural crest and produces catecholamines important in acute stress-induced or "fight-or-flight" responses. The outer adrenal cortex is formed from the intermediate mesoderm, and produces steroid hormones that regulate diverse essential functions, including stress-induced metabolism, blood pressure, and salt homeostasis (*1*). In adult humans, the adrenal cortex is subdivided into three concentric zones with differing steroidogenic functions and cellular architectures **(Figure 1)**.

- The outer **zona glomerulosa (zG)** consists of rosette-like cell clusters that secrete the mineralocorticoid hormone aldosterone, which mediates blood pressure and electrolyte homeostasis, mainly under the control of the renin-angiotensin-aldosterone system (RAAS) and of extracellular potassium levels (*1*).
- The middle layer of the adrenal cortex, **zona fasciculata (zF)** cells, comprise cells organized into parallel cords and are responsible for producing the glucocorticoid hormone cortisol, which is regulated by the hypothalamic-pituitary-adrenal (HPA) axis. Cortisol is a versatile hormone mediating chronic stress-induced metabolism, inflammatory response, and immune function (*1*).
- The inner **zona reticularis (zR)** produces a subset of precursors to sex steroid hormones, including androstenedione and dehydroepiandrosterone (*1*).

The adrenal cortex is encapsulated by a thin layer of cells from the mesothelial lineage, named capsular cells, which, among others, comprises adrenocortical

stem cells and progenitor cells that can give rise to glomerulosa cells, followed by centripetal migration and lineage conversion into fasiculata and reticularis cells to maintain tissue homeostasis (*2-4*). Although there are differences in zonal structure and functions in some species (for instance, rodents lack zR and instead of cortisol as in humans and primates, the rodent zF produces corticosterone), most mammals share the common developmental process and homeostatic maintenance of the adrenal cortex (*5*).

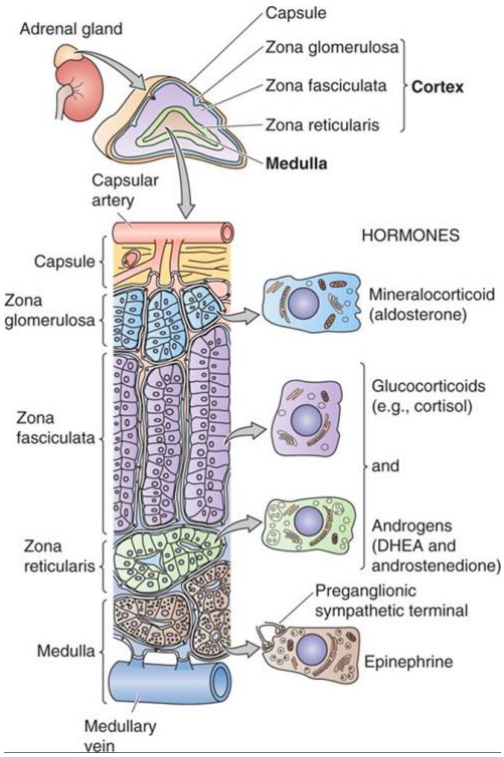

Figure 1: Human adrenal cortex structure

(Barrett J.E., Medical Physiology: A Cellular and Molecular Approach)

1.1.2. Development of the adrenal cortex

The adrenal cortex originates from the intermediate mesoderm (IM), a mesoderm lineage that arises from the primitive streak in early mesodermal development. During gastrulation in vertebrates, the pluripotent epiblast undergoes epithelial-to-mesenchymal transition (EMT) to give rise to the primitive streak, a linear structure of thickened epiblast located at the posterior region of the embryo (*6*) **(Figure 2A)**. In early mesoderm development, the posterior primitive streak gives rise to the paraxial mesoderm (PM), lateral plate mesoderm (LPM), and intermediate mesoderm **(Figure 2B).** The PM generates somites, segmented structures that give rise to the axial skeleton and muscles, while the lateral plate mesoderm contributes to the heart, limbs,

blood vessels, and gut. The IM, located between PM and LPM, originate kidneys, gonads, and the adrenal cortex. Recent lineage tracing studies showed that the specification of IM derivatives is determined by the patterning of IM cells along the anterior-posterior axis (*7, 8*). In kidney development, it has been shown that metanephric mesenchyme is derived from the posterior IM, while the nephric duct (mesonephric duct and Wolffian duct) originates from the anterior IM (*9*) **(Figure 2C-D)**.

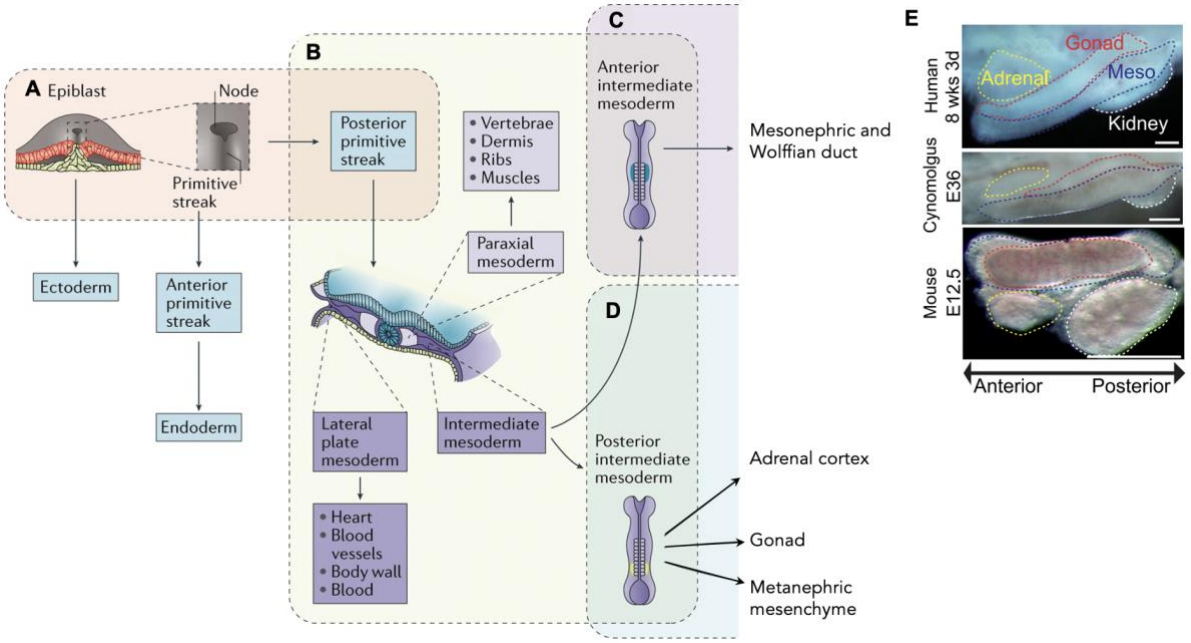

Figure 2: Intermediate mesoderm (IM) and specification of IM derivatives during development (adapted from (*10, 11*))

(A) During gastrulation in vertebrates, the primitive streak is formed by epithelial-to-mesenchymal transition (EMT) of pluripotent epiblast cells. (B) The posterior primitive streak gives rise to mesoderm lineages, including paraxial mesoderm, intermediate mesoderm, and lateral mesoderm, while the anterior primitive streak contributes to the endoderm. The patterning of IM along the anterior-posterior axis determines the specification of IM derivatives. (C) Anterior IM cells give rise to the mesonephric and Wolffian duct of the kidney. (D) Posterior IM cells destine for adrenal cortex, gonad and metanephric mesenchyme of the kidney. (E) Bright-field images of posterior IM derivatives (adrenal: yellow, gonad: red, kidney: white, and mesonephros: blue) in embryos of humans, cynomolgus, and mouse.

It has been shown that in mice, the gonads and the adrenal cortex share a common precursor, the adrenogonadal primordium (AGP) (*8, 12-15*). AGP appears around embryonic day (E) 9.5 in mice, developed from the coelomic epithelium (CE), a descendant of posterior IM. After that, the separation of AGP to form gonad and adrenal primordium marks the first lineage commitment of the gonad and adrenal

cortex, respectively. However, the exact lineage specification during the development of AGP in humans and primates has not been investigated until recently (*8, 11*). Using genetic tracing tools combined with single-cell RNA sequencing (scRNA-seq), these studies showed that the adrenocortical and gonadal lineages originate in spatially and temporally distinct fashion in human. The adrenocortical and gonadal lineages share the posterior IM as the developmental origin **(Figure 2D)**; however, the adrenal cortex emerges earlier and is located anteriorly, while the gonad arises later and extends along the anterior-posterior axis (*8*) **(Figure 2D-E)**. Following the formation of the adrenal primordium, steroidogenic fetal adrenocortical lineages arise and form a fetal zone (FZ). The FZ is then encapsulated by mesenchymal cells and infiltrated by precursors of the adrenal medulla from the neural crest, which becomes the medulla. After the encapsulation, the FZ enlarges rapidly, while a definitive zone (DZ) emerges from the adrenal primordium. With the formation of the DZ, the FZ starts to regress and becomes replaced by the DZ; shortly after birth, the human adrenal cortex comprises mainly DZ adrenocortical cells (*1*). In mice, the FZ (called x-zone in mice) remains after birth and only regresses when puberty starts in males and during the pregnancy of females. Upon the specific expression of *CYP11B2* (aldosterone synthase) in zona glomerulosa (zG) in the perinatal period, the adrenal cortex is separated into distinct steroidogenic zones in a process termed zonation (*16*). In humans and other primates, the zona reticularis (zR) forms only at the beginning of adrenarche, an early step in sexual maturation (*17*).

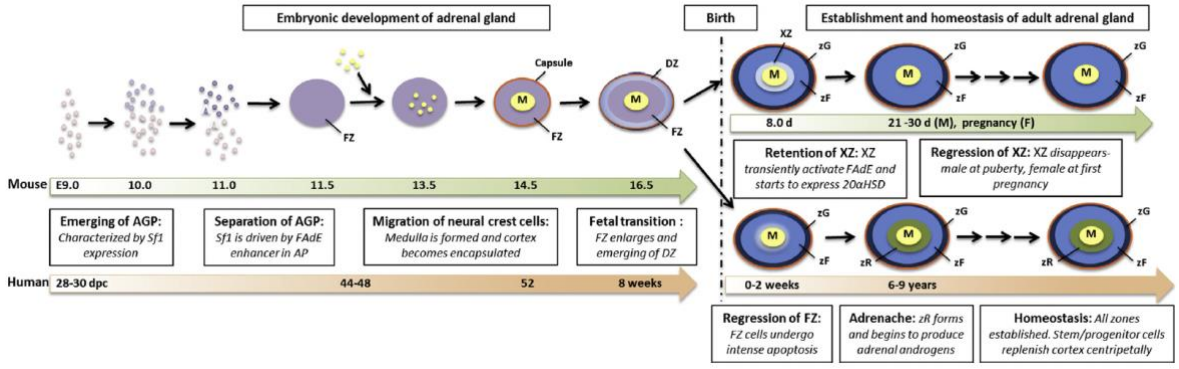

Figure 3: Overview of adrenal organogenesis in humans and mice (*18*).

DZ, definite zone; FZ, fetal zone; XZ: remnant of the fetal zone (x-zone); zF, zona fasiculata; zG, zona glomerulosa; zR, zona reticularis; dpc, days post conception (*18*)

On a molecular level, adrenal and gonadal development critically depends on the expression of the transcriptional activator steroidogenic factor 1 (SF-1), encoded by

the *NR5A1* gene (*15, 19*). SF-1 is the crucial factor controlling cell fate specification and fetal adrenal maturation in the development and is involved in steroidogenesis of the adult adrenal cortex. Indeed, when the *Nr5a1* gene is knocked out in mice, the adrenogonadal primordium undergoes early apoptosis (*19*). In a mouse model lacking SF-1 expression, the adrenal gland was not formed (adrenal aplasia), and the mouse died from adrenal failure within 8 days of birth. Absence of SF-1 results in adrenal failure and sexual differentiation defects in humans (*20*). Overexpression of SF-1 leads to abnormal proliferation, changes in hormone production patterns of human adrenocortical cells, and adrenal tumor formation in mice (*21*). The differential development into adrenal versus gonadal primordium in mice has been linked to fetal adrenal-specific enhancer (FAdE) expression, which drives SF-1 expression during embryonic and early fetal stages (*12*). In mouse AGP, FAdE-mediated SF-1 expression is initiated by the transcription network containing *Pknox1* (PREP1), *Hox9b*, and *Pbx1*. Later in the adrenal primordium, SF-1 controls its own expression by maintaining the FAdE-mediated SF-1 expression (*12*). FAdE expression is lost when the definitive cortex is formed (*22*). Additional transcription factors upstream of SF-1 include PBX1 (PBX homeobox 1) (*23*), WT1 (Wilms tumor suppressor gene 1) (*14*) (both of which are essential for normal development of the urogenital system), and CITED2 (also crucial for cardiac development, among others) (*24*). Their deletion leads to adrenal hypoplasia and other developmental abnormalities in mice.

1.1.3. Adrenal cortex renewal and homeostasis

The adrenal cortex is a highly dynamic organ in which the self-renewal and differentiation of the adult adrenocortical lineages occur throughout life to maintain the function and structure of the gland (tissue homeostasis). The first evidence of self-renewal in the adrenal cortex was reported in the early 1930s; a complete restoration of the adrenal cortex was observed within 6 weeks after removing most of the cortex and the medulla, while the capsule and outermost cortical layer were maintained (*25*). Studies of cells in the capsular and outer adrenal cortex in rodents using Bromodeoxyuridine (BrdU) pulse labeling showed that the labeled cells proliferate and contribute centripetally to the inner layers, where they undergo apoptosis at the corticomedullary junction (*26-29*). Together with other studies, it became known that the homeostasis of the adrenal cortex is balanced by the proliferation of outer cells, centripetal migration and lineage conversion of zona cells, and apoptosis of cells at

the boundary of the cortex and medulla (*2-4*) **(Figure 4)**. In the search for the cell population that possesses the self-renewal capacity in the outer layer, cell lineage analysis in mice identified distinct populations of stem/progenitor cells expressing *Rspo3* (*30*), *Wt1* (*13*), *Gli1* (*31*), *Nr2f2* (*4*) and *Nes* (*32*) in the capsule, while *Shh* (*2*) was found in subcapsular and zona glomerulosa cells **(Figure 5).**

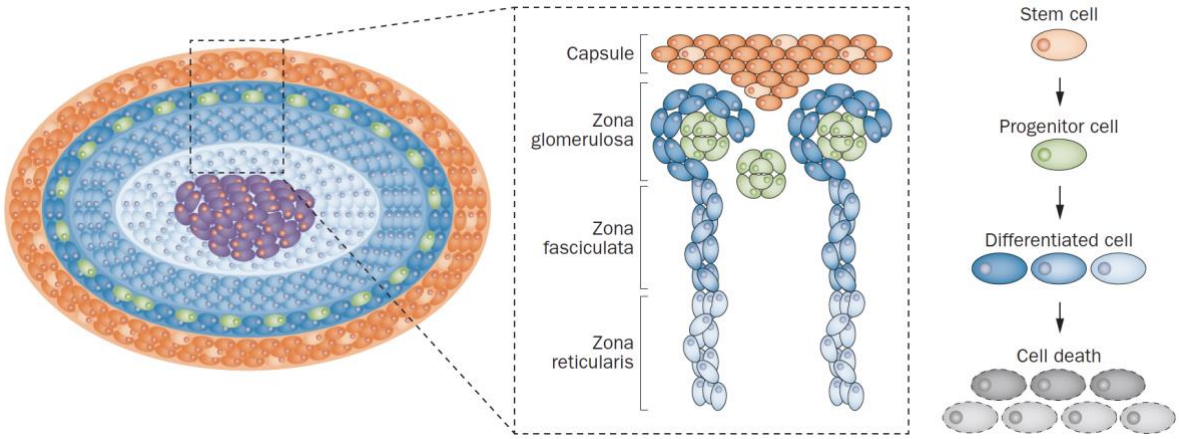

Figure 4: Self-renewal and differentiation of the adrenal cortex lineages (adapted from (*1*)). Graphical illustration of the homeostasis of the adrenal cortex, which is controlled by the self-renewal of stem cells and progenitor cells located at the capsule and zG, and by the differentiation of the undifferentiated cells into steroid-producing cells (glomerulosa, fasciculata, and reticularis cells) until they undergo apoptosis at the corticomedullary junction. Medulla, purple; cortex, blue concentric layers; capsule, orange.

In the fetal and definitive adrenal cortex, a pool of undifferentiated cells in the subcapsular cortex region expresses sonic hedgehog (SHH) protein and co-expresses SF-1. These SHH-expressing cells give rise to the differentiated cells of the adult adrenal cortex, as shown in fate tracing analysis in mice (*2*). In addition, another population of GLI1^{+} progenitor cells (SHH-receiving cells) is located in the capsule **(Figure 5)**. GLI1^{+} cells arise from SF-1-positive cells, temporarily lose SF-1 expression, and re-acquire SF-1 expression when differentiating into adrenocortical cells (*31*). Capsular stem cells also specifically express RSPO3, an activator of canonical Wnt signaling. Deletion of RSPO3 results in impaired zona glomerulosa identity and growth of the adrenal cortex (*30*). Interestingly, RSPO3 released from these capsular cells acts as a ligand to activate Wnt/β-catenin signaling in glomerulosa cells, leading to the activation of SHH. In turn, SHH-expressing cells activate GLI1 as

a downstream target in the capsular cells. This positive feedback loop is considered a signaling center controlling renewal and zonation of the adrenal cortex (*30*).

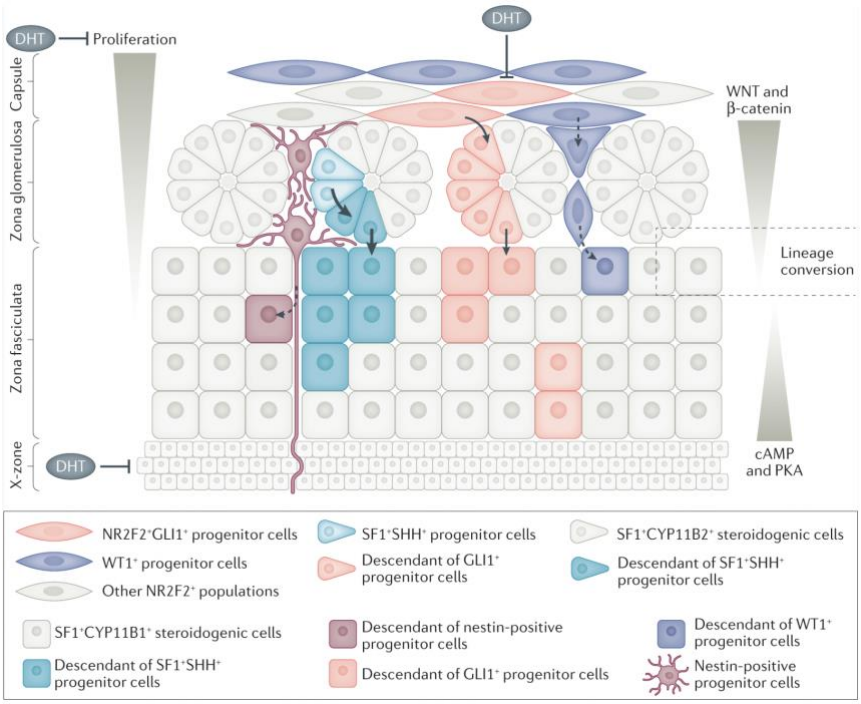

Figure 5: Stem cells and progenitor cells regulate the self-renewal and lineage conversion of the adrenal cortex (*33*).

Several pools of progenitor cells in the capsule (GLI1$^+$ cells, WT1$^+$ cells) and zG (SHH$^+$ cells) contribute to the renewal and lineage conversion of the adrenal cortex by differentiating into their descendant steroidogenic cells.

The underlying mechanisms of adrenal cortex lineage conversion and differentiation are not yet fully understood. Prior studies revealed that nuclear receptor DAX1 plays a vital role in retaining the undifferentiated state of the adrenal cortex progenitor cells (*34*). DAX1, encoded by the *NR0B1* gene (nuclear receptor subfamily 0 group B member 1), is a co-repressor of the SF-1 mediated transcription of steroidogenic genes (*35, 36*). Besides assisting SF-1 in early adrenal development, DAX1 also plays a crucial role in steroid production by activating the transcription of enzymes responsible for adrenal steroidogenesis (*37, 38*). Upregulation of DAX1 was observed as a mechanism to avoid differentiation, thus preventing depletion of the progenitor cell pool (*39*). Canonical Wnt signaling in progenitor cells via β-catenin increases the expression of DAX1, thus keeping progenitor cells in an undifferentiated state (*18, 40*). Similarly, knockout of *Nr0b1* causes early increased zona fasciculata function, followed by stem cell pool depletion and adrenal failure (*34, 35*). In steroidogenic cells,

DAX1 expression is downregulated by the action of adrenocorticotropic hormone (ACTH), a well-known glucocorticoid stimulator, to release the cells from an undifferentiated state. ACTH relieves DAX1-mediated repression of SF-1-dependent steroidogenesis and facilitates steroid production in the differentiated cells (*39*).

Homeostatic maintenance of the adrenal cortex is tightly regulated by a synergy of paracrine and endocrine signaling pathways **(Figure 6)**. The formation of stem/progenitor cells in the capsule and glomerulosa cells mainly depends on paracrine signaling. Canonical β-catenin/Wnt signaling is essential for the proliferation and identity of the zona glomerulosa, as well as for the adrenocortical progenitor cell pool. Ablation of β-catenin expression in mice results in a drastic decrease in the proliferation of prenatal adrenocortical cells and, subsequently, adrenal failure in the postnatal stage (*41*). In the adult adrenal cortex, β-catenin/Wnt is restrictedly active in the zG while inactive in the zF. Constitutive activation of β-catenin in mouse adrenal glands leads to enlargement of the zG and primary aldosteronism, a disease condition with elevated aldosterone secretion (*42*).

On the other hand, SHH signaling has a mitogenic effect on the proliferation and maintenance of adrenocortical growth by supporting the $GLI1^{+}$ capsular progenitor pool (*2, 31*). Targeted inactivation of *Shh* in the adrenal cortex leads to cortex hypoplasia by reducing cortical and capsular proliferation (*43*). Another mitogen factor that controls the proliferation of capsular progenitor cells and glomerulosa cells is fibroblast growth factor (FGF). Conditional deletion of *Fgfr2* (FGF receptor 2) in steroidogenic cells causes reduced capsule and cortex cell proliferation, subsequently leading to hypoplasia observed in fetal adrenal development (*44, 45*).

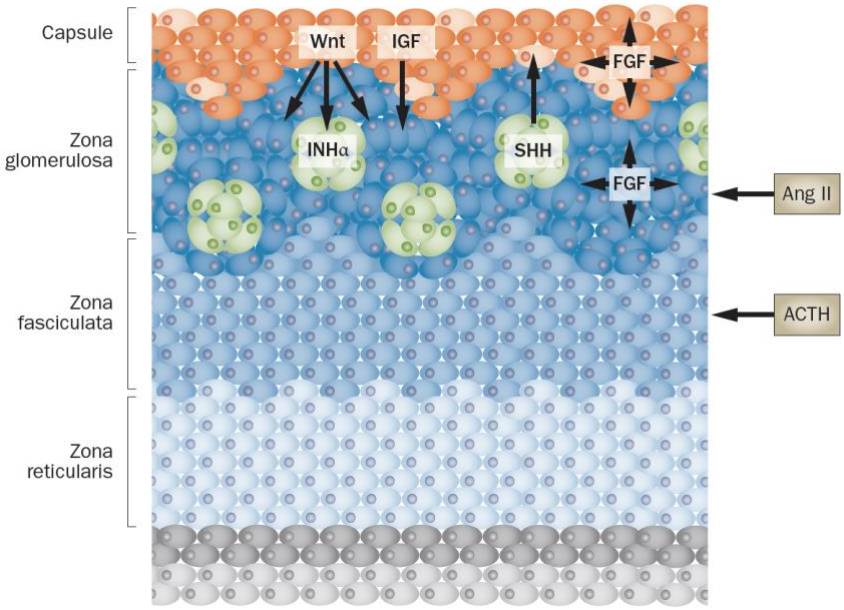

Figure 6: Signaling factors (niche factors) regulate the renewal, differentiation, and steroidogenesis of the adrenal cortex (adapted from (*1*)).

Paracrine signaling factors (Wnt, SHH, FGF2, Inhibin, and cAMP/PKA), endocrine signaling factors (AngII, ACTH), and intracellular cAMP-PKA signaling reciprocally regulate the homeostasis of the adrenal cortex.

The peptide hormones Angiotensin II (AngII) and ACTH comprise endocrine signaling factors that regulate steroidogenesis and zone-specific cell differentiation **(Figure 6)**. Under the control of the renin-angiotensin-aldosterone system (RAAS), AngII acts as a primary activator of aldosterone production in glomerulosa cells by binding to its receptor (type 1 AngII receptors AT1A and AT1B) **(Figure 7)**. The ligand-receptor interaction increases Ca^{2+} influx via two types of calcium channels: low-voltage-activated transient T-type and high-voltage activated long-lasting L-type channels. Consequently, elevated intracellular Ca^{2+} triggers the transcription and activation of *CYP11B2* (encoding aldosterone synthase) via CAMK II complexes (Ca^{2+}/calmodulin-dependent protein kinases) (*46, 47*). In addition, extracellular K^+ is also a potent activator of aldosterone secretion by indirectly increasing Ca^{2+} influx (*48*). Potassium channels in the zona glomerulosa include two-pore domain channels, TASK-1/2/3 and TREK1 (encoded by *KCNK3*, *KCNK*5, *KCNK9*, and *KCNK2* respectively) (*49-51*), as well as G-protein-activated inward rectifying potassium channel Kir3.4 (encoded by *KCNJ5*). Under basal conditions, the two-pore domain channels (TASK-1-3 and TREK1) and Kir3.4 maintain the glomerulosa cell membrane potential hyperpolarized (high K^+ conductance). Under stimulating conditions, the inhibition of potassium

channels by AngII results in depolarization of the cell membrane, leading to Ca^{2+} influx via voltage-gated calcium channels.

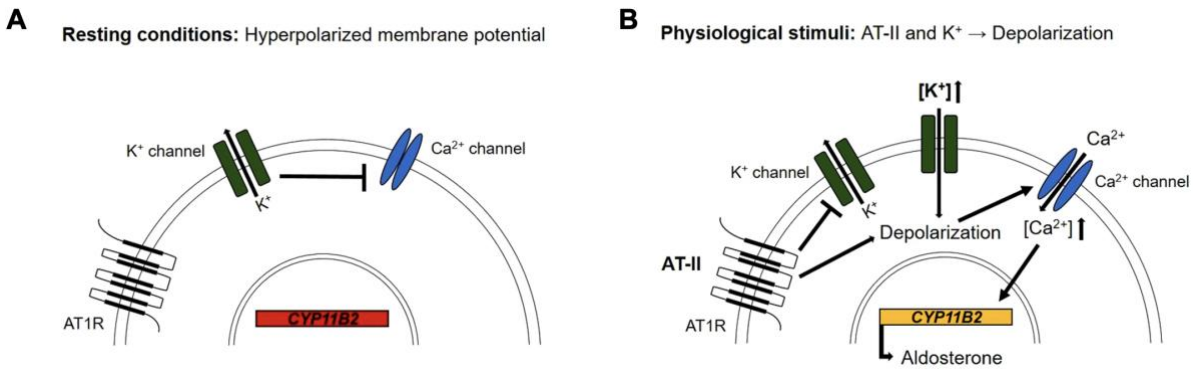

Figure 7: Schematic representation of activation of CYP11B2 (aldosterone synthase) expression in resting conditions and with physiological stimuli (*52*).

(A) In resting conditions, potassium channels maintain the glomerulosa cell membrane hyperpolarized by allowing K^+ efflux. (B) Under physiological stimuli, the binding of AngII to its receptor causes inhibition of potassium channels, leading to depolarization, increasing Ca^{2+} influx via the voltage-gated calcium channels and subsequently activating *CYP11B2* expression.

The regulation of zona fasciculata proliferation and cortisol production (corticosterone in rodents) is crucially governed by ACTH and the intracellular cAMP-PKA (protein kinase A) signaling pathway. Under the control of the hypothalamic-pituitary-adrenal (HPA) axis, the pituitary-derived ACTH hormone induces glucocorticoid steroid production in fasciculata cells by triggering cAMP-PKA signaling (*53*). ACTH binds to its receptor (melanocortin 2 receptor MC2R), initiates the cAMP signal transmission cascade, and activates the transcription factor cAMP response element-binding protein (CREB). This leads to the transcription of target genes, facilitating proliferation and cortisol production (*54*).

1.2. Primary aldosteronism

1.2.1. Clinical features of primary aldosteronism

In 1955, Dr. Jerome W. Conn described a patient who suffered from hypertension and hypokalemia and showed non-specific symptoms, including headache, fatigue, and muscle weakness. Her condition improved after a right adrenalectomy with a removal of an adrenocortical adenoma (*55*). This condition was then defined as primary aldosteronism (PA). PA is a pathological condition characterized by excessive aldosterone production despite low levels of physiologic stimuli (low renin levels, low or normal potassium levels). In physiological conditions, the RAAS regulates blood pressure, fluid, and electrolyte balance. When the body suffers from hypotension or hypovolemia (loss of salt and water), renin is released from the juxtaglomerular cells of the kidney vasculature. Angiotensinogen (secreted from the liver) is then cleaved by renin, resulting in the formation of angiotensin I. Angiotensin-converting enzyme (ACE) catalyzes the conversion of angiotensin I to angiotensin II (AngII), the main effector in the RAAS. AngII binds to its receptor (AT1R) in the zona glomerulosa of the adrenal cortex to induce aldosterone production. Aldosterone is lipophilic and freely diffuses from the zona glomerulosa cells. It then binds to mineralocorticoid receptors in the renal cortical collecting duct, leading to increased numbers of epithelial sodium channels in the apical membrane. Consequently, this reaction leads to an increase in sodium reabsorption and volume retention, as well as potassium secretion (*56*).

PA is the most common cause of secondary hypertension and accounts for increased blood pressure in 6-10% of hypertensive patients, with a higher prevalence in severe or resistant hypertension, up to 29.1% (*57, 58*). PA is also associated with a higher risk of cardiovascular diseases, such as myocardial infarction and atrial fibrillation, than primary hypertension (*59*). The two most common causes of primary aldosteronism are bilateral hyperaldosteronism (BHA), which accounts for 60% of the cases, and aldosterone-producing adenomas (APA), accounting for about 30% (*60, 61*). The remaining cases are rare, including unilateral hyperplasia, adrenocortical carcinoma, or familial hyperaldosteronism (FH). Although PA is potentially curable by surgery (with unilateral disease) or treatable by targeted pharmacotherapy, many if not most patients suffering from PA are not appropriately diagnosed, in part due to complicated and invasive procedures for screening and diagnosis (*62*).

The diagnosis of PA typically includes three phases: screening, confirmation, and subtype classification (*63*). The plasma aldosterone-renin ratio (ARR) is an effective screening test for PA in hypertension patients. PA patients are expected to have high aldosterone secretion, while renin is low or undetectable, leading to an elevated ARR. Confirmatory tests (i.e., saline infusion test, oral sodium loading, fludrocortisone suppression test, and captopril challenge test) are conducted to demonstrate that the administered agents fail to sufficiently lower aldosterone levels as they would in a physiological feedback mechanism. The diagnostic approach to classifying the PA subtype is adrenal vein sampling, an invasive procedure that is based on distinguishing unilateral (mostly APA) from bilateral (usually BHA) PA (*64*). Thereafter, the most suitable clinical intervention is chosen based on this subtype classification. Typically, adrenalectomy is preferred in unilateral cases, while pharmacotherapeutic treatment with mineralocorticoid receptor antagonists is chosen for bilateral cases (*64-66*). However, adrenal vein sampling is a technically difficult and expensive procedure; thus, not many patients are diagnosed or treated optimally. Over six decades since the first description in the 1950s, the recognition of the high prevalence of PA and its association with the severity of cardiovascular and renal damage has led to an increased urgency to understand the cellular/genetic causes and to develop precise diagnoses and treatments (*67, 68*).

1.2.2. Genetic causes of primary aldosteronism and molecular/cellular mechanisms underlying diseases-associated phenotypes.

The progress in exploring genetic causes of PA in the last decade has been impressive, thanks to advances in next-generation sequencing (NGS). The various somatic mutations in aldosterone-producing adenoma (APA) and germline mutations in familial hyperaldosteronism (FH) are summarized in **Table 1**. Most of the affected genes encode ion channels or transporters (*KCNJ5*, *CACNA1D*, *CACNA1H*, *CLCN2*, *ATP1A*, *ATP2B3, SLC30A1*), cell adhesion molecule (*CADM1*), intracellular signaling pathways (*CTNNB1*, *GNAS/Q/11*, *PRKACA*, *ARMC5*), a chimeric *CYP11B1/B2* gene.

Table 1: Somatic and germline variants in APA and FH

Gene and protein	Effects	Transmission	PA Subtype	Prevalence in APA	Reference
Ion channels and transporters					
KCNJ5 Potassium inwardly rectifying channel subfamily J member 5	Increase Na^+ conductance -> Increase Ca^{2+} influx -> activate *CYP11B2* expression	Somatic Germline	APA FH-III	38-63%	Choi M, 2011 (*69*) Scholl UI, 2012 (*70*)
CACNA1D Calcium voltage-gated channel subunit alpha1 D	Increase Ca^{2+} influx -> activate *CYP11B2* expression	Somatic Germline	APA PASNA	14-42%	Scholl UI, 2013 (*71*) Azizan EA, 2013 (*72*)
CACNA1H Calcium voltage-gated channel subunit alpha1 H	Increase Ca^{2+} influx -> activate *CYP11B2* expression	Somatic Germline	APA FH-IV	Rare	Scholl UI, 2015 (*73*) Nanba K, 2020 (*74*)
CLCN2 Chloride voltage-gated 2	Increase Cl^- efflux -> Increase Ca^{2+} influx -> activate *CYP11B2* expression	Somatic Germline	APA FH-II	Rare	Scholl UI, 2018 (*75*) Dutta RK, 2019 (*76*)
ATP1A1 ATPase Na^+/K^+ transporting subunit alpha 1	Depolarize cell membrane -> Increase Ca^{2+} influx -> activate *CYP11B2* expression	Somatic	APA	5%	Beuschlein F, 2013 (*77*) Azizan EA, 2013 (*72*)
ATP2B3 ATPase plasma membrane Ca^{2+} transporting 3	Increase Ca^{2+} influx -> activate *CYP11B2* expression	Somatic	APA	1.5%	Beuschlein F, 2013 (*77*)
CADM1 Cell adhesion molecule 1	Inhibit gap junction communication of aldosterone-producing cells -> activate *CYP11B2* expression	Somatic	APA	n.a	Wu X, 2023 (*78*)
SLC30A1 Zinc transporter 1	Increase Na^+ conductance -> Increase Ca^{2+} influx -> activate *CYP11B2* expression	Somatic	APA	n.a.	Rege J, 2022 (*79*)
Intracellular signaling factors					
CTNNB1 Beta catenin 1	Activate canonical/noncanonical Wnt pathways	Somatic	APA	2.1-5.1%	Tadjine M, 2007 (*80*)
GNA11 & GNAQ G protein subunit alpha 11/Q	Over-produce aldosterone; deregulate cell growth	Somatic	APA (when coincident with CTNNB1 mutation)		Zhou J, 2021 (*81*)
GNAS GNAS complex locus	Activate cAMP/PKA signaling	Somatic	APA	Rare	Nakajima Y, 2016 (*82*)
PRKACA Protein kinase cAMP-activated catalytic subunit alpha	Activate cAMP/PKA signaling	Somatic	APA	Rare	Rhayem Y, 2016 (*83*)
Cytochrome P450 Enzyme					

Chimeric *CYP11B1/B2*	*CYP11B2* under control of *CYP11B1* promoter	Germline	FH-I	Rare	Lifton RP, 1992 (*84*)

APA, aldosterone-producing adenoma; FH, familial hyperaldosteronism; PASNA, PA, seizures, and neurologic abnormalities; n.a., not available.

About 40% of APAs in Caucasian patients are caused by heterozygous somatic mutations in the inwardly rectifying potassium channel KCNJ5 (*69, 85*). The prevalence is higher in patients from East Asia, up to 77% (*86, 87*). Somatic *KCNJ5* mutations appear more frequently in female and younger patients with larger tumors and higher aldosterone production (*88, 89*). Two mutations, Gly151Arg (G151R) and Leu168Arg (L168R), account for almost all cases, while other mutations are rare. The mechanism underlying the excess aldosterone production due to *KCNJ5* mutations has been clearly demonstrated. These mutations are located within (G151R) or close to (L168R) the channel's selectivity filter, causing abnormal sodium permeability. The resulting depolarization of the cell membrane activates calcium influx via voltage-gated calcium channels (*90*), which in turn promotes aldosterone secretion (*69*) **(Figure 8A)**. Germline mutations of *KCNJ5* cause familial hyperaldosteronism type III (FH-III) with massive adrenal hyperplasia and drug-resistant hypertension (*69, 70*). However, the *KCNJ5*-mutation-related pathophysiology of increased proliferation and tumor formation remains unknown. Yet, evidence indicates that mutated KCNJ5 is likely sufficient to cause cellular proliferation besides elevated aldosterone production (*69, 91*). Additional variants, especially ones that account for cellular proliferation, are rarely found in APA associated with *KCNJ5* mutations, suggesting that the effect of the *KCNJ5* mutations themselves likely causes increased proliferation. Additionally, a case of non-hereditary PA in a young patient with germline mosaicism in the *KCNJ5* gene was reported (*92*). Adrenal hyperplasia was only found in the areas of the adrenal gland that carried the *KCNJ5* mutation, suggesting that only the pathogenic *KCNJ5* mutation is required for tumorigenesis and abnormal aldosterone secretion.

Since the discovery of sporadic mutations of *KCNJ5* in APA, progress has been made in identifying inhibitors of aldosterone synthesis due to mutated *KCNJ5*. These are either calcium channel blockers such as verapamil (*93*) or certain macrolide antibiotics (*94, 95*), which are able to inhibit aldosterone secretion *in vitro* by directly blocking mutant KCNJ5. Currently, macrolides are being investigated for their potential in

personalized diagnosis in patients with PA due to their specific affinity towards the most common mutations in KCNJ5 (*96*).

As shown in **Table 1**, heterozygous somatic mutations in the *CACNA1D* calcium channel gene also result in APAs **(Figure 8B)** (*71, 72, 85*). *CACNA1D* encodes the α1 subunit of the Cav1.3 voltage-dependent L-type calcium channel, one of the important calcium channels for zona glomerulosa Ca^{2+} influx. *CACNA1D* mutations that cause APA are gain-of-function mutations that directly cause increased cytosolic Ca^{2+} and subsequently facilitate aldosterone production. The prevalence of somatic mutations of *CACNA1D* is between 14% and 42% of APAs (*97-99*), and is also affected by ethnic differences (the highest frequency, 42%, is found in African-American patients). *De novo* germline *CACNA1D* mutations were identified in two children who exhibited early-onset forms of hyperaldosteronism associated with complex neurologic symptoms in a syndrome called PASNA (primary aldosteronism, seizures and neurologic abnormalities) (*71*). Germline gain-of-function mutations in *CACNA1H*, encoding for the Cav3.2 voltage-dependent T-type calcium channel, cause familial hyperaldosteronism type IV (FH-IV) (*73, 100*). Similar to the pathophysiology of mutated *CACNA1D*, mutations in *CACNA1H* directly induce increased Ca^{2+} influx and *CYP11B2* expression.

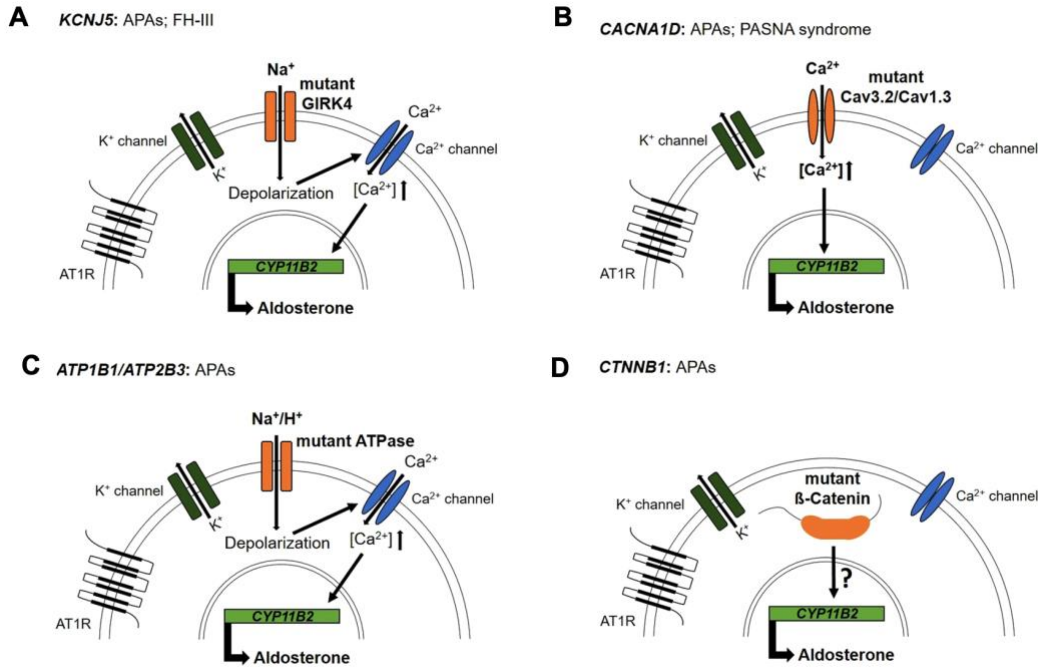

Figure 8: Schematic representation of the mechanism of elevated aldosterone secretion in somatic and germline mutations in aldosterone-producing adenoma (APA) and familial hyperaldosteronism (FH) (*52*).

Four representations of the most recurrent mutations are shown, an updated list of mutations can be found in **Table 1.**

(A) Mutated *KCNJ5* potassium channel (somatic transmission in APA, germline transmission in FH-III) alters the channel selectivity filter, increasing Na^+ conductance which leads to depolarization (B) Mutation in voltage-gated calcium channel *CACNA1D* (as somatic mutations in APA and PASNA syndrome) and *CACNA1H* (as somatic mutations in APA or germline mutation in FH-IV) directly cause increased Ca^{2+} influx. (C) Mutated in ion pumps for sodium/potassium, *ATP1A1*, and calcium, *ATP2B3* cause increased permeability for sodium and protons, leading to cell membrane depolarization. (D) Somatic mutations in *CTNNB1* in APAs show elevated aldosterone secretion; however, the underlying mechanism is not clearly understood.

Somatic mutations in a Na^+/K^+-ATPase subunit and the plasma membrane Ca^{2+}-ATPase (*ATP1A1* and *ATP2B3*) account for 5% and 1.5% of APAs, respectively **(Table 1) (Figure 8C)** (*77*). The Na^+/K^+-ATPase maintains a hyperpolarized cell membrane potential by exchanging two extracellular K^+ ions for three intracellular Na^+ ions. Mutated *ATP1A1* in APAs results in a reduced affinity towards K^+ and a Na^+ or H^+ leak, leading to cell membrane depolarization. On the other hand, *ATP2B3* encodes the Ca^{2+}-ATPase, which is responsible for Ca^{2+} efflux toward the extracellular space. Mutant ATP2B3 promotes aldosterone secretion via two different mechanisms, either by affecting Ca^{2+} binding motif or by causing abnormal Na^+ permeability, which both result in increasing intracellular Ca^{2+} concentration and subsequent membrane depolarization.

Besides aldosterone-driver mutations of ion transporter/channels, somatic mutations of intracellular signaling proteins also contribute to APA, including *CTNNB1* (Wnt/β-catenin signaling) (*80, 101, 102*), *GNAS* and *GNAQ/11* (G-protein signaling) (*81, 82*), and *PRKACA* (cAMP/PKA signaling) (*83*). Unlike the well-understood mechanisms of mutations in ion channels, transporters and pumps in APA, the exact principles for increased aldosterone secretion due to mutated intracellular signaling proteins remain less clear. A common observation of phenotypes associated with these mutations is deregulated cell growth, while autonomous aldosterone production is only recorded in *CTNNB1* and *GNAQ/11* mutations (*103*). Interestingly, Wnt signaling is found constitutively activated in up to 70% of APA **(Figure 8D)** (*104*). About 59% of mutations in the *CTNNB1* gene (encoded β-catenin) co-occur with mutations in G-protein

signaling (*GNAQ/11*) (*81*). Moreover, constitutive activation of Wnt/β-catenin in mice leads to increased proliferation of the adrenal cortex cells, leading to adrenal hyperplasia (*105*). This indicates the important role of Wnt/β-catenin in APA phenotypes and particularly tumorigenesis. Mutations in signaling pathway proteins may suggest a two-hit theory for the tumor formation of APA in selected cases (*106, 107*): The first hit is caused by disruption of signaling pathways resulting in hyperproliferation of adrenocortical cells; the second hit is caused by somatic aldosterone-driver mutations leading to autonomous aldosterone secretion. Nonetheless, the two-hit model of APA development is still unproven, and an adequate APA disease model is needed for further research on this topic.

1.2.3. Disease modeling of primary aldosteronism.

To understand the molecular and cellular mechanism of PA and further develop therapeutic treatments/drug discovery for specific PA subtypes, numerous studies have been established using *in vitro* and *in vivo* models of PA. A summary of genetic animal and cell line models of PA associated with potassium channel mutations is shown in **Table 2**.

In contrast to humans, rodents express low levels of *Kcnj5* in the adrenal gland (*108*); however, knocking out *Kcnj5* in mice still decreases aldosterone levels in females but not in males (*109*). In a previous study, forced expression of human *KCNJ5* mutant under the control of an *Akr1b7* promoter in mouse adrenal glands does not result in a phenotype comparable to that in humans with *KCNJ5* mutation (*110*). Instead of KCNJ5 protein, the main channels for K^+ conductance in rodents are TWIK-related acid-sensitive potassium (TASK) channels. Thus, previous studies have attempted to delete TASK proteins in mice and investigate the pathophysiology of the models. Ablation of *Kcnk3* (encodes TASK-1) leads to severe hyperaldosteronism with low renin levels and hypokalemia, while knocking out *Kcnk9* (encodes TASK-3) shows mild effects on aldosterone production and blood pressure. Although these mouse models do not thoroughly resemble the phenotypes of KCNJ5-associated PA, they emphasize the critical role of potassium channels in regulating aldosterone production and its effects on hypertension.

Table 2: Animal and cell lines models of potassium channel mutations in APA.

Model	Species/Cell lines	Genotype	Reference
Animal model			
Kcnj5 KO	Mice	Reduced aldosterone production in female mice	(*109*)
Akr1b7-driven *KCNJ5* overexpression	Mice	Increased Cyp11b2 expression found only in female mice with overexpressing mutant Aldosterone and renin level were not reported	(*110*)
Kcnk3 (TASK-1) KO	Mice	Cyp11b2 expression in zF and zR Severe hyperaldosteronism (low renin, hypokalemia) Treatable by glucocorticoids	(*111*)
Kcnk9 (TASK-3) KO	Mice	Salt-sensitive, arterial hypertension, low renin Slightly elevated aldosterone production	(*50, 112, 113*)
Kcnk3 (TASK-1) and *Kcnk9* (TASK-3) KO	Mice	Hyperaldosteronism Depolarization in zG	(*114*)
zF-specific TASK-1 and TASK-3 KO	Mice	Mildly elevated aldosterone secretion Chronic high blood pressure	(*115*)
Knock-in germline *KCNJ5*$^{G151R+}$	Pig	Elevated aldosterone renin ratio (ARR) Increased blood pressure	(*116*)
Cell lines			
Ectopic expression of *KCNJ5* mutations	HAC15; H295R	Increased cytosolic Ca^{2+}, increased aldosterone production; decreased cellular proliferation; higher lethality due to massive sodium influx	(*93, 94, 117*)
Conditional expression of KCNJ5 mutations	HAC15	Decreased cellular proliferation; increased apoptosis	(*118*)

HAC15 and H295R: human adrenocortical carcinoma cell lines

In the search for a suitable animal model for PA, the domestic pig is considered to have advantageous features compared to rodents. The physiology of the adrenal cortex of pigs differs from that of humans to some degree, for instance, aldosterone and cortisol synthesis require two different enzymes CYP11B2 and CYP11B1 in human, while only one (CYP11B) is required in pigs. Nevertheless, similarities in the anatomy of the adrenal cortex, and especially the endogenous *KCNJ5* expression in zG, enable pigs to perform as a suitable system for modeling *KCNJ5* mutations in PA. A recent study attempted to knock in germline mutated *KCNJ5* in pigs and investigated their pathophysiology (*116*). This genetic model exhibits a high aldosterone-renin ratio

and high blood pressure; however, the results vary strongly between individuals and even within each individual.

On the other hand, 2D cell lines, usually human adrenocortical carcinoma cell lines, are used to model the pathophysiology of PA *in vitro*. Transfection of HAC15 and H295R cells with mutant KCNJ5 results in increased Na^+ permeability, which in turn raises cytosolic Ca^{2+} and subsequently elevates aldosterone secretion (*93, 117*). Yet, introducing mutant KCNJ5 unexpectedly causes increased apoptosis (*70, 94, 118*); it is also associated with increased lethality in other human cell lines (*70, 94*). This could be explained by the overexpression of mutated *KCNJ5*, which causes a massive sodium influx and depolarization, leading to apoptosis rather than a proliferative effect. Therefore, a model that expresses endogenous mutant KCNJ5 is essential to mimic the proliferative effect of mutant KCNJ5 in patients. The current lack of appropriate disease models hampers further studies of *KCNJ5* proliferative effects in PA as well as other adrenocortical diseases.

1.3. Human induced pluripotent stem cells and stem cell-based disease modeling.

Pluripotent stem cells (PSCs) are defined as cells that possess the ability to proliferate indefinitely and differentiate into all cells of the three primary germ layers. Thanks to these features, PSCs are considered a promising source for regenerative therapy and disease modeling. Embryonic stem cells (ESC) were the first isolated PSCs. ESCs originally comprise the inner cell mass in a blastocyst and were isolated from a mouse embryo (*119, 120*) and later also from human embryos (*121*). ESC can be propagated *in vitro* without losing pluripotency. In 2006, Yamanaka's research group successfully reprogrammed mouse and, subsequently, human somatic cells into cells with a primitive pluripotent state, termed induced pluripotent stem cells (iPSCs) by overexpressing four master transcription factors (SOX2, OCT4, c-MYC, KLF4) (*122, 123*). These cells exhibit properties that closely resemble ESCs, displaying self-renewal and an ability to differentiate into endoderm, mesoderm, and ectoderm cells. Due to the much-reduced ethical issues compared with ESC, there is rapid progress in research using iPSC for drug screening, disease modeling and potential regenerative therapies (*124, 125*).

Stem-cell-derived adrenocortical lineages are promising approaches to solve the lack of plausible disease models and provide a source of cell-based therapy. While the work on other organs, such as the heart, liver, kidney, and central nervous system, has benefited from more established differentiation protocols to derive functional cell types from human pluripotent stem cells (hPSCs) (*126-129*), considerably fewer methods have been developed to facilitate adrenal cortex differentiation. One of the difficulties when generating adrenal cortex from hPSCs is due to the complex organization of its functional units, such as the zG and zF. Over the last decade, several groups have successfully generated steroid-producing cells from hPSCs (*130-132*), human adult stem cells (*133, 134*), or by direct reprogramming from fibroblasts (*135*) **(Table 3).** These studies mainly relied on stable or transient overexpression of steroidogenic factor 1 (SF-1), encoded by *NR5A1*. SF-1 is necessary not only for adrenal but also for gonadal differentiation (*19*). Thus, undesired differentiation into testicular Leydig and ovarian granulosa-luteal cells was obtained in some studies (*132, 133, 136*). In addition, these induced steroidogenic cells do not reflect the full spectrum of adrenocortical cell properties, particularly with limited success in glomerulosa differentiation and aldosterone production (*135, 137*), expression of the adrenal cortex marker *CYP21A2* (*132*) and their proliferative capacity (*135*). Therefore, to precisely direct the cell fate conversion from pluripotent stem cells into adrenocortical lineages, an optimized differentiation system that synergizes niche factors of the adrenal cortex and adrenal-driver transcription factor must be developed.

Table 3: Stem cell-derived/Somatically reprogrammed steroid-producing cells.

Cell types/origin	Methods of induction	Characterization	Hormone production	Ref.
Rat MSCs (bone marrow)	Transplantation	Testicular Leydig cells	Testosterone	(*133*)
Mouse MSCs (bone marrow)	SF-1 (transient expression)	Cortisol-producing cells	Cortisol	(*133, 138*)
Human MSCs (bone marrow)	SF-1 (transient and stable expression) LHR-1 (stable expression)	Steroidogenic cells (zF- and zR-like cells)	Testosterone Cortisol	(*133, 139, 140*)
Human MSCs (Umbilical cord blood)	SF-1 (stable expression)	Ovarian granulosa-luteal cell	Progesterone	(*136*)
Mouse ESCs	SF-1 (inducible expression)	Steroidogenic cells (zF-like cells)	Corticosterone	(*130*)
Human ESCs, iPSCs	SF-1 (transient expression)	Steroidogenic cells	Cortisol DHEA Aldosterone (low levels)	(*131, 141*)

Human urine-derived stem cells (USCs) Fibroblasts (skin)	SF-1 (stable expression)	Steroidogenic cells (zF- and zR-like cells) Limited proliferation capacity	Cortisol Testosterone	(*135*)
Human iPSCs	SF-1 (transient expression)	Testicular Leydig cells Adrenocortical-like cells (not well-characterized)	Testosterone Cortisol, aldosterone	(*132*)

MSC, mesenchymal stem cell; ESC, embryonic stem cell; iPSC, induced pluripotent stem cells; zF, zona fasciculata; zR, zona reticularis

1.4. Research gap and objectives

1.4.3. Research gap

As described in the previous sections, adrenocortical research has long suffered from inadequate models of healthy and diseased tissue. Animal models often do not represent human physiology; in this case, differences in the physiology between animals and humans hamper generating good disease models. Rodents lack the zona reticularis and expression of *Kcnj5*, which is an essential gene to model the most common genetic mutations in APA. In cattle, the steroidogenic pathway is different from humans, for example, aldosterone and cortisol production is catalyzed from a single enzyme instead of two distinct enzymes and pathways in humans (*142*). Meanwhile, research on adrenal cortex biology and disease modeling has strongly relied on the human adrenocortical carcinoma cell line NCI-H295 (H295R, HAC15 cells are sub-strains) (*143, 144*). Even though these cells show adrenocortical gene expression patterns and multiple steroid biosynthesis pathways are present, limitations in their genetic background (H295R cells carry a *CTNNB1* mutation, which leads to upregulated baseline proliferation and may interfere with other signaling pathways (*145*)) and heterogeneity (NCI-H295 originate from multiple zones of the adrenocortical carcinoma, and each sub-strain produces different steroid profiles (*146, 147*)) limit their use as a disease model.

In the same light, stem cell-derived steroidogenic cells that have been generated so far are restricted to the fasciculata and reticularis identity (predominantly produced cortisol and testosterone) (**Table 3**). Moreover, very few studies in this field investigated the proliferation capacity of their cells (*135*), missing out on one of the most important cellular features to model a proliferation-related disorder such as APA. Last but not least, genome editing is considered a laborious technique to perform on animals, especially large animals (pigs, dogs, non-human primates), to introduce PA mutations (*148*). As one of the solutions, CRISPR/Cas9 in hiPSCs is a precise, robust,

and controllable genetic manipulation that is suitable for inserting a somatic KCNJ5 mutation in the cell line (*149*).

Taken together, we realized an evident need for human-derived disease models that allow genomic manipulation and assessment of hormone production and proliferation in a near-physiological context, which prompted us to conduct this study.

1.4.4. Objectives

The overall goal of this study is to advance adrenal cortex research by developing an optimized differentiation system to generate hiPSC-derived adrenocortical cells. The induced cells are expected to exhibit adrenal cortex gene expression profiles and produce adrenal cortex steroids. To overcome the scarcity of preclinical disease models of PA, particularly of APA associated with pathogenic *KCNJ5* mutations, we used our system of adrenal cortex differentiation, combined with the CRISPR/Cas9 technique, to establish a *KCNJ5*$^{G151R/+}$ hiPSC-derived adrenocortical cell model.

Specific aims include:

1. Optimization of the existing differentiation protocols towards the adrenocortical lineage
2. Generation of heterozygous somatic KCNJ5 mutation in hiPSCs
3. Differentiation of the *KCNJ5*$^{G151R/+}$ hiPSCs to adrenal cortex cells under optimized conditions.
4. Characterization of the pathophysiology of the *KCNJ5*$^{G151R/+}$ hiPSC-derived adrenocortical cells.

2. Materials and methods

2.1. Materials

2.1.1. Cell line

The established and fully characterized BIHi005-A hiPSC line (male, https://hpscreg.eu/cell-line/BIHi005-A) was obtained from BIH Stem Cell Core. The cell line was generated using a reprogramming Sendai virus vector on the fibroblasts of a healthy donor. The reprogramming vector carries Yamanaka's transcription factors (OCT4, SOX2, KLF4 and c-MYC). BIHi005-A cells were used in the differentiation from hiPSCs toward adrenocortical cells and generation of the heterozygous *KCNJ5*^{G151R} hiPSC line. The heterozygous *KCNJ5*^{G151R} hiPSC line was banked and registered as BIHi005-A-46 cell line (https://hpscreg.eu/cell-line/BIHi005-A-46). The human adrenal carcinoma NCI-H295R cell line used in this study is a gift of Matthias Haase (Universitätsklinikum Düsseldorf, Germany), authenticated by STR analysis (ATCC Cell Line Authentication Service).

2.1.2. Cell culture reagents

Reagent	Supplier	Cat. No.
StemFlex Medium	Gibco	A3349401
Essential E8 Medium	Thermo Fischer Scientific	A1517001
Advanced RPMI 1640, Reduced Serum Medium	Gibco	12633012
Renal Epithelial Growth Medium 2 Kit	PromoCell	C-26130
DMEM/F-12 (1:1)	Gibco	11320033
KnockOut DMEM/F-12	Gibco	12660012
GlutaMAX-I (100X)	Gibco	35050061
Ultroser-G	Sartorius	15950-017
ITS+ Premix	Corning	354352
BSA 7.5% in DPBS	Sigma	A8412-100ML
Y-27632	Wako	035-24593
Geltrex LDEV-Free (Reduced Growth Factor)	Gibco	A1413201
Penicillin/Streptomycin (100X)	Gibco	10378016
Gentamicin (10 mg/mL)	Gibco	15710064
TrypLE Express, no Phenol Red	Gibco	12604021
UltraPure 0.5 M EDTA, pH 8.0	Invitrogen	15575020

RotiCell PBS without Ca/Mg	Roth	9143.1
Bambanker	Nippon Genetics	BB01
OPTI-MEM (Reduced Serum Medium)	Gibco	31985062
Lipofectamine 2000	Invitrogen	11668019
P3 Primary Cell Nucleofector 4D Kit S	Lonza	V4XP-3032
Human Angiotensin II	Sigma	A9525
Potassium Chloride	Sigma	P5405
8-br-cAMP	STEMCELL Technologies	73602
EZSolution™ CHIR99021	BioVision	1748-5
Human FGF-basic	Peprotech	100-18B
Human Noggin	Peprotech	120-10C
Human/Murine/Rat Activin A	Peprotech	120-14E
Retinoic Acid	Miltenyi Biotec	130-117-339
Human BMP7	Invitrogen	PHC9541

2.1.3. Medium and buffer

H295R growth medium	
DMEM/F-12 (1:1)	**477.5 mL**
Ultroser-G 2.5 %	12.5 mL
ITS+ Premix 1 %	5 mL
Penicillin/Streptomycin (100X) 1%	5 mL

FACS Buffer	
BSA 7.5% in DPBS	1%
UltraPure 0.5 M EDTA	2 mM
in PBS, filtered	

Cell Lysis Buffer	
NaCl	150 mM
Tris-HCl pH 7.5	10 mM
Nonidet P-40	1 % (v/v)
EDTA pH 8.0	1 mM
in dH_2O	
Complete protease inhibitor cocktail (Roche) is added freshly	

Permeabilization/Blocking buffer (Immunocytochemistry)	
BSA 7.5% in DPBS (Sigma)	1%
Saponin (Sigma)	0.2%
in PBS with Ca/Mg (Gibco)	

LB medium		LB agar medium	
Tryptone	1 %	Tryptone	1 %
Yeast extract	0.5 %	Yeast extract	0.5 %
NaCl	0.5 %	NaCl	0.5 %
in dH_2O		Agarose	1.5 %
		in dH_2O	

2.1.4. List of antibodies

Table 4: List of antibodies used for immunofluorescence and FACS.

Intermediate mesoderm differentiation				
Specificity	**Species**	**Dilution**	**Cat. Nr**	**Manufacturer**
WT1	Rabbit Monoclonal	1:100	CAN-R9(ICH)56-2	Novus Biological
OSR-1	Rabbit Polyclonal	1:100	3729	Cell Signaling Technology
TRA1-60-PE conjugated	Monoclonal	1:250	130-122-965	Miltenyi Biotec
OCT3/4-APC conjugated	Monoclonal	1:20	130-123-318	Miltenyi Biotec

Adrenal cortex differentiation				
Specificity	**Species**	**Dilution**	**Cat. Nr**	**Manufacturer**
SF-1	Mouse monoclonal	1:100	sc-393592	Santa Cruz
STAR	Mouse monoclonal	1:100	sc-166821	Santa Cruz
CYP11B2	Mouse monoclonal	1:100	MABS1251	Merck (Sigma-Aldrich)
CYP11B1	Rat monoclonal	1:100	MABS502	Merck (Sigma-Aldrich)
DAX-1	Rabbit monoclonal	1:250	ab196649	Abcam
GLI-1-Alexa Fluor® 647 conjugated	Mouse monoclonal	1:100	sc-515751	Santa Cruz
MKi67-Alexa Fluor® 594 conjugated	Rabbit monoclonal	1:100	IC7617T-100UG	R&D Systems
CD56	Mouse monoclonal	1:100	304602	Biolegend
E-Cadherin-Alexa Fluor® 405-conjugated	Mouse monoclonal	1:100	FAB18381V	R&D Systems
NESTIN	Mouse monoclonal	1:100	sc-23927	Santa Cruz
β-catenin	Rabbit polyclonal	1:250	PA5-16762	Invitrogen

Secondary antibodies				
Specificity	**Species**	**Dilution**	**Clone**	**Manufacturer**
Anti-mouse IgG Alexa Fluor® 546	Goat	1:500	A11030	Invitrogen
Anti-rabbit IgG Alexa Fluor® 555	Goat	1:500	A21428	Invitrogen
Anti-rabbit IgG Alexa Fluor® 647	Goat	1:500	A32733	Invitrogen
Anti-rat IgG Alexa Fluor® 546	Donkey	1:500	A48272	Invitrogen

2.1.5. Reagents and consumables

Name	Supplier	Cat. No.
FoxP3 Staining Buffer Set	Miltenyi Biotec	130-093-142
CellTiter-Glo® Luminescent Cell Viability Assay	Promega	G7571
Annexin V-CF Blue 7-AAD Apoptosis Staining	Abcam	ab214663
Aldosterone ELISA	Cayman	501090
Corticosterone ELISA	Cayman	501320

Name	Supplier	Cat. No.
Cortisol ELISA	Cusabio	CSB-E05111h
Pierce BCA Protein Assay	Thermo Fischer Scientific	23225
QuickExtract DNA Solution	Lucigen	QE09050
4% paraformaldehyde in PBS	Santa Cruz	sc-281692
Dichloromethane (DCM)	Sigma	270997-250ML
DAPI	Thermo Fischer Scientific	62248
DRAG5	BioLegend	424101
QIAprep Spin Miniprep Kit	Qiagen	27106
EndoFree Plasmid Maxi Kit	Qiagen	12362
Chromium Next GEM Single Cell 3' GEM, Library & Gel Bead Kit v3.1	10X Genomics	PN-1000128
Chromium Next GEM Single Cell 3'GEM Kit v3.1	10X Genomics	PN-1000130
Chromium Next GEM Single Cell 3' Gel Bead Kit v3.1	10X Genomics	PN-1000129
Single Index Kit T Set A	10X Genomics	PN-1000213
Cell Scraper S	TPP	353085
Cell Strainer 100 µm Nylon	BD	352360
DNA Gel Loading Dye (6X)	New England Biolabs	B7024S
S.O.C Medium	Invitrogen	15544034
TOP10 Competent Cells	Invitrogen	C404003
RNase-Free DNase Set	Qiagen	79254
Ethidium bromide solution 0.025 %	Roth	HP47.1
1.5 ml Polypropylene Microcentrifuge Tube	Sarstedt	72.706.400
Falcon 15 ml Conical Centrifuge Tube	Greiner Bio-one	500815
Falcon 50 ml Conical Centrifuge Tube	Greiner Bio-one	500817
Falcon Round-Bottom Polystyrene Tubes with snap cap	BD	352054
1 kb Plus DNA Ladder	Invitrogen	10787018
Glycerol	Roth	56-81-5
UltraPure Water	Cayman	400000
NucleoSpin Gel and PCR Clean-up, Mini Kit	Macherey-Nagel	740609.50
Petri Dish 94/16 mm, PS	Greiner Bio-One	Z617636
OneTaq DNA Polymerase	New England Biolabs	M0480S
Kappa2G Hotstart DNA Polymerase	Roche	07960824001
Quick-RNA MicroPrep	Zymo Research	R1050

Name	Supplier	Cat. No.
Restriction enzymes and buffers	New England Biolabs	
QuantiTect Reverse Transcription Kit	Qiagen	205311
RNeasy Mini Kit	Qiagen	74004
PowerSYBR Green PCR Master Mix	Applied Biosystems	4367659
Sterile Culture Tubes with Cap, Polypropylene	Simport	T415-2A
Ampicillin	Life Technologies	11593027
Ambion Nuclease-Free Water	Life Technologies	AM99906
T4 PNK	New England Biolabs	M0201S
EVE Cell counting slide	NanoEntek	NE-EVS-50
TC Plate 12 Well, Standard	Greiner Bio-One	665180
TC Plate 24 Well, Standard	Greiner Bio-One	662160
TC Plate 6 Well, Standard	Greiner Bio-One	657160
TC Plate 96 Well, Standard	Greiner Bio-One	651180
CryoTube 1.8 mL	Thermo Scientific	377267
Biosphere Pipette Filter Tips 2.5 µl	Sarstedt	70.3010.265
Biosphere Pipette Filter Tips 10 µl	Sarstedt	70.3010.255
Biosphere Pipette Filter Tips 100 µl	Sarstedt	70.3050.255
Biosphere Pipette Filter Tips 1000µl	Sarstedt	70.3050.275
UltraPure Agarose	Thermo Fisher Scientific	16500500
Hard-Shell PCR Plates 96-well Low Profiles, Semi-Skirted	Bio-Rad	HSL9601
Microseal ´B´Seals	Bio-Rad	MSB1001
96-well clear bottom white plates	Corning	CLS3367
CellCarrier-96 Black Imaging Plate	PerkinElmer	6055302

2.1.6. Oligonucleotides, primers, and plasmids

Table 5: List of primers and oligonucleotides used for qPCR, genotyping and CRISPR/Cas9.

List of primers used		
Gene	**Forward primer (5' -> 3')**	**Reverse primer (5' -> 3')**
OCT4	ACATGTGTAAGCGCTGCGGCC	GTTGTGCATAGTCGCTGCTTG
NANOG	TCTCCAACATCCTGAACCTC	CCAGTTGTTTTTCTGCCACC
WT1	GAGCGATAACCACACAACGC	ACACGTCGCACATCCTGAATG
PAX2	TGTCAGCAAAATCCTGGGCAG	GTCGGGTTCTGTCGTTTGTATT
HOXD11	ACAGGCTTTCGACCAGTTTTTC	CCTTCTCGGCGCTCTTGTC
LHX1	ATCCTGGACCGCTTTCTCTT	GTACCGAAACACCGGAAGAA

Endogenous *NR5A1*	GCGGGCATGGACTATTCGTA	GAGCAGTCCGTAGTGGTAGC
NR5A1	GAGAGCCAGAGCTGCAAGAT	CTTGTACATCGGCCCAAACT
NR0B1	CCAGGTCCAAGCCATCAAGT	GGCACGTCCGGGTTAAAGA
STAR	GGCATCCTTAGCAACCAAGA	TCTCCTTGACATTGGGGTTC
CYP11B1	GGCAGAGGCAGAGATGCTG	TCTTGGGTTAGTGTCTCCACCTG
CYP11B2	GGCAGAGGCAGAGATGCTG	CTTGAGTTAGTGTCTCCACCAGGA
CYP17A1	TGAGTTTGCTGTGGACAAGG	TCCGAAGGGCAAATAGCTTA
CYP21A2	CACTGAGACCACAGCAAACAC	CTGCAGTCGCTGCTGAATC
18S	GGGAGCCTGAGAAACGGC	GGGTCGGGAGTGGGTAATTT
GAPDH	GCATCTTCTTTTGCGTCG	TGTAAACCATGTAGTTGAGGT
KCNJ5-internal	CGACCAAGAGTGGATTCCTT	AGGGTCTCCGCTCTCTTCTT
KCNJ5-external	TGAATCAGAACAGCCCACTTC	TCTTCTGGAGTCACAGTTGCC

Oligonucleotides (5‘ -> 3‘)	**Supplier**
sgRNA-1-KCNJ5 G151R: ATTGAGACCGAAACAACCAT	Eurofins Scientific
sgRNA-2-KCNJ5 G151R: TTGAGACCGAAACAACCATT	Eurofins Scientific
sgRNA-3-KCNJ5 G151R: AAACCCGGCCCAGGCTCAAGTCTGC	Eurofins Scientific
ssODN-WT: CCTTGTGTTGAAAACCTCAGTGGCTTCGTGTCCGCTTTCCTGTTCTC GATTGAGACCGAAACAACGATTGGATATGGCTTCCGAGTGATCACA GAGAAGTGTCCAGAGGGGATTATACTCCTCTTGGTCCAGGCC	IDT
ssODN-G151R: CCTTGTGTTGAAAACCTCAGTGGCTTCGTGTCCGCTTTCCTGTTCTC GATTGAGACTGAGACAACGATTAGATATGGCTTCCGAGTCATCACA GAGAAGTGTCCAGAGGGGATTATACTC	IDT
U6-Forward: GAGGGCCTATTTCCCATGATTCC	Eurofins Scientific

Plasmid	**Source**
pcDNA3.1(+)-NR5A1-P2A-EGFP	Genscript
pSpCas9(BB)-2A-GFP	Addgene
pCAG-i53-bpA-EF1BFP	Max-Delbrück-Center (Berlin)
pCAG-BCL-XL-bpA-EF1BFP	Max-Delbrück-Center (Berlin)

2.1.7. Equipment

Name	Supplier
EnSpire 2300 Multilabel Reader	PerkinElmer
ChemiDoc XRS+ Imaging System	Bio-Rad
BD FACSAria Fusion Cell Sorter	BD Biosciences
BD LSR II Flow Cytometer	BD Biosciences
CFX Connect Real-Time System	Bio-Rad
Bioanalyzer 2100	Agilent
NanoDrop 2000c Spectrophotometer	Peqlab
WellWash	Thermo Fisher Scientific
4D Nucleofector Transfection System	Lonza
PowerPac Basic Electrophoresis Cell	Bio-rad
Axio Vert.A1 Inverted Phase Contrast Microscope	Zeiss
Mastercyler Nexus SX1 PCR System	Eppendorf
Heraeus Fresco21 Centrifuge	Thermo Fisher Scientific
ThermoMixer C	Eppendorf
Heraeus MegaFuge16R Centrifuge	Thermo Fisher Scientific
Duomax 1030 orbital shaker	Heidolph
AccuBlock Digital Dry Bath	Labnet International
PerfectSpin Plate Centrifuge	Peqlab
Vortex-Genie 2	Scientific Industries
HeraTherm Incubator	Thermo Fisher Scientific
MaxQ 481 HP Shaking Incubator	Thermo Fisher Scientific
HeraCell Vios 160i CO2 Incubator	Thermo Fisher Scientific
Analytical Laboratory Scale	Mettler Toledo
Dry bath	Memmert
Safe2020 Class II Biological Safety Cabinet	Thermo Fisher Scientific
JuLI Live cell movie analyzer	NanoEntek
VacuSafe Aspiration System	INTEGRA Biosciences
Microcentrifuge	Biozym
Milli-Q Water Purification System	Milipore
Mr. Frosty Cryo 1°C Freezing Containers	Nalgene
Multipette Plus	Eppendorf
HiSeq4000 Sequencing System	Illumina
Opera Phenix High-Content Screening System	PerkinElmer
ZEISS906 Transmission Electron Microscope	Zeiss
QTRAP 6500+ LC-MS/MS System	Sciex
Liebherr Laboratory Refrigerator	Liebherr

Liebherr Laboratory Freezer	Liebherr
Ultra-low Temperature Freezer (-80 °C) TDE Series	Thermo Fisher Scientific

2.1.8. Software

Name	Producer
OMERO Imaging System	Glencoe Software Inc.
Columbus Image Data Storage and Analysis System	PerkinElmer
Image Lab 6.0	Bio-Rad
ICE CRISPR Analysis Tool	Synthego
CFX Maestro Software	Bio-Rad
FACSDiva™ Software	BD Biosciences
FlowJo V10	FlowJo, LLC
GraphPad Prism	GraphPad Software
Illustrator CC 2017	Adobe
Multimode Plate Reader Software	PerkinElmer
EndNote 2.0	Clarivate
Microsoft Office 365 ProPlus	Microsoft
NanoDrop 2000 Software	Thermo Fisher Scientific
ZEISS ZEN3.3 (Blue Edition)	Zeiss
SnapGene 4.2.4	GSL Biotech

2.2. Cell biology methods

2.2.1. Culture and maintenance of hiPSCs

Cultivation and maintenance of hiPSCs was performed in Essential E8 medium on a Geltrex-coated 6-well tissue culture plate. For coating, ice-thawed Geltrex was diluted 1:50 in cold KnockOut DMEM/F-12 medium and used to cover the 6-well plates (1.0 mL of diluted Geltrex per well). Geltrex-coated plates were incubated for 30 minutes at 37°C or for 1 hour at room temperature. Depending on the growth rate of the cells, cells were passaged every 3-5 days to maintain the log-phase growth and avoid spontaneous differentiation of the iPSCs. As routine maintenance of the hiPSCs, chemical passaging using EDTA was performed to obtain cell clumps, crucial for hPSC propagation. Briefly, the Geltrex from a coated 6-well plate was aspirated, 1.5 mL of warm E8 medium was added. The medium was then aspirated, and the plates were rinsed with 1 mL of 0.5 mM EDTA. To detach the cell clumps from the previous plates, 1 mL of 0.5 mM EDTA was added and incubated at 37°C for 3 – 5 minutes. EDTA was removed gently, the cell clumps were immersed in 3 mL warm E8 medium. The cells were detached using a cell scraper, and 150 – 500 µL of the cell suspension were

transferred to a pre-warmed and coated 6-well plate with E8 medium. E8 medium was changed daily, passaging was performed when the cells reached 70 – 80% confluency. To freeze hiPSCs, chemical passaging was performed as described above. Instead of transferring the cells to new plates, cell clumps were suspended in 1 mL of ice-cold Bambanker freezing medium and transferred into a cryo-vial. The vial was placed immediately into a freezing container and stored at -80°C overnight, then transferred to liquid nitrogen the next day for long-term storage.

2.2.2. Intermediate mesoderm (IM)

To induce IM differentiation from hiPSCs, hiPSCs were harvested as single cells. In brief, hiPSCs were detached from the plate as single cells using TrypLE-Select at 37°C for 4 minutes. After neutralizing trypsin by resuspending the cells in warm E8, cells were centrifuged at 300 × g. The cell pellet was resuspended in E8 medium supplemented with 10 µM Y-27632, and cell counting was performed with Trypan Blue dye using a Neubauer chamber or a JuLi automatic cell counting system. Single cells were seeded in coated 6-well plates at different cell densities and culture conditions, according to the following protocols:

- Following Mae et al., 2013 (*150*), 1.5 x 10^6 single hiPSCs were seeded in a coated 6-well plate cultured in Stage 1 medium, composed of DMEM/F-12+GlutaMax and 1x B27 Supplement, 3 µM CHIR99021, 100 ng/ml Activin A with 1% Penicillin/Streptomycin and 10 µM Y-27632. The cells were cultured for 2 days and then changed to Stage 2 IM medium, composed of B27 Supplement, 3 µM CHIR99021, 100 ng/ml BMP7 for another 2 days.
- Following Lam et al., 2014 (*151*), 4.0 x 10^5 single hiPSCs were seeded in coated 6-well plate two days before IM induction and cultured in E8 medium supplemented with 10 µM Y-27632. On induction day, the medium was changed to Stage 1 medium, composed of Advanced RPMI, 1X GlutaMax-I, 5 µM CHIR99021 with 1% Penicillin/Streptomycin. The cells were cultured for 1.5 days and then changed to Stage 2 IM medium, composed of 1 µM Retinoic Acid, 100 ng/ml bFGF2 for the next 3 days.
- We followed Morizane et al., 2017 (*128*) with modifications (shortened timing of treating cells with GSK-β inhibitor CHIR99021 (CHIR) and Activin A). 2.0 x 10^5 single hiPSCs were seeded in coated 6-well plates two days before IM induction and cultured in E8 medium supplemented with 10 µM Y-27632. On induction

day, the medium was changed to Stage 1 medium, composed of Advanced RPMI, 1X GlutaMax-I, 10 µM CHIR99021, 5 ng/ml Noggin with 1% Penicillin/Streptomycin. The cells were cultured for 3 days and changed to Stage 2 IM medium, composed of 10 ng/ml Activin A for the next 2 days.

IM cells were harvested on the final day of each protocol and examined for positive expression of IM markers (WT1, OSR-1, PAX2) and negative expression of pluripotency markers (NANOG, OCT4) using immunofluorescence staining and qRT-PCR.

2.2.3. Adrenal cortex differentiation

Approximately 5 x 10^5 IM cells were seeded in one well of a 6-well plate 12-24 hours before transfection. Cells were transfected with 4 µg of a pcDNA3.1(+)-*NR5A1-P2A-EGFP* plasmid. The transfection was performed with 4 µg of the DNA construct in 500 µL of OptiMEM in Tube A; in parallel, 10 µl of Lipofectamine 2000 was diluted with 500 µL OptiMEM in Tube B. Lipofectamine 2000 solution in Tube B was mixed with Tube A and incubated at room temperature for 10 minutes. The transfection mixture was added dropwise to IM cells. After 6 hours, the transfected cells were cultured in adrenal cortex differentiation medium. The components and concentrations were: human Angiotensin II (AngII), 100 nM; Potassium Chloride (KCl), 12 mM; 8-bromo-cyclic AMP (8-br-cAMP), 100 µM; human FGF2, 100 ng/ml. These reagents were mixed in renal epithelial cell growth medium 2 Kit supplemented with Penicillin/Streptomycin and 5% FCS. Medium was changed every 2 days and collected for characterization after one week of differentiation. To examine the effect of the Wnt signaling pathway on adrenocortical differentiation, CHIR99021 (1 µM) was added to the culture system on day 10 of the experimental scheme **(Figure 20)** for 2 days.

2.2.4. CRISPR/Cas9 knock in of the KCNJ5 G151R mutation

sgRNAs were designed using the CRISPR Design Tool (Horizon Discovery). The construction of the pSpCas9(BB)-2A-GFP plasmid is described in Section 2.3.1. A single-stranded oligonucleotide (ssODN) containing the G151R mutation (ssODN-G151R) on exon 2 of *KCNJ5* was designed with 50 bp 5' and 3' homology arms. A silent mutation was added to generate a new DdeI restriction site in ssODN-G151R. A ssODN carrying the WT codon at G151 (ssODN-WT) with 50 bp homology arms was used to increase the efficiency of heterozygous edits. To screen for the sgRNAs

with the highest genome editing efficiency, we performed a T7E1 assay by transfecting individual sgRNA-Cas9-GFP plasmid into BIHi005-A iPSCs. After 48 hours, the GFP^+ cells were harvested to collect total genomic DNA by using the QuickExtract DNA extraction kit. PCR was performed using the KAPA2G Fast HotStart polymerase with primers specific for the targeted *KCNJ5* region (KCNJ5-internal). Half of the PCR products were denatured, annealed, and treated with T7E1. Cleaved fragments were visualized on a 1% agarose gel along with untransfected cells as WT. The other half of the PCR products were sent for Sanger sequencing (Eurofins Genomics). Indel percentage of sgRNA-3-KCNJ5 G151R was determined and calculated using the ICE CRIPSR Analysis Tool (Synthego).

For optimized plasmid transfection into the BIHi005-A iPSC line, cells were seeded as single cells in a 6-well plate 1 day before plasmid transfection. 8 x 10^5 cells were harvested and suspended with a mixture containing P3 electroporation buffer, 6 µg sgRNA-Cas9 carrying plasmid, and 100 pmol of each ssODN. To facilitate the HDR pathway and improve iPSC survival after transfection, 1 µg of i53-BFP plasmid (Ku, Yumlu, and Bashir 2019) and 1 µg of BCL-XL-BFP plasmid (Li et al. 2018) were added to the cell suspension. Cells were transferred to a 100 µl Nucleocuvette and electroporated using a 4D Nucleofector X unit. Then, cells were transferred to pre-warmed StemFlex medium supplemented with 10 µM Y-27632 and incubated for 48 hours before FACS sorting. 10^3 GFP/BFP^+ cells were sorted and cultured in a 6-well plate for 5 – 7 days before picking up the emerging single colonies using StemFlex. iPSC clones were expanded for 2 weeks before analysis. Total DNA was extracted using the QuickExtract DNA extraction kit. To genotype Cas9-mediated clones, RFLP assay and Sanger sequencing were performed using PCR products amplified by *KCNJ5* internal and external primer sets. PCR was performed using KAPA2G Fast HotStart PCR on a Mastercycler Nexus SX1 to amplify the regions of interest with the PCR program following the manufacturer's instructions. Sanger Sequencing (performed by TubeSeq Sanger Sequencing Service of Eurofins Genomics) verified the correct knock-in mutation by two primer sets: *KCNJ5*-internal (exon), and *KCNJ5*-external (intron-exon spanning), which covered the region of interest. In a RFLP assay, the PCR products were digested with DdeI for 30 minutes and visualized by gel electrophoresis with Ethidium bromide.

2.2.5. Characterization of CRISPR/Cas9-modified hiPSC cell lines

Karyotyping (G-banding and SNP array) and characterization of the iPSC line (pluripotency markers, morphology, viability) were performed by the BIH Stem Cell Core and did not show any abnormalities. The heterozygous *KCNJ5*$^{G151R/+}$ hiPSC line was banked and registered as BIHi005-A-46 cell line.

2.2.6. Proliferation by luminescent viability assay

The proliferation rate was measured using CellTiter Glo Luminescent Cell Viability Assay. 4,000 cells of each cell line were seeded onto four wells of 96-well clear bottom white plates. Luminescence was measured 2-5 hours after seeding (considered as day 0), day 1, day 2, and day 3, according to the manufacturer's instructions, using an EnSpire 2300 Multilabel Reader. Briefly, CellTiter-Glo reagent was added in the same volume to the volume of cell culture medium present in each well. Cell culture medium without cells was added into three individual wells as a control for background luminescence. Readings from the blank control wells were subtracted from test well readings.

2.2.7. Proliferation and apoptosis assay

To determine the fraction of Ki67$^+$ (proliferation marker) and Annexin V$^+$ (apoptosis marker) cells, hiPSC-derived adrenocortical cells were collected on day 10 of differentiation and separated into two tubes for Ki67 and Annexin V staining. For intracellular Ki67 staining, the cells were fixed and permeabilized using FOXP3 staining buffer set followed by incubation with antibody Ki67-AlexaFluor594 for 30 min at 4^{o}C in the dark. For Annexin V, the cells were suspended in binding buffer and incubated with Annexin V and 7-AAD for 15 min using Annexin V-CF Blue 7-AAD Apoptosis Staining according to the manufacturer's instruction. Both Ki67- and AnnexinV/7-AAD- stained tubes were washed with FACS buffer, directly followed by flow cytometry analysis.

2.2.8. Flow cytometric analysis and cell sorting

SF-1-overexpressing cells were harvested into centrifuge tubes and washed with cold FACS buffer (1% BSA and 2 mM EDTA in PBS without Ca^{2+}/Mg^{2+}). To quantify GFP$^+$ transfected cells, the cells were directly measured using FACS (FACS Aria, FACS AriaII at Max Delbrück Center for Molecular Medicine, Berlin). For sorting, Cas9-GFP transfected iPSCs were harvested and suspended in cold FACS buffer supplemented

with Gentamicin (final concentration is 10 µg/mL) and collected in an FCS-coated catching tube using FACS AriaIII Sorter (BIMSB, Berlin). Sorted cells were spun down at 300 g for 5 minutes, re-suspended in fresh pre-warmed StemFlex medium with ROCKi, and plated onto a 6-well plate for further cultivation.

2.2.9. Electron microscopy

hiPSCs and hiPSC-derived adrenal cortex cells were seeded at 80% confluency on a 6-well plate. On day 1, hiPSCs were fixed with ½ strength Karnovsky's fixative (2.5% glutaraldehyde and 2% paraformaldehyde in 0.1M phosphate buffer), while hiPSC-derived adrenal cortex cells were fixed in 2.5% glutaraldehyde, 0.1M Cacodylate buffer. Both cell lines were fixed at 4°C overnight. On day 2, the fixed cells were rinsed with 0.1M cacodylate buffer and post-fixed in 1% aqueous OsO_4/0.8% potassium hexacyanoferrate for 90 minutes at room temperature, then washed with Caco buffer before embedding. The cells were then embedded in 1% agarose and solidified overnight at 4°C. On day 3, cells were progressively dehydrated using ethanol in the following order: 70% for 30 min, 85%, 95%, and 100% for 10 minutes each and 100% for 5 minutes. Then, cells were infiltrated with a mixture of propylene oxide (PO) and Epon resin (PO/Epon resin) for 60 minutes each: 2:1; 1:1; 1:2 and finally 100% Epon resin overnight at room temperature. On day 4, the cells were embedded in Beem capsules using fresh Epon resin at 60°C for 3 days. Thereafter, samples were cut into ultra-thin sections (60 nm) and imaged using a ZEISS906 microscope.

2.3. Molecular biology methods

2.3.1. Construction of Cas9-sgRNA expressing vector

In this study, the construction of the Cas9-sgRNA expressing vector was adapted from (*152*). Briefly, the top and bottom strands of sgRNA oligos were phosphorylated by T4 PNK and annealed with the thermocycler program: 37˚C for 30 min; 95˚C for 5 min; ramp down to 25˚C at 5˚C/min. Then, the phosphorylated and annealed oligos were cloned into pSpCas9(BB)-2A-GFP at the restriction site BbsI, followed by ligation by T4 Ligase. The constructs were amplified by transformation into OneShot Top10 competent cells. 10 µL of ligation mixture was mixed with 50 µL of competent cells, then incubated on ice for 30 minutes, followed by heat shock at 42˚C for 30 sec, and immediately placed back on ice for 5 minutes. 100 µL of SOC medium were added to the mixture and plated on an LB Agar plate with 100 µg/ml Ampicillin. The plate was

incubated at 37˚C overnight. Three to five colonies were picked up and incubated individually in 3 mL of LB medium with 100 µg/ml Ampicillin at 37˚C overnight. The plasmid DNA was isolated using QIAprep Spin Minikit following the manufacturer's instructions. Sanger sequencing (performed by TubeSeq Sanger Sequencing Service of Eurofins Genomics) verified the correct insertion using the U6-Forward primer. After confirmation by Sanger sequencing, the bacteria stocks were revived by scraping a small amount of 50% Glycerol stocks using a pipette tip and added to 3 mL LB-Ampicillin for 8 hours as a pre-culture. An amount of 300 µL bacteria pre-culture was then transferred to 100 mL LB-Ampicillin medium and incubated in 37˚C for 16 hours before harvesting. Plasmids were then extracted by using the EndoFree Plasmid Maxi Kit (QIAGEN), and used for transfection.

2.3.2. Gene expression analysis

Total RNA was extracted from cultured cells using RNeasy Mini Kit or Quick-RNA Microprep according to the manufacturer's instructions. cDNA was synthesized from 500 ng of total RNA using QuantiTect Reverse Transcription. The cDNA obtained was then used as a template for quantitative PCR using SYBR Green Master Mix on a CFX Connect Real-time PCR machine. Primers used in this study are listed in Table S1. Levels of mRNA expression were normalized to those of a housekeeping gene, *GAPDH,* or 18S *rRNA*.

2.3.3. Immunofluorescence

The cultured cells were fixed using 4% paraformaldehyde in PBS for 10 minutes at room temperature. Permeabilization and blocking were performed using a buffer containing 0.2% Saponin and 1% BSA in PBS for 30 minutes. All antibodies used here were diluted in permeabilization/blocking buffer at a ratio recommended by the manufacturer. The cells were incubated with primary antibody overnight at 4˚C, followed by the equivalent secondary antibody for 1 hour at room temperature. Nuclear staining was performed using DAPI. The stained cells were imaged by High-Content Screening System Opera Phenix.

2.3.4. Hormone quantification and steroid profiling

Cell culture supernatant was collected 24 h after the last medium change. To remove particulates, the samples were centrifuged at 1.500 rpm for 10 minutes at 4ºC. The supernatant was transferred to a clean tube and stored at -80°C. Hormone production

in the media was detected by either steroid profiling or ELISA. The cell culture supernatants were sent on dry ice to Klinisches Labor, Universitätsklinikum Erlangen (Prof. Manfred Rauh) for steroid profiling using LC-MS/MS technique. In this method, the steroid hormones 17-OHP, progesterone, and testosterone, among other steroids, are detected in deproteinated samples of tissue culture supernatant. For sample preparation, proteins are precipitated using zinc sulfate followed by filtration of the sample. The LC-MS/MS system used is the QTRAP 6500+ combined with two 1200 series Agilent pumps. The prepared samples are purified using an in-line C18-extraction column combined with a methanol/water solvent system as a mobile phase. After that, the sample is back-flushed to a reverse phase chromatography using a C18-column and gradient eluted using a methanol/water-based solvent buffered with ammonium formate as mobile phase. For detection, electrospray ionization in positive mode and data acquisition in MRM mode are used.

Aldosterone and corticosterone were measured using Aldosterone ELISA Kit (Cayman), and Corticosterone ELISA Kit (Cayman). Cortisol was detected using the human cortisol ELISA Kit (Cusabio). All ELISA assays were performed according to the manufacturer's instructions. The absorbance was read using EnSpire 2300 Multilabel Reader.

2.3.5. Aldosterone ELISA post-DCM extraction

Aldosterone ELISA was performed after extraction using Dichloromethane (DCM). DCM extraction was adapted from a published protocol (*153*). Briefly, 3 mL of DCM was gently mixed with 0.6 mL of cell culture supernatant. After letting the hydrophobic and hydrophilic phases separate for 30 min at RT, 1.5 mL of the hydrophobic fraction was dried down at 45˚C under a continuous stream of nitrogen in a Schlenk tube. The dried extracts were reconstituted in 350 µl of ELISA Buffer, and further steps of the ELISA followed the manufacturer's instructions.

2.3.6. Single-cell RNA sequencing

Single-cell RNA sequencing was performed on IM cells (day 5), day 10, and day 12 from one experiment. Cells were suspended in PBS-BSA 0.04% and processed according to the experimental workflow of Chromium Single Cell 3' v3.1 at the Single-Cell Technologies Unit (Scientific Genomics Platform, BIMSB, Berlin) by Michaela

Seeger (BIMSB). Briefly, cells were partitioned and barcoded using Chromium Automation (10X Genomics) before sequencing using a HiSeq4000 (Illumina).

2.4. Others

2.2.2. Statistical methods

Data were analyzed and visualized using GraphPad Prism (Version 9.2.0, GraphPad Software). Used statistical methods are stated in each figure legend. All values are depicted as mean ± SEM. Data are estimated to be statistically significant when $p < 0.05$. Significance levels are represented as follows: ns, $p > 0.05$; *, $p \leq 0.05$; **, $p \leq 0.01$; ***, $p \leq 0.001$; ****, $p \leq 0.0001$.

2.2.3. Bioinformatic analysis of scRNA-seq data

Sequencing libraries were processed using Cellranger multi (v3.1.0), and the GRCh38 genome annotation was extended with an extra chromosome containing the eGFP sequence and analyzed with Seurat v4.0.11 (doi: 10.1016/j.cell.2019.05.031). We filtered out cells with > 10% mitochondrial gene content and cells with fewer than 500 or more than 8000 genes. Batch effect between samples was removed using Seurat's IntegrateData workflow. Clustering and UMAP embedding were performed with 20 principal components. This scRNA-seq data was analyzed by Dr. Benedikt Obermayer-Wasserscheidt (Core Unit Bioinformatics, Berlin Institute of Health at Charité – Universitätsmedizin Berlin, 10117 Berlin, Germany).

3. Results

3.1. Establishment of an optimized differentiation protocol from human induced pluripotent stem cells towards adrenal cortex lineages

Optimizing the differentiation system from pluripotent stem cells to adrenocortical cells involved two steps: (1) inducing hiPSCs into intermediate mesoderm (IM) cells, the origin of the adrenal cortex; and (2) directing the IM cells towards adrenal cortex lineages. Differentiating pluripotent stem cells into IM has been systematically studied to derive renal lineages (*150, 151, 154, 155*), while protocols for other IM derivatives, including gonadal and adrenal cortex lineages are not well-established. Therefore, we set out to screen extrinsic factors and further optimize the differentiation method to obtain IM cells suitable for the efficient derivation of adrenocortical cells.

3.1.1. Differentiation of hiPSCs into intermediate mesoderm

The *in vitro* IM induction from hPSCs was developed in prior studies by mimicking early embryonic development **(Figure 9)**. These approaches commonly require a transitional differentiation step from PSCs into the mesodermal precursors of IM, which are either early bi-potent mesendoderm (ME) or late primitive streak. Bi-potent mesendoderm differentiation is achieved by activating Wnt/β-catenin, the essential signaling pathway in mesoderm specification during the gastrulation (*156, 157*). Chemical mesoderm induction using the small molecule GSK-3β inhibitor CHIR99021 (CHIR) is widely used to activate canonical Wnt signaling *in vitro* (*151*). Besides the Wnt signaling pathway, multiple pathways including Nodal and Bmp regulate the primitive streak formation (*158-160*). Based on this knowledge, Mae et al. (*150*) introduced Activin A to activate the TGF-β/Nodal/Activin pathway together with CHIR and obtain mesendoderm. At the same time, Morizane et al. (*154*) supplemented the medium with Noggin, an extracellular antagonist of BMP proteins, to promote primitive streak formation. However, in the second stage of these systems, the IM was generated using different culture conditions. This resulted in distinct sets of gene expression resembling the IM patterning in the anterior-posterior axis during development **(Figure 9)**. $PAX2^{+}LHX1^{+}$ IM cells are expressed in the anterior region (*7, 9*), while $WT1^{+}$ (Wilms tumor 1) cells are located in the posterior region (*8, 11, 154*). OSR1 (Odd-skipped related 1) is the earliest marker whose expression is not only restricted to the anterior-posterior IM axis but also extends laterally (*161, 162*). In

recent studies (*8, 11*), the specification of adrenal primordium and gonadal primordium are spatially and temporally different, even though they share the same precursor: the posterior IM. These findings in the specification of IM derivatives during the development provide a finer characterization of iPSC-derived IM generated from different protocols. Furthermore, the reproducibility of stem cell differentiation protocol relies on the differentiation potential of each stem cell line (*163*). Therefore, to evaluate the optimal differentiation condition to induce IM from our hiPSC line used in this study, we tested previously established 2-stage iPSC – IM differentiation protocols and examined the expression of IM markers.

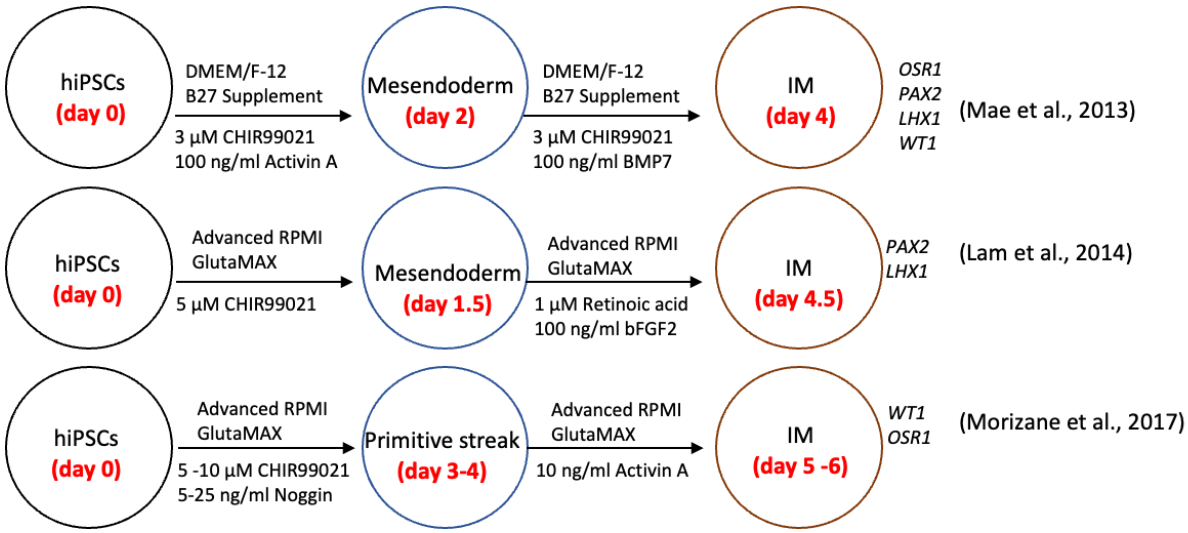

Figure 9. Experimental scheme for optimizing differentiation condition of Intermediate mesoderm (IM).

We adapted three established protocols of IM induction from iPSC/ESCs toward renal lineages (*128, 150, 151*)

IM cells generated in each protocol were collected for gene expression analysis using qPCR **(Figure 10**). All methods successfully downregulated the expression of pluripotency markers (*NANOG* and *OCT4*). On the contrary, the expression levels of IM markers *WT1* and *PAX2* were significantly upregulated under several conditions. The highest expression of *WT1* and *PAX* could be found in cells following Morizane's protocol (*128*) (treatment with 10 µM CHIR99021 combined with 5 ng/ml Noggin).

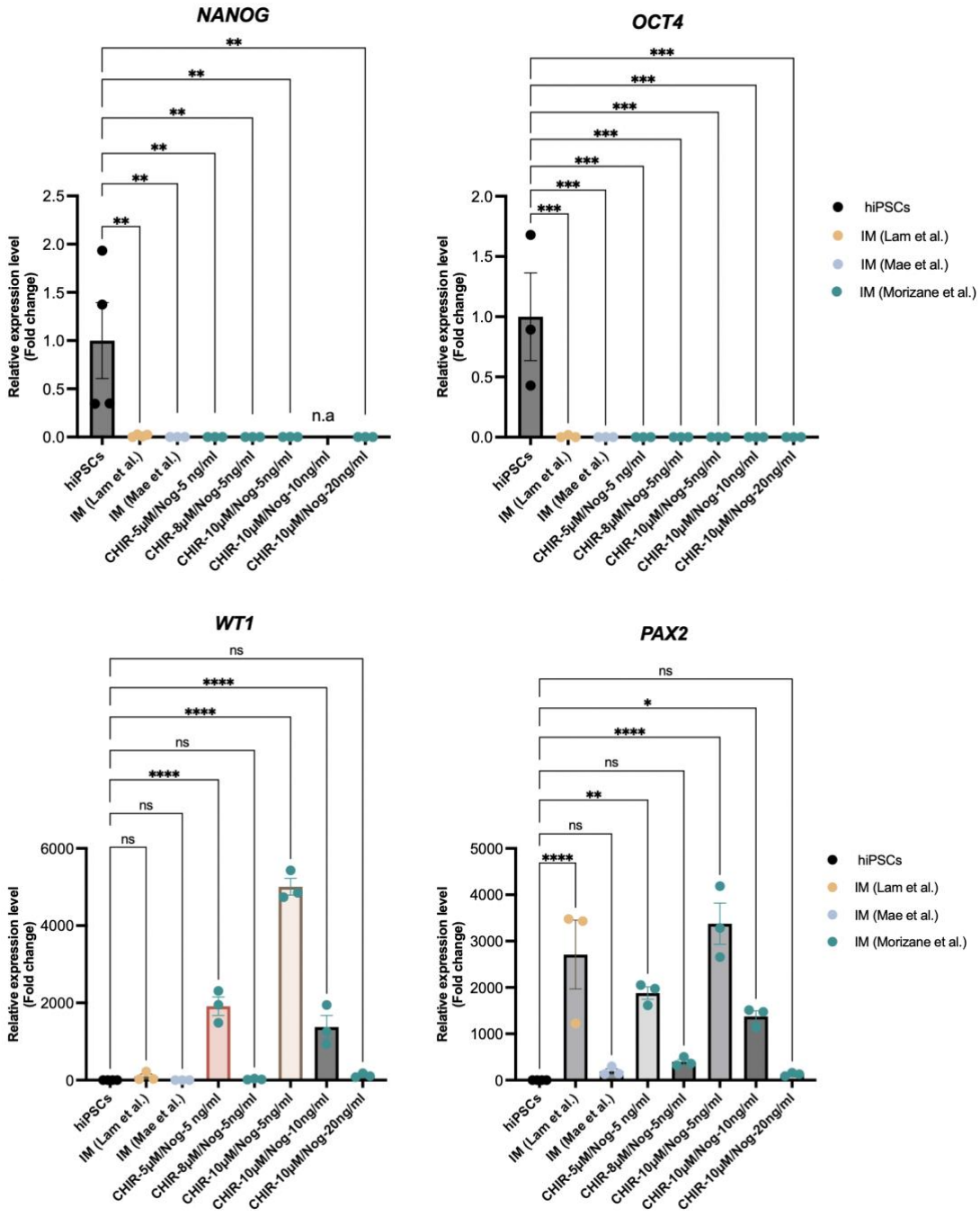

Figure 10: Screening the optimal iPSC – IM differentiation conditions.

qRT-PCR analyses of hiPSC markers (*NANOG*, *OCT4*) and IM markers (*WT1*, *PAX2*) mRNA expression in hiPSCs and IM cells following three protocols (n = 3). For statistical analysis, one-way ANOVA tests with Tukey's correction were used. *P < 0.05, **P < 0.01, ***P < 0.001, ****P < 0.0001.

Protein expression of IM and hiPSCs was examined by flow cytometric analysis. We compared the percentage of $OCT4^+$ cells in the IM cell population using the protocols from Mae et al. and Morizane et al. (in the Morizane group, we also compared the effectiveness of different concentrations of Noggin) **(Figure 11)**. Consistent with the

gene expression profile, the OCT4-expressing population was strongly reduced in all conditions. Treatment with 20 ng/ml Noggin showed lower effectiveness in differentiating iPSCs, and 20% of the cell population still expressed OCT4. Both protocols successfully induced the expression of OSR-1 in differentiated cells (**Figure 11**, lower panel). Among the tested conditions, the largest OSR-1+ population was found when using the Morizane protocol modified by using 10 µM CHIR and 5 ng/ml Noggin. With these results, the IM conversion process from hiPSC following Morizane's protocol had the highest differentiation efficiency, as shown in IM marker expression. The optimal condition for our in-house hiPSCs was a Morizane-based treatment, with 10 µM CHIR and 5 ng/ml Noggin in the first stage and 10 ng/ml of Activin A in the second stage. We applied this IM differentiation condition to all further experiments.

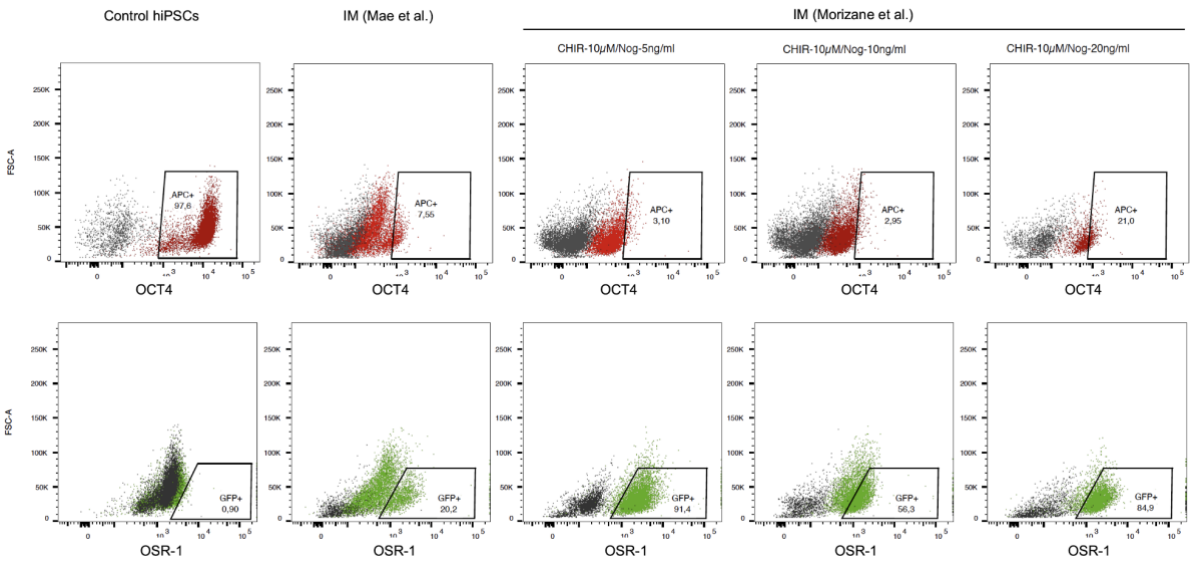

Figure 11: FACS analysis of pluripotency marker OCT4 and IM marker OSR-1.

IM cells were differentiated based on two protocols: Mae et al., 2013 and Morizane et al., 2017. The percentage of OCT4-APC$^+$ and OSR-1-GFP$^+$ cells were measured by FACS analysis. Gating was performed using negative controls. In OCT4 expression analysis, unstained samples were used as a control to set a positive gate for each cell line, depicted as gray. In OSR-1 expression analysis, a sample stained with secondary antibodies was used as a control to set the positive gate for each cell line, depicted as black. Untreated hiPSCs were as control.

Among IM-specific genes, WT1 is a crucial transcription factor determining the adrenogonadal primordium (AGP) cell fate in early urogenital development (*13, 14*). A lineage tracing study on mouse and human embryos discovered that posterior IM WT1$^+$ cells develop into WT1$^+$ coelomic epithelium (posterior IM derivative), which

gives rise to the AGP and directly regulates the expression of SF-1 to specify the adrenal and gonadal separation (*8*). Thus, we further performed immunostaining of WT1 and OCT4 on IM cells differentiated by the optimized protocol **(Figure 12)**. Immunofluorescent staining revealed more than 80% of cells as WT1+, while OCT4+ cells were almost undetectable. Altogether, by optimizing the IM differentiation system, we successfully differentiated our in-house hiPSCs cell line into an IM cell population containing posterior IM ($WT1^{+}OSR1^{+}$), which can further develop into adrenal cortex cells (*11*).

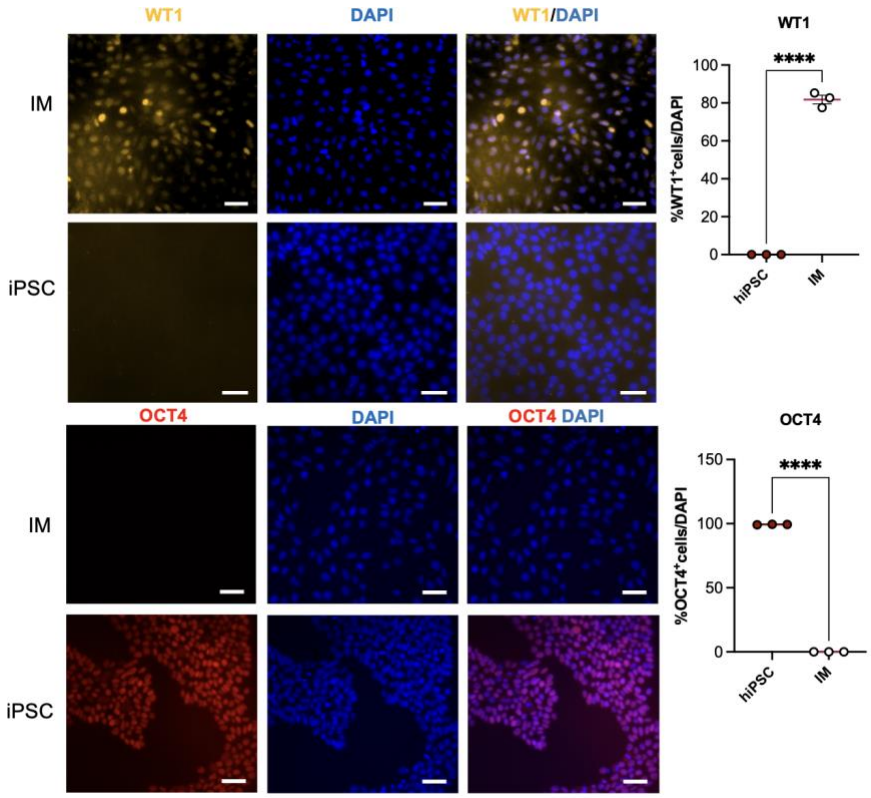

Figure 12: Expression of IM-specific and iPSCs-specific markers by immunofluorescence staining.

Immunofluorescence staining of WT1 and OCT4 in hiPSC and IM cells at day 5 following Morizane et al. protocol. Scale bar: 50 µm. The fraction of WT^{+} and $OCT4^{+}$ cells in total cell numbers are shown. Two-tailed unpaired Student's t-tests were used, ****P < 0.0001.

3.1.2. Adrenal cortex differentiation from IM

In the second step of differentiation, we aimed to optimize conditions for specific and efficient differentiation of IM towards the adrenocortical lineages.

To direct the cell fate conversion from IM to its derivative, the adrenal cortex, we forced expression of a key transcription factor in adrenal cortex development, steroidogenic

factor-1 (SF-1), encoded by the *NR5A1* gene. The ectopic *NR5A1* expression was introduced by an *NR5A1-EGFP* vector with a CMV promoter **(Figure 13A)**. We introduced the vector to IM cells on day 5 of the experimental scheme by lipid-based transfection. **Figure 13B** shows the morphology of the cells 48 h after transfection, with GFP as a reporter of SF-1 expression. The percentage of GFP^+ cells, determined by FACS, was >30% after 24 hours **(Figure 13C)**.

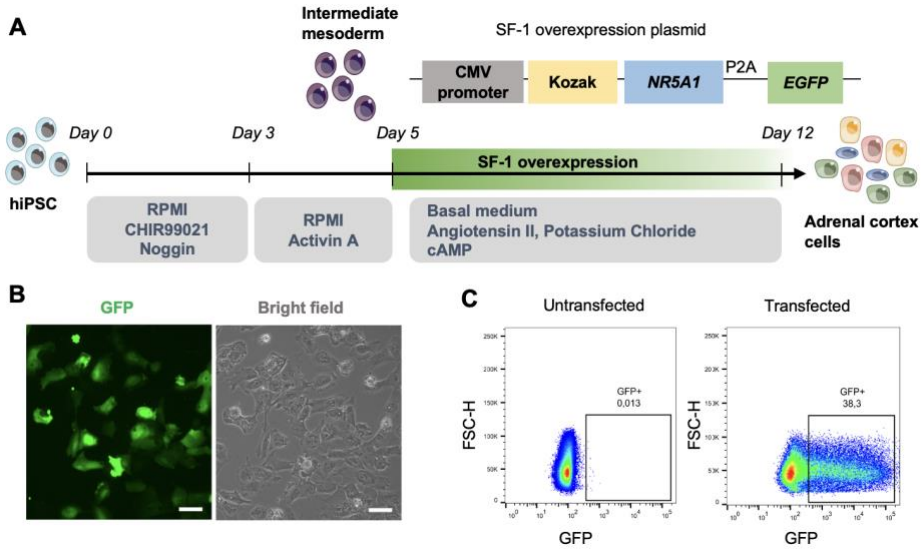

Figure 13: hiPSC-derived adrenocortical differentiation system.

(A) Schematic representation of the differentiation from hiPSCs into adrenocortical cells through intermediate mesoderm induction followed by SF-1 overexpression in a defined differentiation media. (B) Cell morphology and GFP expression 48 hours after transfection, a representative result of one experiment is shown. (C) Transfection efficiency of SF-1-GFP overexpression plasmid after 24 hours (n = 4). FCS-H: Forward Scatter Height. Scale bar: 50 µm

To establish optimal culture conditions for differentiating IM towards adrenocortical lineages, in addition to SF-1 overexpression, we screened niche factors that may regulate adrenal cortex development and adrenal steroidogenesis. In the zG of the adrenal cortex, aldosterone synthesis is mainly controlled by AngII (Angiotensin II) and potassium (*164*). In contrast, the cAMP/PKA pathway is the main regulator of zF proliferation and cortisol synthesis (*165*). The peptide hormone ACTH induces cAMP formation and is involved in steroidogenesis and cell differentiation of zF and zR cells in the adrenal cortex. Therefore, to stimulate the differentiation towards glomerulosa and fasiculata cells, we tested a culture system containing AngII and K^+ in combination with either ACTH or activators of cAMP/PKA signaling, which are Forskolin and 8-br-cAMP.

A human adrenocortical carcinoma cell line, H295R, was used to preliminarily assess the effects of different factors **(Figure 14)**. We monitored the expression of genes involved in hormone synthesis, *CYP11B2* (encoding aldosterone synthase) and *CYP11B1* (11 β-hydroxylase), to evaluate the efficacy of the factors. The gene products of *CYP11B2* and *CYP11B1* catalyze the final steps in the synthesis of aldosterone and cortisol. Untreated H295R cells were cultured in a starvation medium (containing low serum) and used as a control. As shown in **Figure 14**, *CYP11B2* expression was significantly up-regulated in the culture condition where both aldosterone stimulators, AngII and K^+, were added with 8-br-cAMP. Similarly, combining these factors also highly induced *CYP11B1*, besides the combination of AngII and Forskolin. Therefore, by testing adrenal cortex niche factors on the H295R cell line, we determined a condition in which AngII, K^+ and 8-br-cAMP were supplemented to stimulate the highest expression of both *CYP11B2* and *CYP11B1*. This culture condition was then applied in our hiPSC-derived adrenocortical differentiation system.

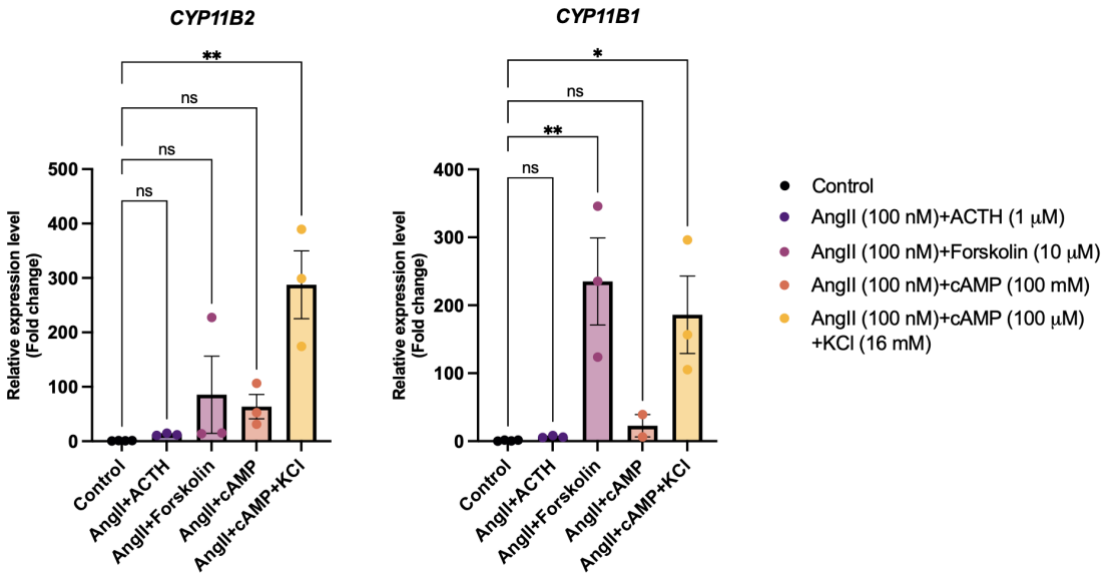

Figure 14: Screening adrenal cortex niche factors on H295R cell line.

qRT-PCR showing *CYP11B2* and *CYP11B1* mRNA expression in H295R cells. H295R cells cultured in starvation medium were used as controls (n = 3). Cells were cultured under the indicated conditions and were collected for RNA extraction after 48 hours. A one-way ANOVA analysis followed by Tukey's correction test was used. *P < 0.05, **P < 0.01.

The hiPSCs-derived IM generated as described in 3.1.1 were further differentiated into adrenocortical cells. After transfection with an *NR5A1-EGFP* overexpression vector

on day 5, IM cells were cultured for 7 days (day 12 on the experimental scheme) in a medium containing 8-br-cAMP, AngII, and KCl to direct the cell fate towards adrenocortical lineages **(Figure 13A)**. To characterize the hiPSC-derived differentiated cells, we first analyzed the gene expression pattern of the transfected cells. Compared to IM cells, the total expression of *NR5A1* was significantly increased in transfected cells **(Figure 15)**. By using a primer specific to the 5' UTR of *NR5A1* that is not contained in the expression plasmid, we also detected an elevated expression of endogenous *NR5A1*. Enzyme-encoding genes involved in steroidogenesis of the AC (*STAR*, *CYP17A1*, *CYP21A2*), as well as *CYP11B2* and *CYP11B1,* were significantly induced in transfected cells. Interestingly, we detected an expression of *NR0B1*, which encodes for DAX1 (nuclear receptor subfamily 0 group B member 1), a marker for progenitor cells located in the zG, in the transfected cells.

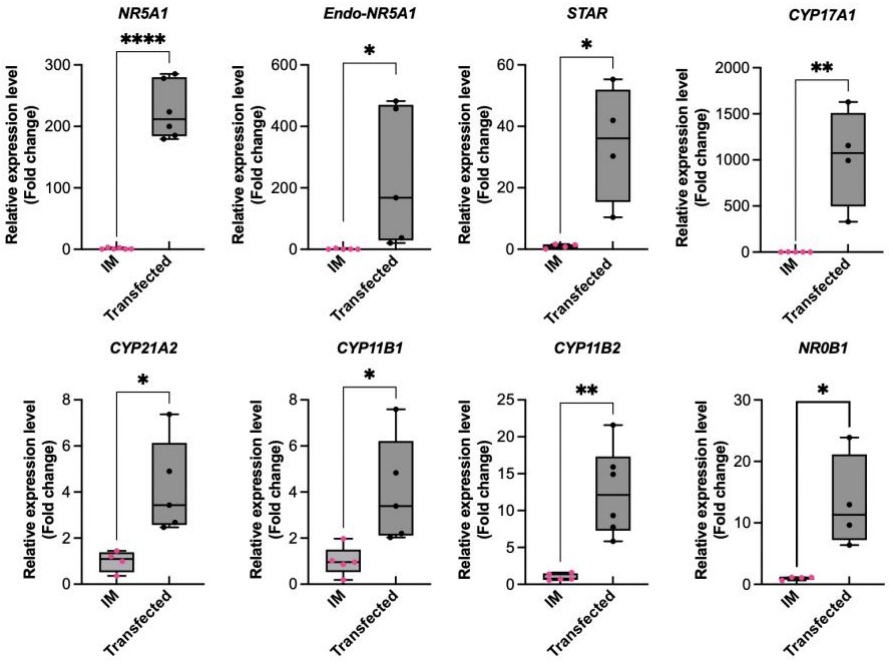

Figure 15: Gene expression profile of hiPSC-derived adrenocortical cells.
qRT-PCR showing transcription factor SF-1 (*NR5A1)* and steroidogenic enzymes (*STAR*, *CYP17A1*, *CYP21A2*, *CYP11B2*, and *CYP11B1*) mRNA expression in transfected cells. Briefly, IM cells (day 5) were transfected with an *NR5A1* construct. Transfected cells were cultured in differentiation medium supplemented with niche factors and harvested for qRT-PCR on day 12. Untransfected IM (on day 5) was used as a control ($n \geq 4$). Multiple two-tailed unpaired Student's t-tests were used. *P < 0.05, **P < 0.01, ***P < 0.001.

We further characterized the differentiated cells by immunofluorescence staining. Besides GFP^+ cells, we noted that GFP^- cells were also positive for SF-1, StAR, and

CYP11B2 **(Figure 16A)**. This could be explained by endogenous SF-1 expression (as shown in **Figure 15**), loss of plasmid expression with time, differentiation through paracrine effects of GFP^+ neighboring cells, or effects of factors added to the media. We also detected expression of other adrenal cortex markers, including DAX1 (a marker of progenitor zG cells), NESTIN (a marker of capsule stem cells), and CD56 (encoded by NCAM, a marker of mesenchymal-derived zG cells) **(Figure 16B)**.

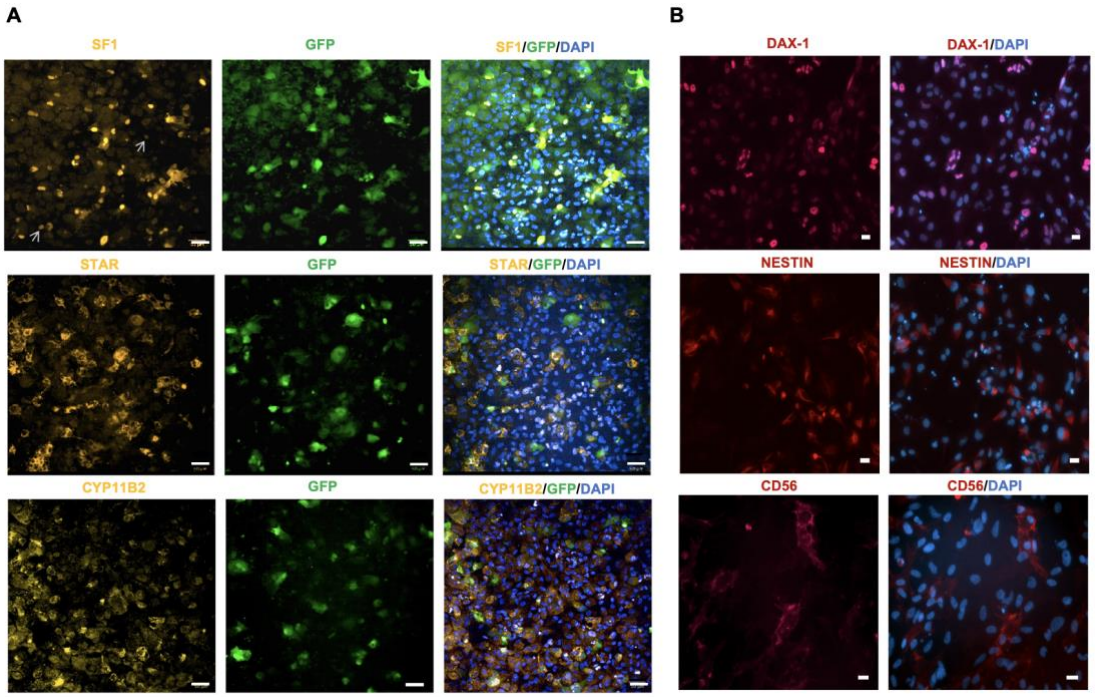

Figure 16: Protein expression of hiPSC-derived adrenocortical cells.
Immunofluorescence staining of (A) adrenal steroidogenesis-related proteins (SF-1, STAR, and CYP11B2) and (B) adrenal non-steroidogenesis proteins (DAX1, NESTIN, CD56) in transfected cells on day 12, one of three biological replicates is shown. Scale bar: 50 µm (A) and 25 µm (B). GFP^-/$SF\text{-}1^+$ are shown by the white arrows.

To study morphological changes at the ultrastructural level, we performed electron microscopy and found elongated mitochondria of lamellar shape with regular cristae in transfected cells, whereas round-shaped mitochondria with irregular cristae were present in iPSCs **(Figure 17)**.

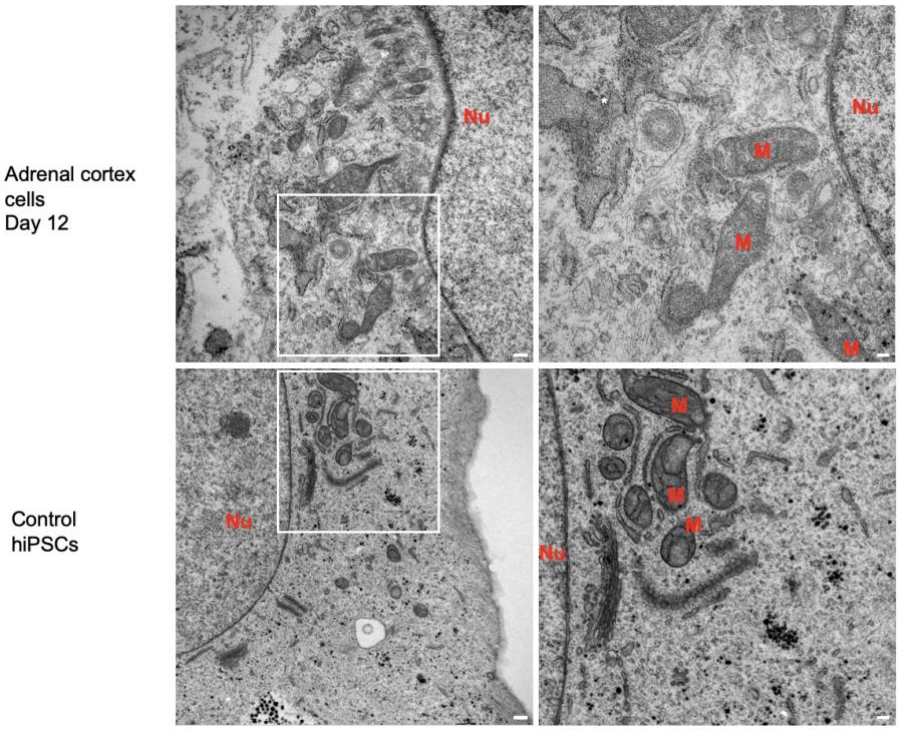

Figure 17: Morphology of hiPSC-derived adrenocortical cells at the ultrastructural level.
Transmission electron microscopy of transfected cells on day 12 and iPSCs, one of three biological replicates is shown. The right panels are magnified sections indicated in white squares. M, mitochondria; Nu, nucleus. Scale bars: 250 nm (left panels) and 200 nm (right panels).

To assess the function of differentiated cells, we quantified the production of steroids in cell culture supernatants, using steroid profiling **(Figure 18B)** and ELISA **(Figure 18C)** based on adrenal steroidogenesis as a reference **(Figure 18A)**. Transfected cells showed significantly elevated production of adrenal steroids, including progesterone, deoxycorticosterone, 17OH-progesterone, 11-deoxycortisol, testosterone and cortisol. Importantly, aldosterone was significantly produced by transfected cells, as detected by ELISA. Aldosterone was surprisingly not detected in the steroid profiling; this will be further investigated in 3.3.

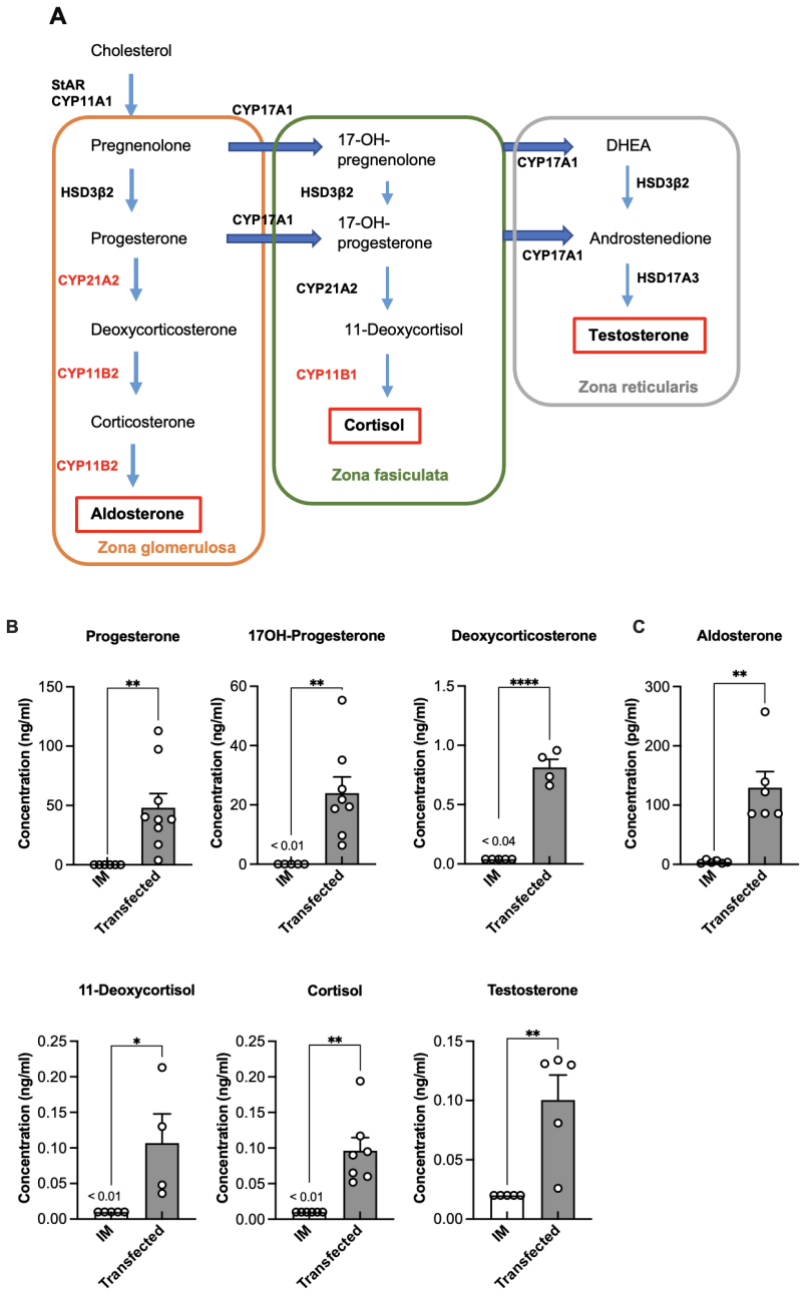

Figure 18: Hormone production of hiPSC-derived adrenocortical cells.

(A) Steroidogenesis in the human adrenal cortex. (B) Steroid profiling by LC-MS/MS shows adrenal steroid secretion of cells (day 12), compared to IM cells (day 5) ($n \geq 4$). (C) ELISA shows aldosterone production of adrenal cortex cells compared to IM cells ($n \geq 4$). The hiPSC-derived adrenocortical cells were cultured in medium supplemented with KCl (12 mM), AngII (100nM) and 8-br-cAMP (100 µM). Multiple two-tailed unpaired Student's t-tests were used. *P < 0.05, **P < 0.01, ***P < 0.001, ****P < 0.0001.

To examine whether our iPSC-induced adrenal cortex cells respond to physiologic stimuli of aldosterone production, we treated the cells with increasing levels of AngII, from a physiologic concentration (30 pM) to a high concentration of 100 nM (**Figure**

19, left panel). Similarly, a range of KCl concentrations starting from physiologic concentration (3.5 mM) to high concentration (12 mM) was added into the culture system to stimulate aldosterone synthesis (**Figure 19**, right panel). Both stimuli significantly and dose-dependently increased aldosterone production. Collectively, by forced expression of SF-1 and providing niche factors of the adrenal cortex, IM cells were differentiated into steroid-producing cells with a gene expression pattern characteristic of adrenocortical lineages. These cells respond to key physiologic stimuli with increased production of aldosterone.

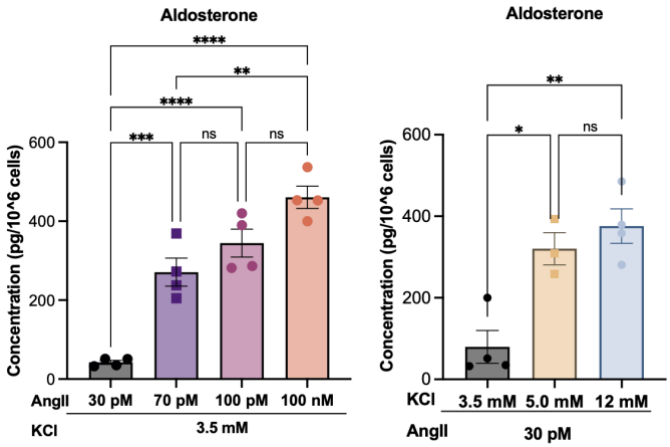

Figure 19: iPSC-induced adrenal cortex cells respond to physiologic stimuli of aldosterone production.

ELISA shows aldosterone secretion of adrenocortical cells on day 12 in response to AngII (left) and KCl (right) compared to IM (n = 3). One-way ANOVA tests with Tukey's correction were used. *P < 0.05, **P < 0.01, ***P < 0.001.

3.1.3. Single-cell RNA sequencing analyses of hiPSC-derived adrenal cortex lineages

To unveil the transcriptomic signature of our differentiated cells, we performed single-cell RNA sequencing (scRNA-seq) of IM cells and of cells at day 10 of adrenocortical differentiation (5 days after SF-1 transfection) **(Figure 20)**. Additionally, using our *in vitro* differentiation system, we also examined how activation of Wnt signaling affects adrenal cortex differentiation. Prior studies have shown that activation of Wnt inhibits adrenal steroidogenesis (*166*). Indeed, qPCR analysis showed a significant decrease in *STAR* expression when CHIR99021 (CHIR), a canonical Wnt signaling activator, was added for 2 days **(Figure 20B)**. This prompted us to include a 48-hour CHIR

treatment in our scRNA-seq experiment to investigate the gene expression profile of Wnt-activated adrenocortical cells **(Figure 20A)**.

The transcriptomic profiles of 9000 cells that passed quality-control criteria were analyzed. Unsupervised graph-based clustering defined 14 clusters of the pooled dataset **(Figure 20C)**. These clusters were annotated based on unique transcript expressions found in existing RNA-seq data and the literature **(Table 6)**. Cluster 9 expresses genes representing adrenocortical fate (*STAR*, *CYP11A1,* and *HSD3B2*), indicating adult adrenocortical cells **(Figure 20D)**. Cluster 8 cells were defined as fetal-like adrenal cortex cells **(Table 6)**, which also highly expressed *RSPO3,* an activator of the canonical WNT pathway and a marker of adrenal stem cells (*30*). *NR0B1*, a marker of adrenal cortex progenitor cells, was abundantly expressed in cluster 8 and 9, suggesting that cluster 8 and 9 is a mixed population of adrenal progenitor cells and differentiated cells. Expression of *DLK1*, a recently described adrenal cortex marker (*167*), was elevated in IM-derived differentiated cells (day 10 and day 12, **Figure 20E**) indicating IM commitment to adrenal cortex lineage. The mesoderm fate indicator, *TMEM88*, was strongly expressed in IM clusters and lower in more differentiated cells.

To understand the short-term effect of Wnt signaling in our differentiation system, we compared transcriptional profiles of day 10 and day 12 **(Figure 20E).** Steroidogenic markers (*STAR*, *CYP11A1*) were down-regulated, while transcription factors representing fibroblast-like/smooth-muscle cells (*NR2F2*, *PITX1*) (*4*) (*168*) were upregulated in day 12 cells. This could indicate a spontaneous cell fate conversion of day 10 differentiated cells upon CHIR treatment. In addition, Wnt/β-catenin-induced cells expressed high levels of canonical Wnt modulators (*DKK2*, *TRIB3)* (*169, 170*), confirming the activation of the canonical Wnt pathway. Taken together, the scRNA-seq analysis described transcriptional profiles of our adrenal cortex lineages derived from specifically committed mesoderm precursors. Moreover, extrinsic interference by activation of Wnt signaling in the iPSC-derived differentiated cells caused changes in their transcriptome profiles.

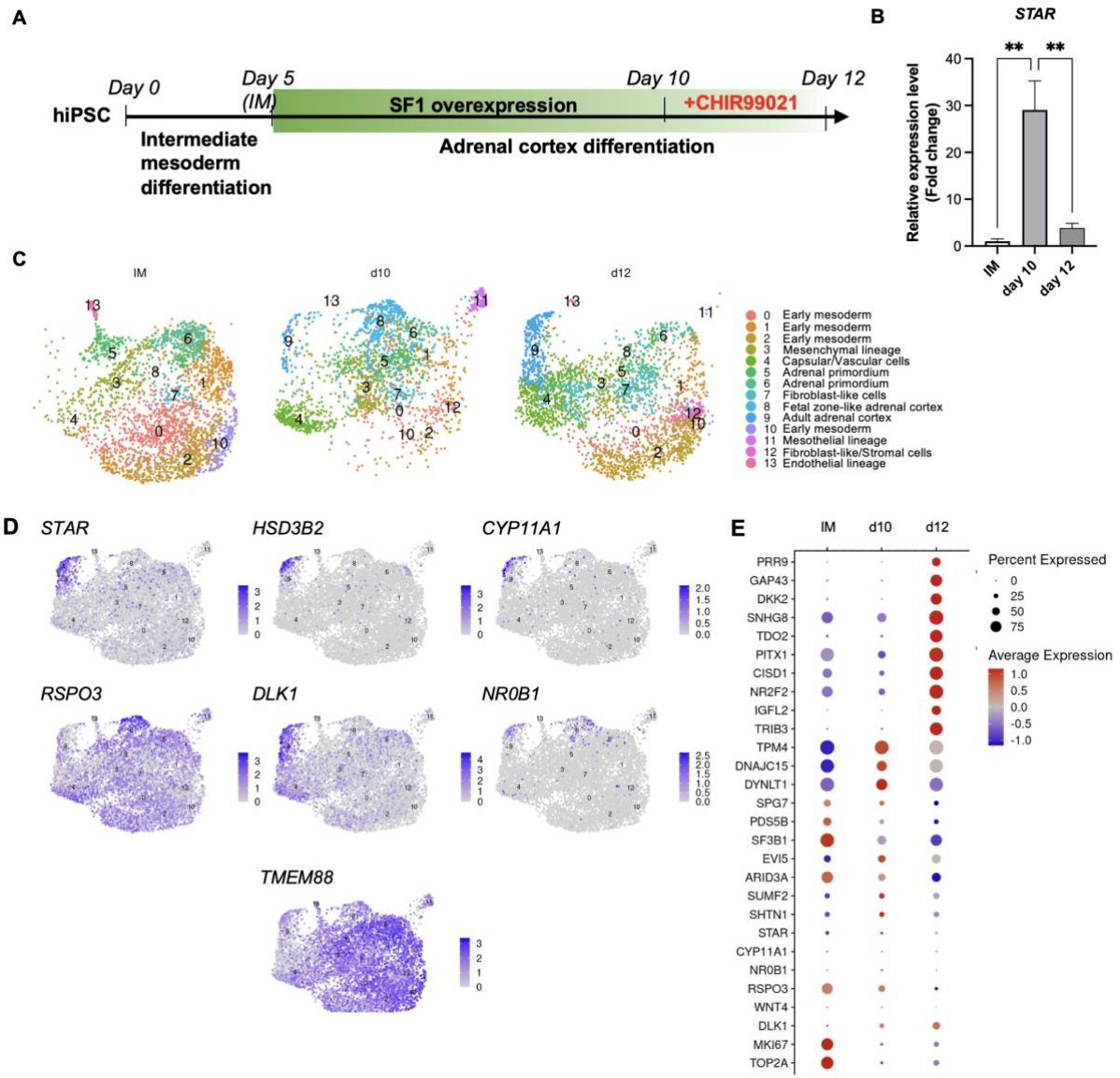

Figure 20: Single-cell RNA sequencing analyses of hiPSC-derived adrenal cortex lineages.
(A) Schematic setting for sample harvesting, including IM (day 5), cells before CHIR addition (day 10), and after CHIR addition (day 12). (B) qRT-PCR for *STAR* on day 10 and day 12 of differentiation, according to A. One-way ANOVA with Tukey's correction was used (n = 3). (C) UMAP visualization of 14 clusters in the adrenal cortex differentiation system (n = 1). Clusters were annotated based on the expression of conserved markers. (D) Expression of adrenocortical lineage (*STAR*, *HSD3B2*, *CYP11A1*), adrenal stem/progenitor cell (*RSPO3*, *DLK1*, *NR0B1*), and mesoderm (*TMEM88*) marker genes. (E) Dot plot depicting the top 10 differentially expressed genes in IM, day 10, and day 12 cells.

Table 6: Literature curated cell type marker genes used for cell type annotation.

Cell type	Gene	Reference
Adult adrenal cortex (C9)	*STAR*, *CYP11A1*, *APOA1*, *FDXR*, *GSTA1*, MT2A	**(*8*)**

Cell type	Gene	Reference
Fetal zone-like adrenal cortex (C8)	*APOA1*, *APOPE, APOC1*, *MT2A*, *S100A6*	(***8***)
Adrenal primordium (C5, C6)	*KRT8, KRT18, KRT19, ID3, MDK, APOA1, CYB5A, APOE*	(***8***)
Mesenchymal lineage (C3)	*LUM, DCN, MME, SPARC, ITGA6*	(***171***)
Capsular/Vascular cells (C4)	*MGP, IGFBP3, COL1A1, COL1A2, DCN*	(***8***) (***172***)
Mesothelial lineage (C11)	*PTN, SPP1, KRT7, KRT19, EPCAM*	(***173***)
Early mesoderm (C0, C1, C2, C10)	*TOP2A, CENPF, CENPW, MEIS1, TMEM88, PRRX, DKK1*	(***174***)
Fibroblast-like/Stromal (C7, C12)	*ACTG2, THY1, NR2F2, TAGLN, ANXA1*	(***175***) (***176***)
Endothelial lineage (C13)	*SOX17, SOX18, SOX7, PECAM1*	(***177***)

C: cluster, referred to clusters shown in **Figure 20C.**

3.2. Heterozygous *KCNJ5*^{G151R} hiPSC-derived adrenal cortex cells exhibit phenotypes of primary aldosteronism

3.2.1. CRISPR/Cas9 mediated *KCNJ5* modifications in hiPSCs

To demonstrate the suitability of our system as a disease model, we used CRISPR/Cas9 to generate hiPSCs carrying a heterozygous PA-associated *KCNJ5*$^{G151R/+}$ mutation **(Figure 21)**. The point mutation G151R is located on exon 2 of the *KCNJ5* gene and affects the channel's selectivity filter. We designed three sgRNAs close to the mutation and two donor single-strand oligonucleotides containing 50 nucleotide homology arms **(Figure 21A)**, which are ssODN-G151R and ssODN-WT. The strategy of introducing one donor template containing the mutation and one containing the wildtype sequence is to enhance the efficiency of heterozygous homology repair (*178*). To facilitate the screening of the edited clones, we introduced a DdeI restriction site by inserting a silent mutation in the ssODN-G151R. The cleavage efficiency of sgRNAs was evaluated by T7E1 assay **(Figure 21B)**, in which individual sgRNA-Cas9 plasmids were transfected without ssODNs into hiPSCs cells. Among three sgRNAs, sg3 gave the highest percentage of indel formation (74%), thus,

we transfected hiPSCs with sg3-Cas9-GFP plasmid combined with donor ssODNs to proceed with the knock-in experiment.

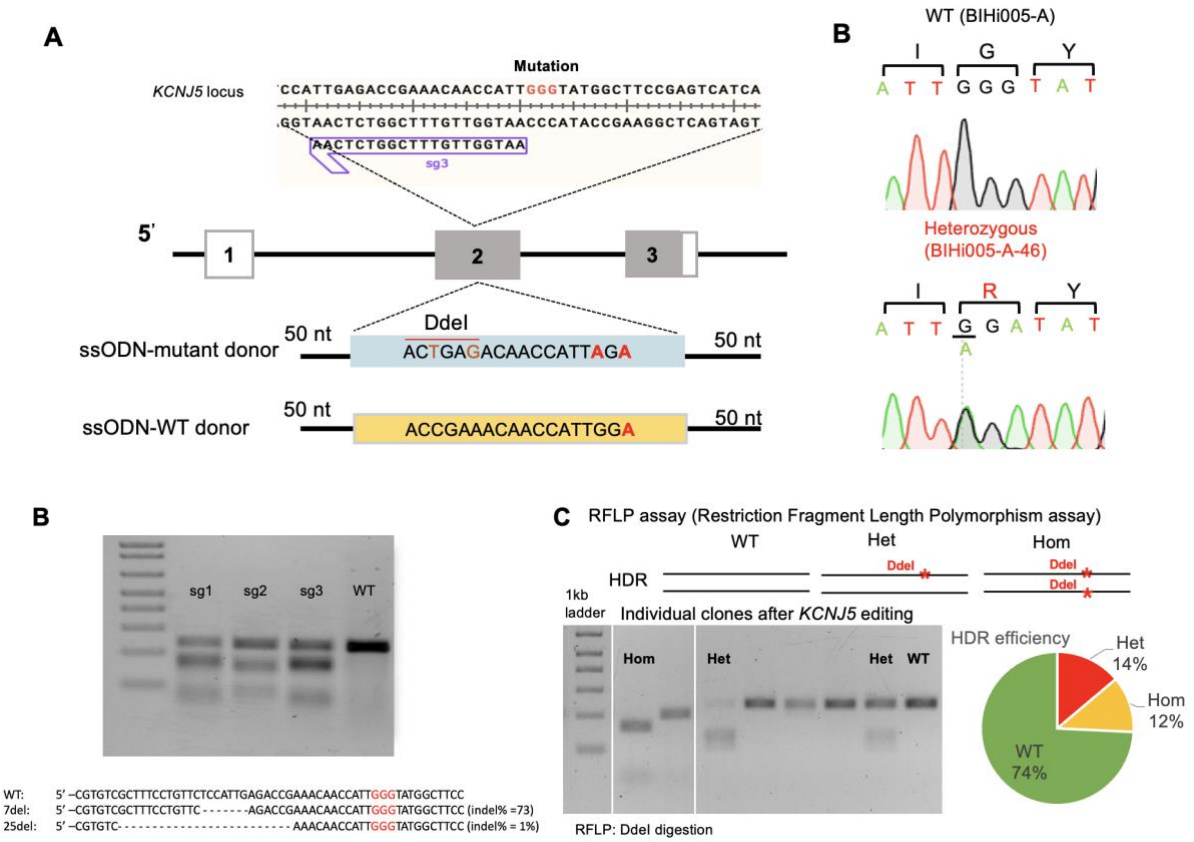

Figure 21: CRISPR/Cas9 mediated *KCNJ5* modifications in hiPSCs.

(A) Schematic representation of targeting strategy to insert point mutation G151R in exon 2 of the human *KCNJ5* locus by CRISPR/Cas9. (B) T7E1 assay shows the cleavage efficiencies of three sgRNAs (above) at the targeted KCNJ5 sequence. Below, sequencing data showed indels and indel efficiencies mediated by sg3 computationally calculated by ICE CRIPSR Tool (Synthego). (C) DdeI-mediated restriction fragment length polymorphism (RFLP) assay showed HDR efficiency of heterozygous and homozygous mutant clones. A processed image of one intact gel is shown, see **Supplementary Figure 1A** for unprocessed image (D) Genotyping of WT and *KCNJ5*$^{G151R/+}$ by Sanger sequencing.

After three weeks of clonal expansion, the total genomic DNA of each clone was extracted, and the targeted region was amplified by PCR. To access HDR efficiency, a DdeI-based RFLP assay was performed, and cleaved fragments were visualized on an agarose gel **(Figure 21C)**. Heterozygous and homozygous mutant clones were determined by the monoallelic and biallelic integration of the DdeI restriction site, respectively. The total HDR efficiency was 26%, including 14% heterozygous mutant clones and 12% homozygous mutant clones **(Figure 21C)**. The genotype of the heterozygous *KCNJ5*$^{G151R/+}$ hiPSC clones was confirmed by Sanger sequencing

(Figure 21D). Characterization of heterozygous iPSC line generated and banked included: Karyotyping (G-banding **(Supplementary Figure 1 B)** and SNP array)) and assessment of undifferentiated state markers, morphology, and viability. None of the tests showed any abnormalities.

3.2.2. Differentiation of *KCNJ5*$^{G151R/+}$ hiPSC towards the adrenocortical lineage

We differentiated *KCNJ5*$^{G151R/+}$ hiPSCs towards the adrenocortical lineage following our established method (See 3.1). We compared the gene and protein expression patterns of the mutant *KCNJ5*$^{G151R/+}$ hiPSCs-derived adrenal cortical cells with those from the same hiPSCs that were only differentiated to IM cells **(Figure 22)**. The *KCNJ5*$^{G151R/+}$ hiPSC-derived differentiated cells clearly showed higher expression of adrenal cortex-specific markers compared to IM at the transcriptional **(Figure 22A)** as well as the translational level **(Figure 22B)**.

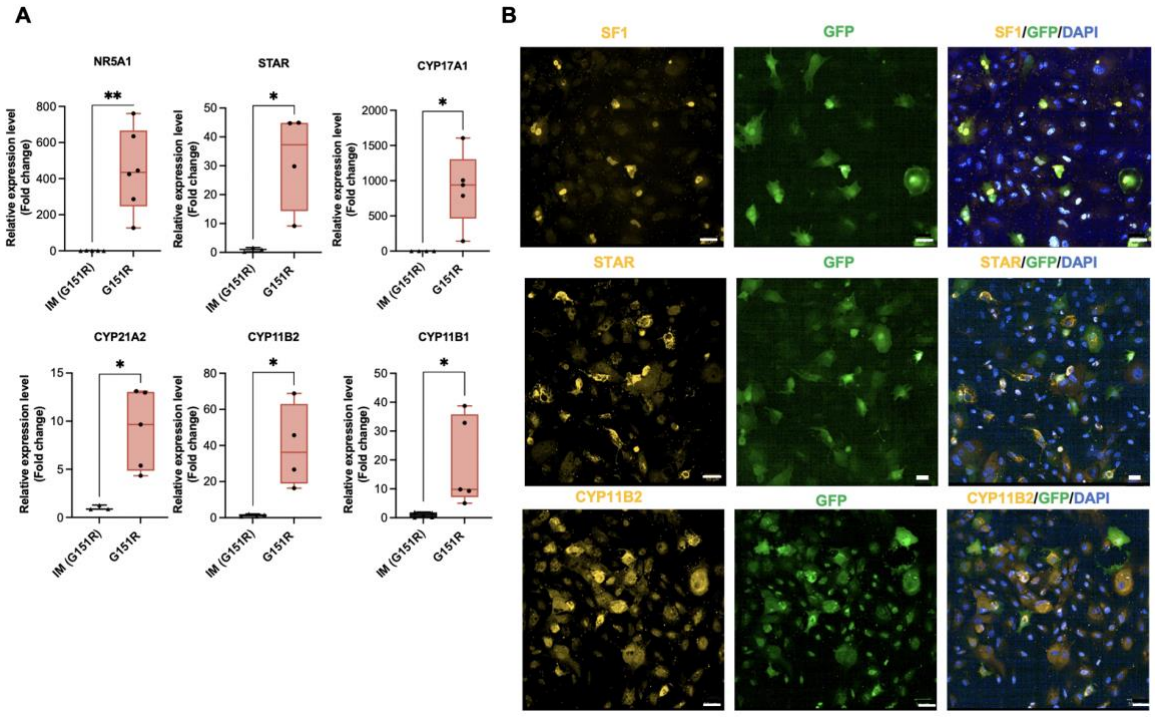

Figure 22: Characterization of the *KCNJ5*$^{G151R/+}$ iPSC-derived adrenocortical cells.
(A) qRT-PCR analyses presenting mRNA expression of *NR5A1* and steroidogenic enzymes (*STAR*, *CYP17A1*, *CYP21A2*, *CYP11B1*, and *CYP11B2*) in G151R mutated SF-1 transfected cells on day 12 (according to the procedure in **Figure 5A**). IM on day 5 was used as a control (n = 6). (B) Immunofluorescence staining of SF-1, StAR, and CYP11B2 in G151R mutated SF-1 transfected cells after 7 days of differentiation, one of at least three biological replicates is shown. Scale bar: 50 µm. Two-tailed unpaired Student's t-tests were used. *P < 0.05, **P < 0.01, ****P < 0.0001.

We next compared the hormonal profile of the *KCNJ5*$^{G151R/+}$ iPSC-derived adrenocortical cells to IM cells by LC-MS/MS **(Figure 23A)** and ELISA **(Figure 23B)**. Adrenal steroids, which are produced by adrenal cortex lineages, were detected at high levels in the mutant adrenocortical cells. Average cortisol production showed a non-significant trend to be higher in mutant cells. Additionally, incubation of mutant cells with Roxithromycin, a macrolide antibiotic (*94*), significantly inhibited aldosterone secretion compared to untreated cells. **(Figure 23C)**.

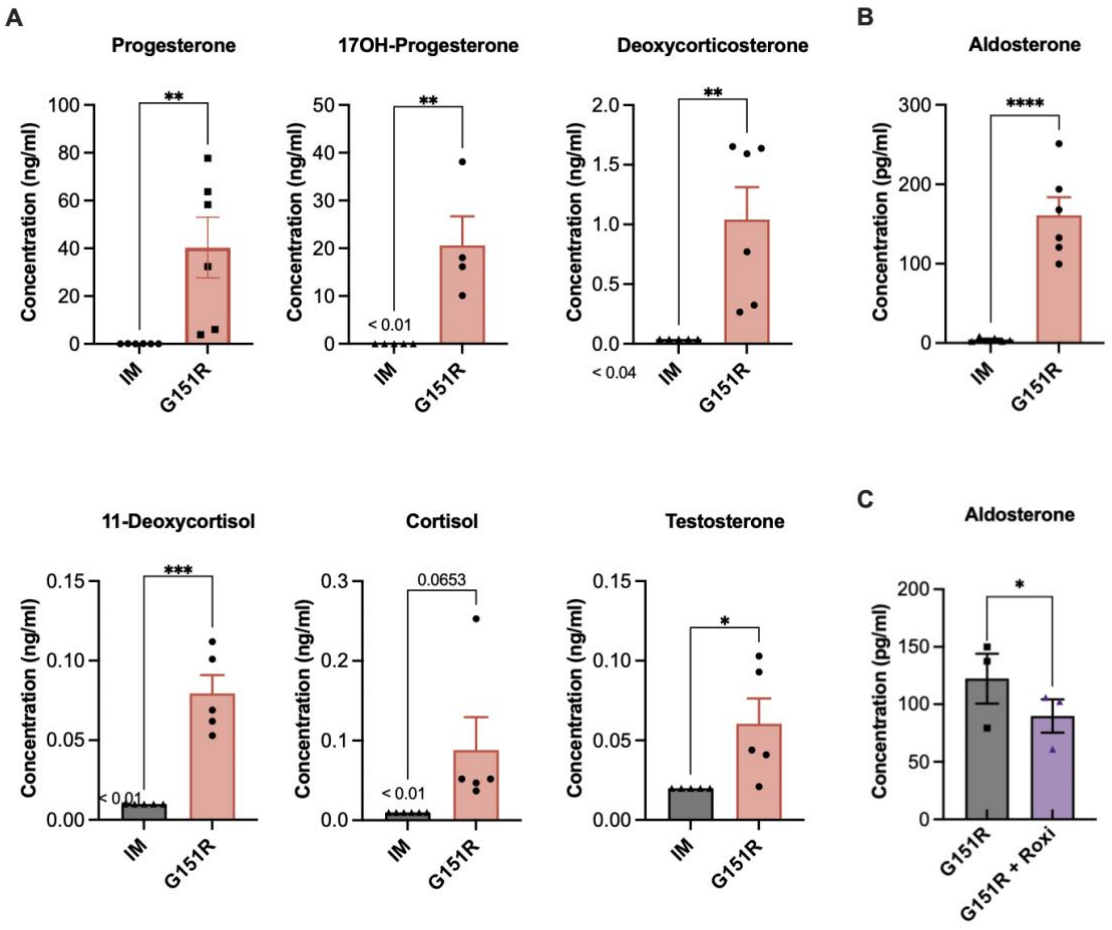

Figure 23: Hormone production of *KCNJ5*$^{G151R/+}$ iPSC-derived adrenocortical cells.
(A) Steroid profiling by LC-MS/MS shows adrenal steroid secretion in the cultivation media of *KCNJ5*$^{G151R/+}$ adrenal cortex cells on day 12, compared to IM cells (n ≥ 4). (B) ELISA showed aldosterone production in the cultivation media of *KCNJ5*$^{G151R/+}$ adrenal cortex cells on day 12, compared to IM cells (n = 6) (C) Inhibition of *KCNJ5*$^{G151R/+}$-induced aldosterone production by Roxithromycin (Roxi) treatment for 2 days compared to untreated *KCNJ5*$^{G151R/+}$ cells (n = 3). Multiple two-tailed unpaired Student's t-tests (Figure A, B) or two-tailed paired Student's t-test (Figure C) were used. *P < 0.05, **P < 0.01, ***P < 0.001, ****P < 0.0001.

3.2.3. Characterization of heterozygous *KCNJ5*^{G151R} hiPSC-derived adrenal cortex cells

To assess whether the G151R-mutated iPSC-induced adrenocortical cells show features of PA, we compared them to wild-type (WT) iPSC-induced adrenocortical cells. Steroid profiling showed no significant differences in the amount of progesterone, 17-OH-progesterone, deoxycorticosterone, 11-deoxycortisol, cortisol, and testosterone between WT and the G151R adrenal cortex cells **(Figure 24A)**. Interestingly, the amounts of aldosterone produced by mutant cells were significantly elevated **(Figure 24B)**. Real-time PCR analyses revealed notably increased expression of *CYP11B2* in the mutant cells, while other genes encoding steroidogenic enzymes were not strongly affected **(Figure 24C)**. These data suggest that our system can adequately model the primary symptom of PA, which is elevated aldosterone production, associated with *KCNJ5* mutations.

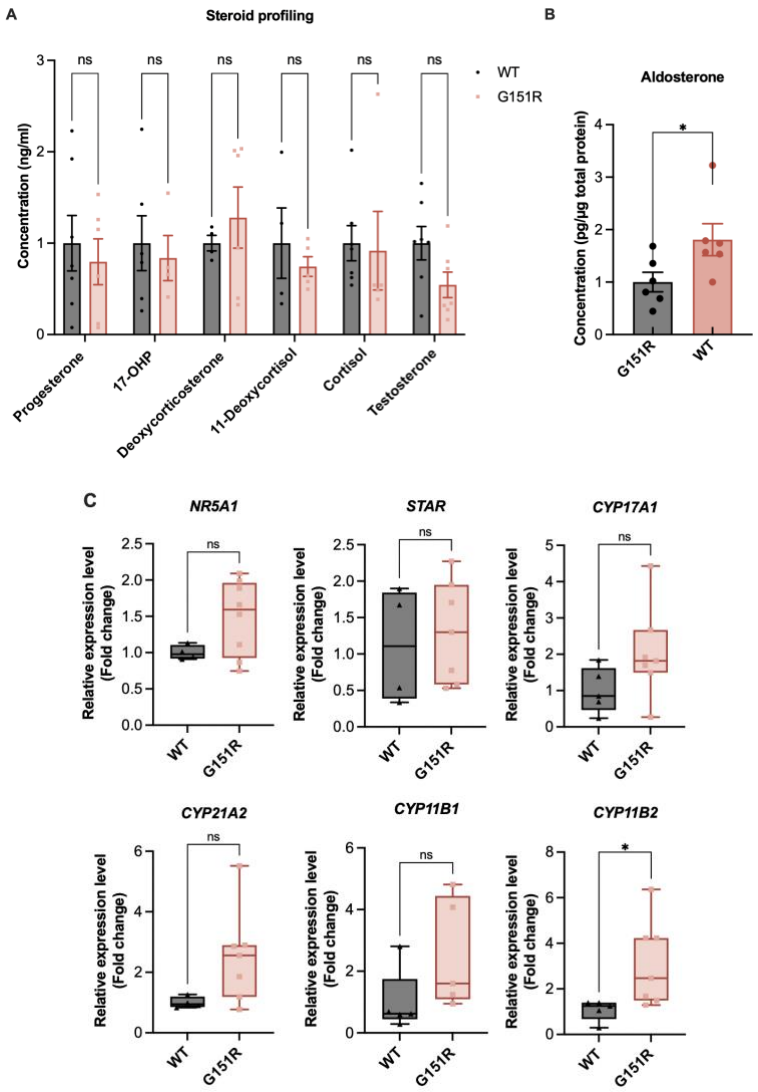

Figure 24: Elevated aldosterone production of *KCNJ5$^{G151R/+}$* adrenocortical cells.

(A) Steroid profiling analyses in media of the KCNJ5$^{G151R/+}$ adrenal cortex cells on day 12, compared to WT cells (n ≥ 4). (B) ELISA shows aldosterone production in the media of *KCNJ5$^{G151R/+}$ adrenal cortex* cells on day 12, compared to WT cells (n = 6). (C) qRT-PCR analyses of *NR5A1* and steroidogenic enzymes (*STAR*, *CYP17A1*, *CYP21A2, CYP11B1, CYP11B2)* mRNA expression of *KCNJ5$^{G151R/+}$* adrenal cortex cells on day 12, compared to WT adrenal cortex cells (n ≥ 4). Multiple two-tailed Student's t-tests were used. *P < 0.05, ns, not significant.

Next, we investigated the proliferation rate of *KCNJ5$^{G151R/+}$* adrenocortical cells using a luminescent cell viability assay **(Figure 25A)**. The luminescence, which is proportional to the cell number, was considerably higher in *KCNJ5$^{G151R/+}$* cells than in WT cells (from day 1 on), suggesting a higher proliferation rate. Proliferation in *KCNJ5$^{G151R/+}$* cells also exceeded that of the H295R adrenocortical cancer cell line **(Figure 25B)**. We also compared proliferation and apoptosis between *KCNJ5$^{G151R/+}$* and WT by quantitating Annexin V (apoptosis marker) and Ki67 (proliferation marker)-positive cells using flow cytometry **(Figure 25C)**. Annexin V positivity was indistinguishable between WT and *KCNJ5$^{G151R/+}$;* however, the Ki67^{+} percentage was markedly higher in *KCNJ5$^{G151R/+}$*, indicating stronger proliferation activity than in WT cells.

Increased proliferation is one of the features associated with *KCNJ5* mutation but could not be observed in any of the previously established model systems. We now show for the first time that our iPSC-derived model also resembles this feature. Taken together, by using genetic modification and lineage-directed differentiation of hiPSC, we successfully generated an adrenocortical cell model representing *KCNJ5*-mutated PA, demonstrated by increased hormone production and proliferation.

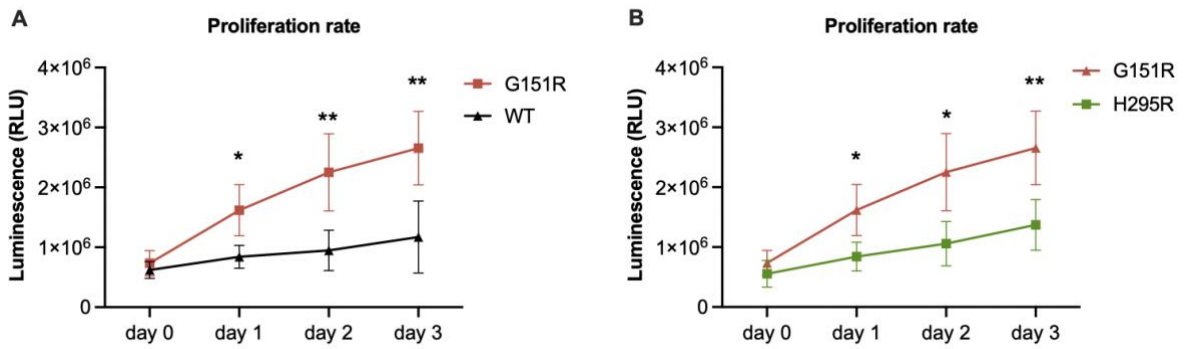

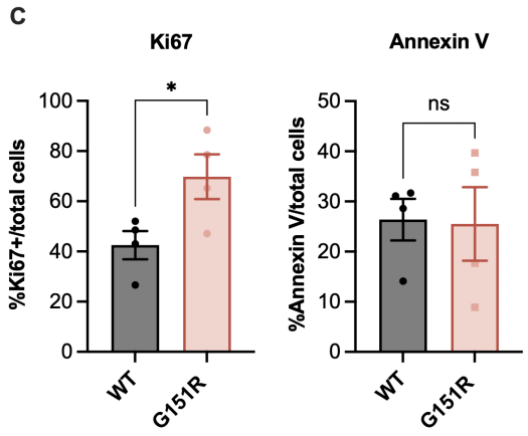

Figure 25: *KCNJ5*$^{G151R/+}$ adrenal cortex cells show high cellular proliferation

(A) Cell viability assay showing luminescence (as a readout of cell number) of *KCNJ5*$^{G151R/+}$ at day 0, day 1, day 2, and day 3 compared with WT cells (n = 6). (B) Cell viability assay showing luminescence (as a readout of cell number) of *KCNJ5*$^{G151R/+}$ at 0h, 24h, 48h, and 72h compared with H295R (n = 6). (C) Flow cytometry analysis of Ki67^{+} (left) and Annexin V+ (right) of WT and *KCNJ5*$^{G151R/+}$ cells (n = 4). In A-B, a two-way ANOVA analysis followed by Tukey's correction tests was used. In C, two-tailed Student's t-tests were used. *P < 0.05, **P < 0.01, ns, not significant.

3.3. Quantitation of aldosterone in cell culture supernatant

In this study, measuring aldosterone secretion in cell culture supernatant is essential to characterize the function of hiPSC-derived adrenocortical lineage cells. Serum and plasma aldosterone is commonly measured either by immunoassay (IA) or LC-MS/MS in clinical laboratories (*179*). Although IAs for hormone quantification are technical easier and less time- and cost-consuming, their disadvantages include lower analytical sensitivity and specificity, exogenous and endogenous interferences such as pre-analytical factors, cross-reacting substances, and endogenous interfering antibodies. In contrast, LC-MS/MS has the advantage of higher analytical performance and fewer interferences caused by the unspecific binding of antibody/immunoglobulin (*180, 181*). On the other hand, the quantitation of adrenal steroids, especially aldosterone secreted from *in vitro* cell culture, has not yet been systematically reviewed. To measure the aldosterone-producing capacity of our hiPSC-derived cells in our study, we used the ELISA method as previously described in other similar studies (*131-133, 135, 141*) **(Figure 18C, Figure 23B, and Figure 24B)**. Measurements of aldosterone levels by LC-MS/MS were further performed to strengthen our data, however, aldosterone could not be detected in cell culture supernatants of hiPSC-derived adrenocortical cells (data not shown). We noted that in other reference studies,

aldosterone measurements by LC-MS/MS were not reported either (*131-133, 135, 141*). This may indicate a technical difficulty that requires further investigation.

One of the possible explanations for the positive ELISA results is the cross-reactivity of aldosterone metabolites, which could be recognized by ELISA antibodies. A prior study by Lam et al. (*153*) showed that aldosterone in patients' plasma with renal impairment was overestimated by a common automated chemiluminescent IA, which could be eliminated by solvent extraction. The aldosterone levels were significantly reduced when post-extracted samples were measured, which could be explained by the presence of aldosterone glucuronide, an inactive hydrophilic aldosterone derivative metabolized by hepatic and kidney cells (*182*). Although glucuronidation of aldosterone only exists in the liver and kidney metabolism (*183*), we cannot exclude the possibility of contamination of other aldosterone metabolites in our differentiation system, which may be potentially synthesized in our differentiated cells. Therefore, we performed an aldosterone extraction using an organic solvent, dichloromethane (DCM), to eliminate potential hydrophilic interferences and performed aldosterone ELISA with the solvent-extractable fraction.

First, to test the efficiency of the extraction method by DCM, we performed a spike-in experiment in which a range of aldosterone levels (from 2000 pg/ml to 15.6 pg/ml) was added into the basal culture medium. The spike-in samples were extracted by DCM, reconstituted, and measured by ELISA. The ratio of post-extraction versus actual aldosterone levels represented the recovery percentage of the extraction method. **Figure 26A** shows the recovery percentage after the spike-in samples' extraction. The extraction gave a recovery ranging from 78.8% to 98%. Next, we compared the pre- and post-extraction aldosterone secreted by WT and G151R-mutated adrenocortical cells. Both cell lines had significantly decreased aldosterone amounts detected after the extraction **(Figure 26B)**. This indicates that a proportion of hydrophilic aldosterone derivatives or other hydrophilic interfering substances were abolished after the extraction, and their presence before extraction possibly resulted in falsely elevated values measured by ELISA. Of note, the aldosterone detected post-extraction was still significantly higher in the mutated cells compared to WT, indicating that our mutant cells, in fact, produced elevated aldosterone and perhaps its derivatives **(Figure 26C)**. More detailed investigation on aldosterone detection is needed and will be further discussed. Nevertheless, as evidenced by both pre-and post-extraction ELISA results,

our mutant adrenocortical cells could prove themselves as an adequate model for primary aldosteronism.

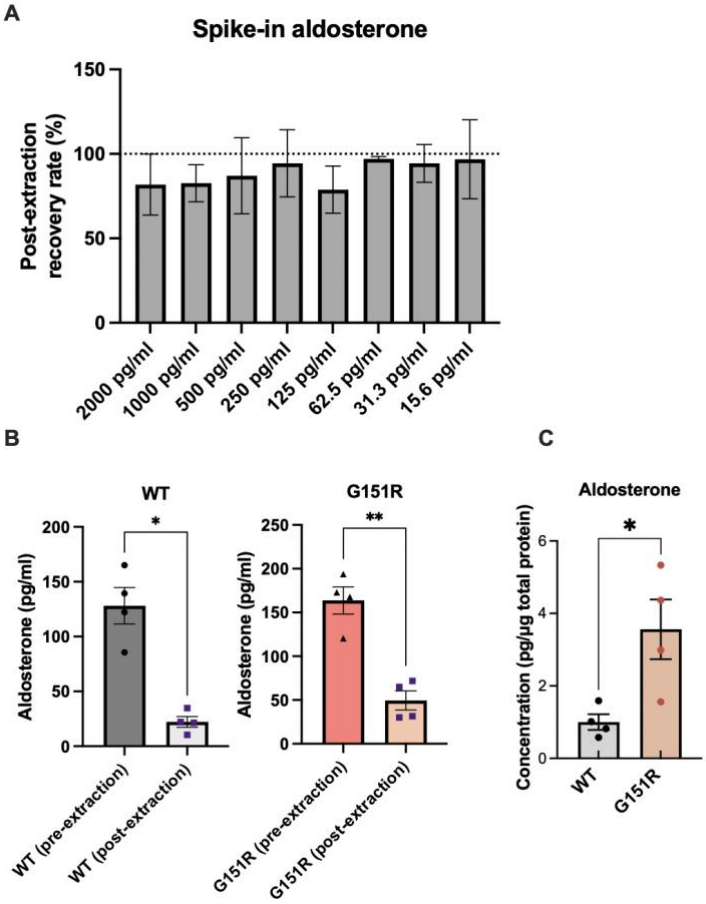

Figure 26: Quantitation of aldosterone in cell culture supernatant with solvent extraction

(A) The efficiency of solvent extraction was examined by the recovery rate of spike-in aldosterone samples. The spike-in samples were extracted by DCM, and the post-extracted aldosterone was measured by ELISA. The percentage of recovery was calculated by the post-extracted aldosterone and the actual spike-in aldosterone (n = 2). B) ELISA quantification of aldosterone production in the cultivation media of WT and *KCNJ5*$^{G151R/+}$ adrenocortical cells before and after solvent extraction (n ≥ 4). (B) ELISA quantification of aldosterone production in the solvent-extracted supernatant of WT and *KCNJ5*$^{G151R/+}$ adrenocortical cells (n = 4). In B-C, two-tailed Student‘s t-tests were used. *P < 0.05, **P < 0.01.

4. Discussion

4.1. Adrenal cortex differentiation from hiPSCs

Advances in adrenocortical research have been hampered by the lack of adequate disease models, which hinder the understanding of disease mechanisms and the development of more specific therapies for adrenal cortex diseases. In this study, we established an optimized differentiation system to generate hiPSC-induced adrenocortical cells through intermediate mesoderm (IM), the mesenchymal precursor of the adrenal cortex.

Resembling the embryonic development of the adrenal cortex, the transient step from pluripotent stem cells to IM is crucial to direct the differentiation towards adrenal cortex lineages. Although there are numerous studies establishing efficient and robust differentiation protocols focusing on the iPSCs-IM-kidney lineages axis, the iPSCs-IM-adrenocortical lineages axis has not yet been systematically investigated. By adapting three established IM induction protocols and optimizing the cultivation conditions of our in-house hiPSCs **(Figure 9)**, we generated a population of mesenchymal cells that can be characterized as a mix of posterior ($WT1^+/OSR1^+$) and anterior IM ($PAX2^+$) **(Figure 10-12)**. The origin and separation of human adrenogonadal primordium (AGP) were not clear until the recent findings of Sasaki et al., 2021 (*11*) and Cheng et al., 2022 (*8*). These findings highlight the differences in spatial and temporal development of these organs: the adrenal cortex precursor exits the primitive streak early, while the gonadal precursor emerges later from the late primitive streak; however, they are both localized at the posterior region of the IM. Therefore, to generate the precise IM derivatives (kidney, adrenal cortex or gonads) *in vitro*, there should be a comprehensive study on restoring the specification and patterning of IM in correlation with those *in vivo* studies.

When differentiating IM to adrenal cortex cells, we showed that forced expression of SF-1, the key adrenal transcriptional modulator, in combination with adrenocortical niche factors cAMP, AngII, and increased extracellular potassium levels, induced cell fate commitment from mesenchymal precursors into adrenocortical lineages. The differentiated cells expressed markers of the adrenal cortex and released adrenal steroid hormones, especially aldosterone and cortisol, proving their functional capacity **(Figure 15-18)**. Importantly, the differentiated cells also responded to physiologic

stimuli of aldosterone production (angiotensin II, extracellular potassium) in a dose-dependent manner **(Figure 19)**.

Previous studies attempted to generate steroid-producing cells from iPSCs, adult stem cells, and fibroblasts **(Table 3)**; nonetheless, the production of aldosterone was rarely reported, except Li et al. (*132*) and Matsuo et al. (*141*), or only indirectly shown by an induced CYP11B2 expression (*135*). Besides cells expressing steroidogenic-related genes, we also found adrenal stem/progenitor-like cells, including $RSPO3^+$ capsular stem cell- and $DAX1^+$ subcapsular progenitor cell-like populations in our differentiation system **(Figure 20)**. DAX1 (*NR0B1* gene), a nuclear receptor, is critical for maintaining the undifferentiated state of progenitors located the zG (*1, 34*). Capsular stem cells control adrenal tissue homeostasis by replacing damaged cortical cells and maintaining zonation throughout life via the RSPO3/WNT4 pathway (*30*). Some of the other adrenal cortex markers were identified by immunostaining, including NESTIN (stressed-induced adrenal stem cells) (*32*) and CD56 (mesenchymal-derived zG cells) (*184*) **(Figure 16B)**. Taken together, we demonstrated that by overexpressing SF-1 and supplementing niche factors in the cultivation system, we generated a mix of different adrenocortical lineages, including steroidogenic and non-steroidogenic cells, resembling the cell components of the *in vivo* adrenal cortex.

Our stepwise differentiation system, which includes an iPSCs-to-IM differentiation followed by an IM-to-adrenocortical lineage differentiation, gave rise to lineage-committed cells and precursor cells. IM induction may support early differentiation events from IM into mesenchymal-like capsular stem cells and subcapsular progenitor-like cells. The advantage of maintaining an undifferentiated state in our system is the preserved self-renewal of the transfected cells, contrary to the directly reprogrammed steroidogenic cells (hiSCs) from fibroblast and adult stem cells, which become proliferation arrested 3-5 days after SF-1 overexpression (*135*). It may also explain the lack of zG in hiSCs-derived cells, as this zone is closer to the progenitor state than zF and zR (*3*). Future strategies could be aimed at purifying progenitor cells in our system and differentiation into cortical cells using zone-specific niche factors.

The scRNA-seq analysis revealed a cell fate conversion from mesoderm precursors to adrenocortical cells, which provides a better understanding of the adrenal cortex differentiation **(Figure 19)**. We observed a down-regulation of mesoderm marker genes and an up-regulation of adrenocortical marker genes in our system.

Additionally, our *in vitro* adrenal cortex differentiation system exhibited a change in gene expression profile when Wnt/β-catenin was activated. Previous studies have reported that constitutive activation of this pathway results in adrenal hyperplasia and inhibits steroidogenesis (*42, 185*). On the other hand, interference with intrinsic molecular pathways could induce abnormal adrenal development. A recent study showed that disruption of the Hippo pathway results in hyperactivation of YAP/TAZ signaling in the adrenal cortex, leading to an impaired conversion from steroidogenic cells to myofibroblast-like cells (*186*); however, the mechanism is still unknown. We found an increased expression of genes representing fibroblast, connective tissue, and Wnt/β-catenin modulators, which suggests further investigation of constitutive activation of the Wnt pathway in the adrenal cortex development. Although we observed a change in the gene expression profile of hiPSC-derived cells with the expression of adrenal cortex markers (STAR, CYP11A1, HSD3B2), CYP11B1 and CYP11B2 was undetected. The percentage of adrenal cortex lineage cells (Cluster 8, Cluster 9; Figure 20C) in the total cell population was relatively low compared to other cell types (e.g., mesenchymal, fibroblast-like cells).

This can be explained by the low differentiation efficiency, thereby, considerable heterogeneity in the cell population is presented in our differentiation system. There is a need to optimize our differentiation system to improve the homogeneity of derived cells. A purification method to separate adrenocortical cells from untargeted cells could be done by fluorescence-activated sorting using specific cell surface markers, for instance, CD56, which is a marker for zG cells. Another approach to improve the homogeneity of the cells is enhancing differentiation efficiency. Screening an optimal differentiation condition from different niche factors or increasing the SF-1 overexpression could be appropriate strategies.

Finally, we observed an inconsistency between measurements of aldosterone in tissue cell culture supernatants by immunoassays, in our case ELISA, and LC-MS/MS. Although we were able to detect aldosterone in the supernatant by ELISA, aldosterone was undetectable in LC-MS/MS steroid profiling, unlike other steroids. Surprisingly, in other studies of stem cell-derived steroidogenic cells, aldosterone levels reported in the articles were measured exclusively by ELISA, even though steroid profiling was also conducted in the same studies (*132, 135*). The first possible explanation is the analytical sensitivity issue of LC-MS/MS. The levels of aldosterone (20-30 pg/ml) could

be below the detection limits of the LC-MS/MS. To investigate this, a spike-in experiment by LC-MS/MS was performed to examine the detection of aldosterone added to media ranging from 15 pg/ml to 1000 pg/ml in concentration (data not shown). This experiment showed that the LC-MS/MS can indeed detect small amounts of aldosterone (20 pg/ml); thus, the possibility of low sensitivity is excluded. Another possible cause would be the presence of aldosterone derivative, metabolites or other interfering substances, which are detected by the antibodies in the ELISA, resulting in over-estimation of aldosterone. This issue has been discussed and assessed in clinical diagnostics, and a solvent extraction using dichloromethane (DCM) reduced the measured aldosterone levels. The falsely elevated aldosterone levels were possibly caused by the accumulation of aldosterone glucuronide, an inactive hydrophilic aldosterone derivative that is produced as a result of hepatic and kidney cell metabolic activity (*182, 187*). Although such a glucuronidation process would be unlikely to occur in our cell culture system, the aldosterone levels were reduced after the extraction in both mutant and WT cells **(Figure 26A)**. To answer whether aldosterone glucuronide or other hydrophilic aldosterone derivatives or interfering substances lead to an overestimation of the actual aldosterone in our cell culture supernatants, LC-MS/MS would be helpful (*187*). Even though LC-MS/MS confirmation is still pending, as evidenced by both pre-and post-extraction ELISA results, our mutant adrenocortical cells show elevated aldosterone secretion compared to WT cells. This finding demonstrates that hiPSC-derived KCNJ5$^{G151R/+}$ are an adequate model for primary aldosteronism **(Figure 26B)**.

4.2. Modeling primary aldosteronism (PA) by heterozygous *KCNJ5^{G151R}* hiPSC-derived Adrenal Cortex Cells

Over the last ten years, numerous somatic mutations in genes encoding ion pumps and channels (*KCNJ5, CACNA1D, ATP1A1*, *ATP2B3*, *CACNA1H*, *CLCN2*) were discovered in APAs **(Table 1)** (*69, 71, 72, 77, 188*). While their contribution to increased aldosterone production is well studied, the exact mechanisms underlying proliferation and tumor formation in APAs remain unsolved. Existing mouse models of hyperaldosteronism do not display tumor formation or hyperplasia (*189-191*). Pitfalls associated with the use of the human adrenocortical cancer cell line H295R as a model system include the limited response to ACTH stimulation, variable aldosterone

production (*147, 192*), and an upregulated baseline proliferation rate as well as a *CTNNB1* mutation that may interfere with Wnt pathway analysis (*145*).

Utilizing our new system, we successfully modeled PA by generating adrenocortical cells with a heterozygous somatic *KCNJ5*^{G151R} mutation. Unlike the H295R/HAC15 line, our *in vitro* cell line reproduced the two key APA features observed *in vivo* (hormone production and proliferation). Given that lethality was previously observed in HAC15 cells overexpressing *KCNJ5*^{G151R} (*118*) we propose that endogenous promoter-driven expression of the heterozygous allele is the key to adequately model *in vivo* effects. For *KCNJ5* mutations, our data argue against the second-hit hypothesis (*193*), which proposes that signaling pathways such as Wnt/β-catenin (*104*) or Shh (Sonic hedgehog) signaling (*194*) lead to abnormal proliferation as the first hit. In our study, *KCNJ5* mutations appear to be sufficient to interfere with both hormone production and proliferation; however, it is still worth examining β-catenin activity in the mutant cells compared to the WT cells. To further study the proliferative effects of *KCNJ5* mutations, we propose an experiment to test whether upregulated cellular proliferation in the mutant cells is dependent/independent of the Ca^{2+} signaling by blocking voltage-gated calcium channels. Similarly, future RNA sequencing may help to uncover additional pathways involved in mutant KCNJ5-induced proliferation. Such experiments would help to shed light on understanding the causes of tumorigenesis in APA.

4.3. Future perspective

In the clinical context, patients with adrenal insufficiency show inadequate production of cortisol and aldosterone. Mimicking the diurnal (morning peak) and stress-induced pattern of cortisol production through life-long substitution is challenging. Increased needs for glucocorticoids due to infections, injuries and/or surgeries can precipitate life-threatening adrenal crises (*195*), while over-replacement can lead to Cushing's syndrome, including obesity, osteoporosis, hypertension, and impaired glucose tolerance (*196*). One important potential application of hiPSC-derived adrenocortical cells could be cell therapy for adrenal insufficiency, for which self-renewal of cells would be crucial and was evident in our system. SF-1 in our study and several previous studies was introduced by transient plasmid-based methods (*131, 132*); stable expression by genome-integrated virus methods has also been used (*134, 135*). While these methods are well suited for generating disease models, they may lead to

integration at undesired positions therefore a less harmful introduction of the transgene would be beneficial. This could be achieved using an mRNA-based approach in the future. Alternatively, extrinsic factors, leading to direct conversion from mesenchymal precursors into adrenocortical lineages, could be applied. The latter approach is challenging because SF-1 is a critical modulator of AC development and regulator of steroidogenesis; however, candidate factors such as activin and bone morphogenetic proteins, BMPs (*197, 198*), dopamine D receptor agonists (*141*) or insulin-like growth factors, IGFs (*199*) have been described in the literature and could be screened. Another challenge would be the observed heterogeneity of our differentiated cell population. Contamination with undifferentiated cells in transplanted populations could cause proliferative clusters of cells. Thus, a purification method to separate undifferentiated cells from adrenocortical precursors and steroid producing cells should be considered. CD56 could be a promising marker that allows to isolate aldosterone-producing steroidogenic cells by immunomagnetic beads as described previously (*200*).

In addition, our hiPSC-derived adrenocortical cells could be applied to recreate the 3D structure of the adrenal cortex. The generation of 3D organoids is required to mimic complex multicellular and functional organs, particularly the adrenal cortex, which is a complex concentric organ, with each layer representing distinct histological and functional features. Currently, 3D organoids have been successfully created from hiPSCs for organs including the brain, intestine, liver, and kidney (*127, 201-203*). However, adrenal organoids are still lacking. Our preliminary data on the generation of a 3D structure called adrenal spheroid showed that after 30 days of induction, a compacted cell organization of multiple adrenocortical lineages, including $STAR^+/CYP11B2^+$ steroidogenic cells, $E\text{-}CAD^+$ epithelial cells, $WT1^+$ progenitor cells, and especially endogenous $SF\text{-}1^+$ cells can be achieved **(Supplementary Figure 1B)**. These results indicate that, in a 3D structure, the hiPSC-derived adrenal cortex cells maintained their cell identity as adrenal cortex lineages; however, a complex structure with zonation is still missing. To trigger the self-organization into concentric zonation as the adult adrenal cortex, we will further examine the effects of the extracellular matrix (ECM), a crucial component needed to trigger the self-organization of an organoid.

Additionally, the 3D structure of the adrenal cortex and the whole structure of the adrenal gland, including cortical and medullary chromaffin cells, could also be generated. Previous studies have shown that co-culturing bovine adrenocortical cells and chromaffin cells significantly enhances steroidogenesis up to ten times (*204*). Importantly, the precursors of the adrenal cortex and medulla come from different origins: the adrenal cortex cells derive from the mesoderm, while medullary cells originate from the neural crest. As such, the differentiations of hiPSCs into each cell type have to be performed under different conditions, then two cell lineages are prepared to be assembled in the same tissue culture dish. Such structures are called assembloids, a new concept of generating 3D structures of multiple organoids from different origins (*205*).

Disease modeling of other adrenal genetic diseases using our hiPSC-derived adrenocortical cells is a promising application. Thanks to the advance in the improvement of genome editing using the CRISPR/Cas9 technique, the generation of cell lines carrying somatic mutations is now more robust, efficient, and precise. Under our described differentiation methods, these mutation-harboring iPSC lines can be differentiated into adrenocortical lineages and potentially model the pathophysiology of the associated disorders. Besides disease modeling, personalized medicine, including transplantation and drug screening are possible applications **(Figure 27)**. Patient-derived iPSCs can be reprogrammed *in vitro* from the patient's somatic cells. The CRISPR/Cas9 technique allows a precise genetic modification to "correct" the patient-derived iPSCs, followed by adrenal cortex differentiation to generate corrected adrenal cortex cells. Corrected differentiated cells could serve as a source of cells for auto-transplantation, while mutant cells could be used for drug screening **(Figure 27)**.

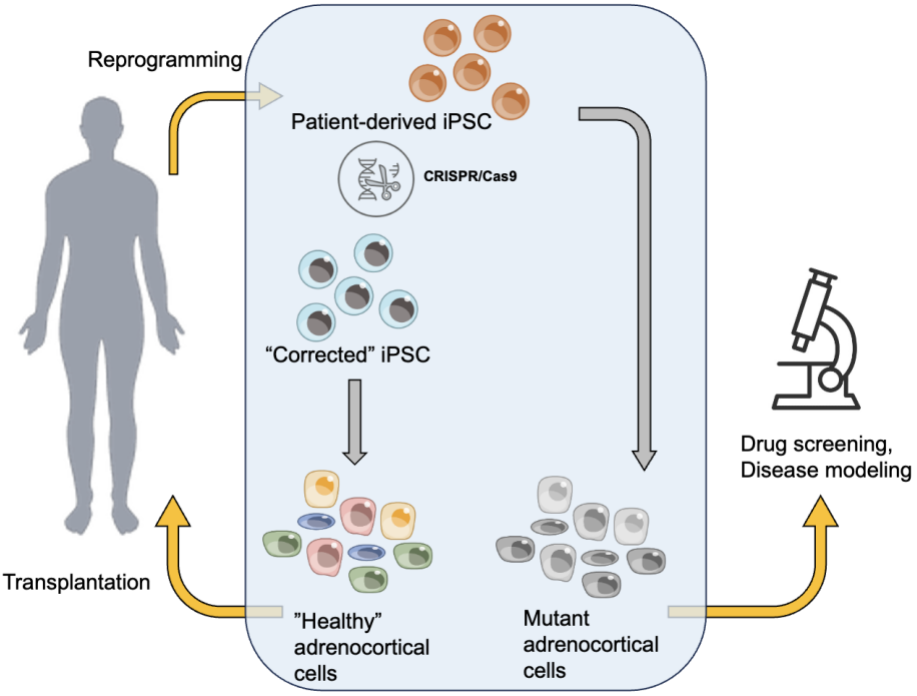

Figure 27: A proposed application of hiPSC-derived adrenocortical cells.
CRISPR/Cas9 is used to correct mutation-harboring patient-derived iPSCs, which are reprogrammed from somatic cells. Patient- and corrected iPSC cells undergo differentiation towards adrenocortical cells under our optimal differentiation conditions. While "healthy" adrenocortical cells could be used as a source of cell-based therapy, mutant adrenocortical cells could serve as models for disease or personalized drug screening.

4.4. Conclusion

To sum up, we addressed challenges in adrenocortical research by establishing an optimized system to differentiate adrenocortical lineages from hiPSCs. As proof of principle, using CRISPR/Cas9, we successfully modeled PA associated with pathogenic *KCNJ5*^{G151R} mutations. We propose that our system is a versatile tool to investigate mechanisms underlying other adrenocortical genetic disorders. hiPSC generation from patients might even obliterate the need for genome editing. 3D adrenocortical organoids could further improve this system and pave the way for future transplantation strategies.

5. Supplementary data

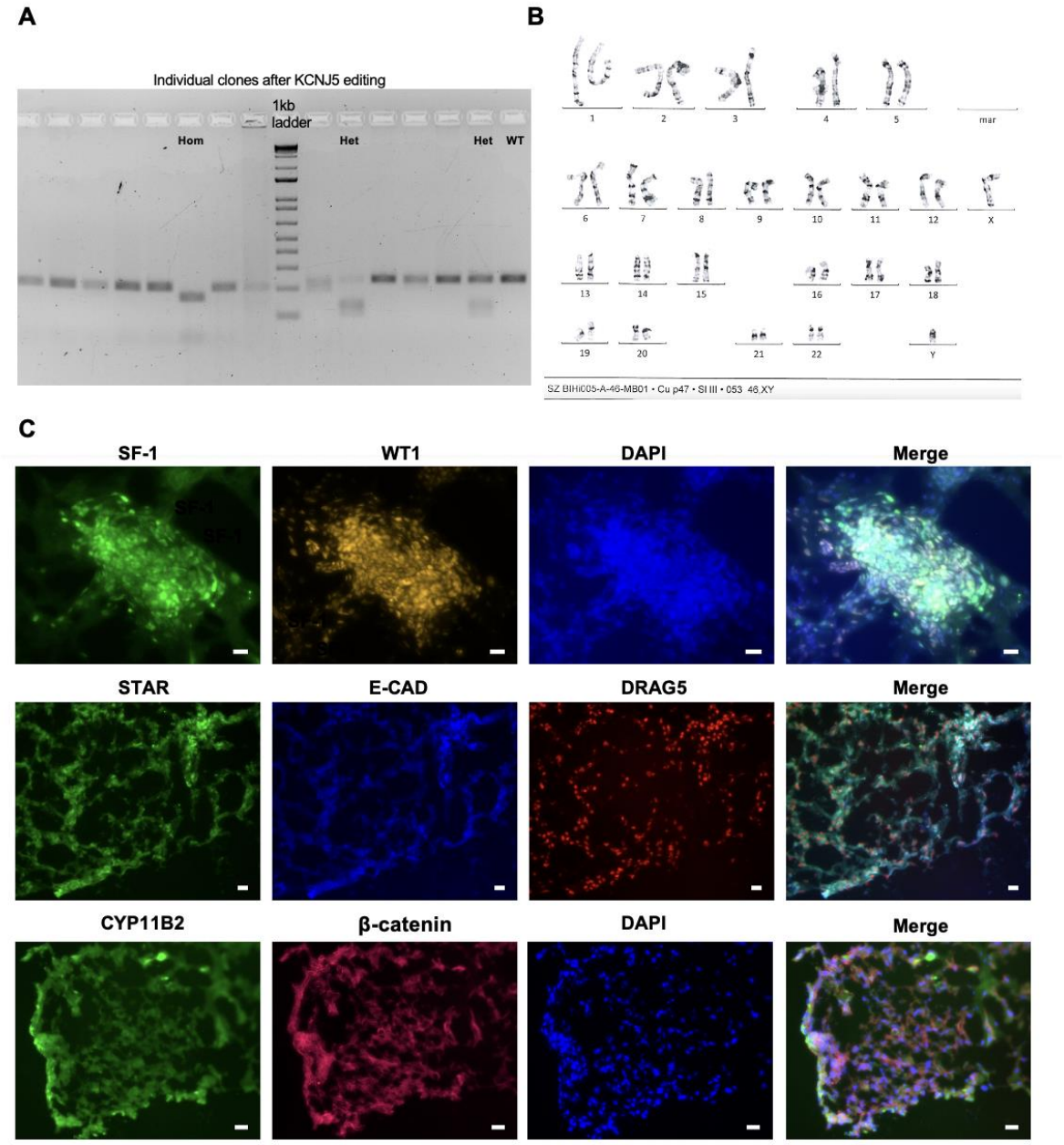

Supplementary Figure 1

(A) Unprocessed image of **Figure 21C**. DdeI-mediated restriction fragment length polymorphism (RFLP) assay showed HDR efficiency of heterozygous and homozygous mutant clones.

(B) G-banding karyotyping of *KCNJ5*$^{G151R/+}$ hiPSC line (BIHi005-A-46).

(C) Immunostaining of hiPSC-derived adrenal spheroids after 30 days of induction of steroidogenic cells (SF-1$^+$, STAR$^+$, CYP11B2$^+$ cells), WT1$^+$ progenitor cells, E-CAD$^+$ epithelial cells, and β-catenin$^+$ cells. The nuclei were stained with DAPI (blue) or DRAG5 (red). Scale bar: 25 µm.

Supplementary data 2: Top 20 differentially expressed genes in each cluster from the scRNA-seq data ranked by fold change.

Cluster	Gene	Fold change	p-value	Cluster	Gene	Fold change	p-value	Cluster	Gene	Fold change	p-value	Cluster	Gene	Fold change	p-value
0	MGP	2.1	2.3e-130	4	H4C3	1.8	0	8	GSTA1	3.0	2.3e-139	12	EGFP	3.7	9.5e-100
0	IGFBP3	2.0	2.4e-115	4	H1-5	1.8	0	8	STAR	3.0	7.5e-100	12	LRRC17	2.7	2.4e-153
0	DCN	1.6	7.8e-224	4	H1-3	1.8	0	8	MT2A	2.8	3.9e-31	12	ITGA1	2.5	2.5e-94
0	COL3A1	1.5	0	4	H1-2	1.3	0	8	EGFP	2.5	1.5e-129	12	APCDD1	2.3	3.3e-104
0	LUM	1.5	6.3e-215	4	H1-4	1.3	0	8	DLK1	2.5	8.3e-78	12	VGF	2.3	9.7e-38
0	COL1A2	1.4	0	4	H1-1	1.3	1.9e-237	8	GSTP1	2.4	8.3e-197	12	CLDN11	2.2	9.7e-67
0	NEAT1	1.4	1.3e-230	4	NASP	1.0	0	8	CYP11A1	2.2	2.4e-87	12	LGALS3	2.2	3.5e-46
0	APCDD1	1.4	4.8e-100	4	H3C2	0.99	0	8	AC022075.1	2.2	1.5e-53	12	NOTUM	2.0	1.3e-117
0	POSTN	1.1	0	4	H2AC20	0.95	0	8	HIGD1A	2.1	7.8e-28	12	CRYGS	2.0	6.5e-54
0	COL1A1	1.1	3.3e-256	4	CLSPN	0.95	0	8	NEFL	2.0	1.3e-56	12	LYPD1	2.0	7.1e-49
0	ITGA1	1.1	1.3e-227	4	DUT	0.95	0	8	CLTB	2.0	8.1e-20	12	ITM2B	1.8	2.3e-57
0	SST	1.1	3.3e-49	4	HELLS	0.94	0	8	CDKN1C	2.0	4.7e-7	12	RBP1	1.8	1.6e-53
0	VCAN	1.0	3.6e-291	4	DEK	0.94	0	8	RBP1	1.9	7.2e-61	12	IGFL2	1.8	3.3e-40
0	IL6ST	1.0	6.4e-118	4	PCLAF	0.9	0	8	FDXR	1.8	1.1e-20	12	IGFBP2	1.8	2.1e-30
0	IFI6	0.99	2.9e-189	4	CYB5A	0.89	7.1e-89	8	TUBB2A	1.8	2.1e-11	12	SLC2A1	1.8	5.1e-23
0	ITM2B	0.98	5.7e-161	4	ATAD2	0.87	0	8	MYL9	1.7	9.6e-71	12	STT3B	1.8	3.1e-15
0	TDO2	0.97	7.6e-84	4	HMGN2	0.85	4.1e-238	8	CALM3	1.7	3.1e-33	12	CST3	1.8	1.2e-12
0	IFITM3	0.94	1.1e-272	4	TYMS	0.82	7.2e-271	8	S100A13	1.7	7.8e-14	12	CRABP2	1.7	6.1e-48
0	CXCL14	0.94	2E-97	4	TMPO	0.81	2.4e-245	8	GLRX	1.7	0.000062	12	TDO2	1.6	3.6e-38
0	PDPN	0.92	3.1e-105	4	HMGB2	0.8	6.8e-222	8	RPS27L	1.6	2.1e-82	12	DKK	1.6	6E-35
1	CCN2	1.1	5.4e-64	5	PRTG	2.2	0	9	SPP1	3.7	0	13	APOA1	3.8	1.1e-79
1	TAGLN	1.0	1.7e-291	5	TMEM88	2.1	0	9	DLK1	3.0	3.6e-229	13	TTR	2.8	1.3e-199
1	TIMP3	0.98	1.6e-136	5	HAS2	2.1	8.4e-243	9	GSTA1	3.0	2E-208	13	CST1	2.8	2.5e-162
1	INHBA	0.8	3.8e-109	5	HAND1	1.9	0	9	CCN2	2.5	2.1e-135	13	S100A16	2.7	2.8e-80
1	ACTA2	0.79	6.1e-85	5	RPS29	1.7	0	9	MEG3	2.4	1.9e-136	13	APOC1	2.6	2.8e-70
1	SERPINE1	0.75	2E-212	5	HAPLN1	1.7	9.1e-303	9	IGFBP7	2.0	9E-83	13	MYL4	2.6	3.6e-53
1	FN1	0.75	2.6e-116	5	HOXB-AS3	1.6	0	9	TFPI2	2.0	9E-29	13	S100A6	2.6	1.8e-26
1	ACTC1	0.75	6.4e-32	5	BMP4	1.6	0	9	STAR	1.8	1E-57	13	GPX2	2.5	5.7e-244
1	NNMT	0.73	2E-115	5	SLC9A3R1	1.6	1.1e-261	9	PRSS23	1.8	8.8e-51	13	SLC2A3	2.4	1E-85

Cluster	Gene	Fold change	p-value	Cluster	Gene	Fold change	p-value	Cluster	Gene	Fold change	p-value	Cluster	Gene	Fold change	p-value
1	ACTG2	0.72	4.3e-71	5	ACTC1	1.6	3.2e-197	9	SFRP1	1.8	1.3e-30	13	CKB	2.3	1.1e-51
1	PAPPA	0.71	2.9e-117	5	FGF19	1.5	0	9	EGFP	1.6	1.7e-141	13	PTGR1	2.3	1.2e-42
1	IGFBP5	0.69	3.9e-30	5	RGS5	1.5	0	9	S100A13	1.5	2.4e-55	13	EPCAM	2.2	0
1	C12orf75	0.67	3.6e-164	5	PSAT1	1.5	0	9	AC022075.1	1.5	1.1e-24	13	NTS	2.2	1.1e-232
1	CNN1	0.66	1.1e-161	5	CITED2	1.5	0	9	CDKN1C	1.5	0.0000027	13	FST	2.2	1.3e-108
1	PRSS23	0.66	1.1e-127	5	TMEM185A	1.4	0	9	RPS27L	1.4	6.4e-56	13	MIR302CHG	2.1	5.6e-42
1	ACTN1	0.65	1.1e-175	5	CTSV	1.4	0	9	RAP1B	1.4	3E-11	13	IGFBP6	2.0	0
1	CDC42EP3	0.64	1.7e-125	5	PHGDH	1.3	0	9	GASK1B	1.4	0.00067	13	APOE	2.0	2.8e-52
1	ANXA1	0.63	3E-154	5	H19	1.3	4.7e-176	9	ITPRID2	1.4	17	13	APELA	1.9	1E-278
1	ANXA2	0.62	1.1e-203	5	RPS27	1.2	0	9	CPE	1.4	0.54	13	RSPO3	1.9	1.5e-83
1	MYH9	0.62	2.7e-156	5	WLS	1.2	1.5e-270	9	HIGD1A	1.4	1	13	APOA2	1.8	0
2	APOA1	1.3	7.7e-38	6	GADD45A	0.99	1.9e-35	10	HOXB-AS3	1.8	6.7e-169	14	CRHBP	2.7	1.2e-151
2	S100A6	1.0	1.7e-28	6	LAYN	0.8	4.2e-20	10	DOK4	1.7	7.7e-175	14	KDR	2.0	6E-105
2	S100A16	1.0	9.1e-24	6	H4C3	0.72	2.7e-64	10	RPS29	1.6	3.9e-166	14	EGFL7	2.0	5.1e-42
2	CKB	0.97	6.8e-85	6	DIAPH3	0.71	1.2e-89	10	ID2	1.4	3.6e-106	14	NRP2	1.6	2.9e-53
2	CSRP2	0.76	1.3e-113	6	TXNRD1	0.71	6.8e-27	10	RPS27	1.3	1.2e-176	14	HAPLN1	1.5	1.7e-28
2	IGFBP6	0.7	1.1e-24	6	H1-5	0.7	7.2e-74	10	TERF2IP	1.3	1.4e-103	14	TFPI	1.4	8.8e-54
2	PTGR1	0.69	1.5e-21	6	TNFRSF-12A	0.7	2.1e-68	10	TMEM88	1.3	3.2e-84	14	IER2	1.3	3.8e-46
2	CYB5A	0.63	1.8e-34	6	DEK	0.67	1.1e-86	10	KDR	1.3	3.9e-84	14	LIMCH1	1.2	7.4e-127
2	APOC1	0.63	0.02	6	H1-3	0.67	1.1e-54	10	MCOLN3	1.2	2.2e-201	14	CCDC85B	1.2	2.3e-41
2	ISG15	0.61	1.2e-13	6	H1-2	0.66	1.2e-62	10	H4C3	1.2	1.2e-58	14	H1-5	1.2	1.8e-28
2	DNAJC15	0.59	3.6e-76	6	OGFRL1	0.66	3.3e-56	10	URAD	1.1	4.8e-270	14	H1-3	1.2	2.4e-22
2	S100A10	0.55	2.5e-134	6	NCL	0.63	4.1e-77	10	CDX2	1.1	9.9e-268	14	GNG11	1.2	1.4e-7
2	FST	0.55	9.3e-20	6	EZR	0.61	3.6e-59	10	MLLT3	1.1	2.3e-142	14	SOX17	1.0	1.4e-257
2	GNAS	0.54	2.3e-126	6	ATF3	0.61	8.6e-51	10	AMIGO2	1.1	1.3e-140	14	H1-1	1.0	9.9e-12
2	RPL10P9	0.53	2.8e-128	6	ATAD2	0.58	1.2e-86	10	HOXB9	1.1	4.6e-100	14	IFITM2	0.96	1.7e-32
2	PTTG1	0.53	4.9e-11	6	PFKP	0.58	1.9e-64	10	HAND1	1.1	5.1e-90	14	H4C3	0.96	7.3e-16
2	MYL6	0.49	1.9e-141	6	ORC6	0.57	1.7e-70	10	SPRY1	1.1	1.3e-88	14	TM4SF-18	0.95	3E-82
2	FTL	0.49	3.4e-73	6	MCM4	0.57	1.2e-67	10	LIN28A	1.0	3.3e-188	14	RAMP2	0.95	1.6e-63

Cluster	Gene	Fold change	p-value	Cluster	Gene	Fold change	p-value	Cluster	Gene	Fold change	p-value	Cluster	Gene	Fold change	p-value
2	LGALS1	0.46	1.2e-35	6	DDX21	0.57	1.6e-51	10	HOPX	1.0	3.3e-127	14	ID3	0.88	4.8e-23
2	NDUFS6	0.43	1.3e-129	6	C12orf75	0.57	4.2e-46	10	TOP2A	1.0	6.8e-127	14	ESAM	0.86	6.7e-185
3	CENPF	1.5	4.9e-286	7	NPPB	4.1	6.3e-233	11	DLK1	2.7	1.4e-175	15	CRYGS	2.9	3.8e-135
3	TOP2A	1.4	1.6e-276	7	ANKRD1	3.6	0	11	EGFP	2.5	0	15	PLAT	1.9	3E-59
3	CENPE	1.3	0	7	CCN1	2.9	0	11	STAR	2.4	0	15	TDO2	1.8	2.6e-22
3	CCNB1	1.2	2E-303	7	SERPINE1	2.9	0	11	GSTA1	2.3	1.2e-256	15	MAFB	1.7	4.1e-87
3	MKI67	1.2	2.1e-302	7	IER3	2.7	3.2e-274	11	MT2A	2.2	1.8e-142	15	GAP43	1.7	5.2e-45
3	TPX2	1.2	1.2e-287	7	FLNC	2.5	0	11	PEG10	2.1	5E-77	15	ENC1	1.7	2.1e-34
3	ASPM	1.2	7.6e-284	7	EDN1	2.3	0	11	HSD3B2	1.9	0	15	TIMP1	1.7	9.1e-31
3	DLGAP5	1.0	1.6e-275	7	CCL2	2.1	0	11	FDXR	1.7	3.4e-223	15	ITGA1	1.7	8E-26
3	UBE2C	1.0	5.6e-253	7	UGP2	2.1	7.4e-280	11	GAL	1.7	6E-86	15	SLC7A8	1.6	3.3e-47
3	AURKA	0.99	1.2e-263	7	DDIT4	2.0	5.1e-268	11	GDF15	1.7	1.8e-77	15	CYP1B1	1.6	8E-43
3	HMMR	0.95	3.3e-280	7	TAGLN	2.0	2.1e-187	11	HPGD	1.6	3E-202	15	MMP10	1.6	1.9e-32
3	CDKN3	0.93	2.3e-285	7	THBS1	1.9	0	11	HES6	1.6	8.5e-90	15	CTSC	1.6	3.4e-28
3	KPNA2	0.88	1.6e-177	7	KRT8	1.9	4E-279	11	CDKN1C	1.6	5.2e-39	15	VGF	1.5	7.8e-32
3	DEPDC1	0.86	0	7	KRT18	1.9	6.5e-266	11	S100A13	1.5	2.7e-279	15	PHLDA1	1.5	1.8e-31
3	SGO2	0.86	2.1e-274	7	UPP1	1.9	4E-180	11	NEFL	1.4	3.6e-34	15	NEAT1	1.5	3E-14
3	UBE2S	0+G28.86	4.7e-223	7	TNFRSF-12A	1.7	6.9e-276	11	APOA1	1.4	0	15	CXCL14	1.5	0.0000041
3	PTTG1	0.85	4.7e-203	7	ACTC1	1.7	2.6e-81	11	SCARB1	1.4	2.8e-194	15	IL7R	1.3	2.8e-65
3	SMC4	0.82	4.2e-217	7	LTB	1.6	0	11	CCN3	1.3	7.7e-156	15	CTSB	1.3	8.5e-31
3	HMGB2	0.82	3.1e-154	7	IGFBP4	1.5	5.2e-226	11	RARRES2	1.3	8.7e-182	15	NR2F2	1.3	1.1e-25
3	KIF20B	0.81	4.5e-211	7	FHL2	1.4	0	11	FDX1	1.3	4.5e-146	15	COL1A2	1.3	0.00013

6. References

1. E. M. Walczak, G. D. Hammer, Regulation of the adrenocortical stem cell niche: implications for disease. *Nat Rev Endocrinol* **11**, 14-28 (2015).
2. P. King, A. Paul, E. Laufer, Shh signaling regulates adrenocortical development and identifies progenitors of steroidogenic lineages. *Proc Natl Acad Sci U S A* **106**, 21185-21190 (2009).
3. B. D. Freedman, P. B. Kempna, D. L. Carlone, M. Shah, N. A. Guagliardo, P. Q. Barrett, C. E. Gomez-Sanchez, J. A. Majzoub, D. T. Breault, Adrenocortical zonation results from lineage conversion of differentiated zona glomerulosa cells. *Dev Cell* **26**, 666-673 (2013).
4. M. A. Wood, A. Acharya, I. Finco, J. M. Swonger, M. J. Elston, M. D. Tallquist, G. D. Hammer, Fetal adrenal capsular cells serve as progenitor cells for steroidogenic and stromal adrenocortical cell lineages in M. musculus. *Development* **140**, 4522-4532 (2013).
5. S. Mesiano, R. B. Jaffe, Developmental and functional biology of the primate fetal adrenal cortex. *Endocr Rev* **18**, 378-403 (1997).
6. S. J. Arnold, E. J. Robertson, Making a commitment: cell lineage allocation and axis patterning in the early mouse embryo. *Nat Rev Mol Cell Biol* **10**, 91-103 (2009).
7. H. Barak, L. Rosenfelder, T. M. Schultheiss, R. Reshef, Cell fate specification along the anterior-posterior axis of the intermediate mesoderm. *Dev Dyn* **232**, 901-914 (2005).
8. K. Cheng, Y. Seita, T. Moriwaki, K. Noshiro, Y. Sakata, Y. S. Hwang, T. Torigoe, M. Saitou, H. Tsuchiya, C. Iwatani, M. Hosaka, T. Ohkouchi, H. Watari, T. Umazume, K. Sasaki, The developmental origin and the specification of the adrenal cortex in humans and cynomolgus monkeys. *Sci Adv* **8**, eabn8485 (2022).
9. A. Taguchi, Y. Kaku, T. Ohmori, S. Sharmin, M. Ogawa, H. Sasaki, R. Nishinakamura, Redefining the in vivo origin of metanephric nephron progenitors enables generation of complex kidney structures from pluripotent stem cells. *Cell Stem Cell* **14**, 53-67 (2014).
10. M. H. Little, A. N. Combes, M. Takasato, Understanding kidney morphogenesis to guide renal tissue regeneration. *Nat Rev Nephrol* **12**, 624-635 (2016).
11. K. Sasaki, A. Oguchi, K. Cheng, Y. Murakawa, I. Okamoto, H. Ohta, Y. Yabuta, C. Iwatani, H. Tsuchiya, T. Yamamoto, Y. Seita, M. Saitou, The embryonic ontogeny of the gonadal somatic cells in mice and monkeys. *Cell Rep* **35**, 109075 (2021).
12. M. Zubair, K. L. Parker, K. Morohashi, Developmental links between the fetal and adult zones of the adrenal cortex revealed by lineage tracing. *Mol Cell Biol* **28**, 7030-7040 (2008).
13. R. Bandiera, V. P. Vidal, F. J. Motamedi, M. Clarkson, I. Sahut-Barnola, A. von Gise, W. T. Pu, P. Hohenstein, A. Martinez, A. Schedl, WT1 maintains adrenal-gonadal primordium identity and marks a population of AGP-like progenitors within the adrenal gland. *Dev Cell* **27**, 5-18 (2013).
14. P. Val, J. P. Martinez-Barbera, A. Swain, Adrenal development is initiated by Cited2 and Wt1 through modulation of Sf-1 dosage. *Development* **134**, 2349-2358 (2007).

15. O. Hatano, A. Takakusu, M. Nomura, K. Morohashi, Identical origin of adrenal cortex and gonad revealed by expression profiles of Ad4BP/SF-1. *Genes Cells* **1**, 663-671 (1996).
16. F. Mitani, K. Mukai, H. Miyamoto, M. Suematsu, Y. Ishimura, Development of functional zonation in the rat adrenal cortex. *Endocrinology* **140**, 3342-3353 (1999).
17. A. J. Conley, R. M. Bernstein, A. D. Nguyen, Adrenarche in nonhuman primates: the evidence for it and the need to redefine it. *J Endocrinol* **214**, 121-131 (2012).
18. Y. Xing, A. M. Lerario, W. Rainey, G. D. Hammer, Development of adrenal cortex zonation. *Endocrinol Metab Clin North Am* **44**, 243-274 (2015).
19. X. Luo, Y. Ikeda, K. L. Parker, A cell-specific nuclear receptor is essential for adrenal and gonadal development and sexual differentiation. *Cell* **77**, 481-490 (1994).
20. J. C. Achermann, M. Ito, M. Ito, P. C. Hindmarsh, J. L. Jameson, A mutation in the gene encoding steroidogenic factor-1 causes XY sex reversal and adrenal failure in humans. *Nat Genet* **22**, 125-126 (1999).
21. M. Doghman, T. Karpova, G. A. Rodrigues, M. Arhatte, J. De Moura, L. R. Cavalli, V. Virolle, P. Barbry, G. P. Zambetti, B. C. Figueiredo, L. L. Heckert, E. Lalli, Increased steroidogenic factor-1 dosage triggers adrenocortical cell proliferation and cancer. *Mol Endocrinol* **21**, 2968-2987 (2007).
22. A. M. Lerario, I. Finco, C. LaPensee, G. D. Hammer, Molecular Mechanisms of Stem/Progenitor Cell Maintenance in the Adrenal Cortex. *Front Endocrinol (Lausanne)* **8**, 52 (2017).
23. C. A. Schnabel, L. Selleri, M. L. Cleary, Pbx1 is essential for adrenal development and urogenital differentiation. *Genesis* **37**, 123-130 (2003).
24. S. D. Bamforth, J. Braganca, J. J. Eloranta, J. N. Murdoch, F. I. Marques, K. R. Kranc, H. Farza, D. J. Henderson, H. C. Hurst, S. Bhattacharya, Cardiac malformations, adrenal agenesis, neural crest defects and exencephaly in mice lacking Cited2, a new Tfap2 co-activator. *Nat Genet* **29**, 469-474 (2001).
25. D. J. INGLE, G. M. HIGGINS, AUTOTRANSPLANTATION AND REGENERATION OF THE ADRENAL GLAND. *Endocrinology* **22**, 458-464 (1938).
26. J. Y. Bertholet, Proliferative activity and cell migration in the adrenal cortex of fetal and neonatal rats: an autoradiographic study. *J Endocrinol* **87**, 1-9 (1980).
27. G. Zajicek, I. Ariel, N. Arber, The streaming adrenal cortex: direct evidence of centripetal migration of adrenocytes by estimation of cell turnover rate. *J Endocrinol* **111**, 477-482 (1986).
28. A. M. McNicol, A. E. Duffy, A study of cell migration in the adrenal cortex of the rat using bromodeoxyuridine. *Cell Tissue Kinet* **20**, 519-526 (1987).
29. S. P. Chang, H. D. Morrison, F. Nilsson, C. J. Kenyon, J. D. West, S. D. Morley, Cell proliferation, movement and differentiation during maintenance of the adult mouse adrenal cortex. *PLoS One* **8**, e81865 (2013).
30. V. Vidal, S. Sacco, A. S. Rocha, F. da Silva, C. Panzolini, T. Dumontet, T. M. Doan, J. Shan, A. Rak-Raszewska, T. Bird, S. Vainio, A. Martinez, A. Schedl, The adrenal capsule is a signaling center controlling cell renewal and zonation through Rspo3. *Genes Dev* **30**, 1389-1394 (2016).
31. C. C. Huang, S. Miyagawa, D. Matsumaru, K. L. Parker, H. H. Yao, Progenitor cell expansion and organ size of mouse adrenal is regulated by sonic hedgehog. *Endocrinology* **151**, 1119-1128 (2010).

32. C. Steenblock, M. F. Rubin de Celis, L. F. Delgadillo Silva, V. Pawolski, A. Brennand, M. Werdermann, I. Berger, A. Santambrogio, M. Peitzsch, C. L. Andoniadou, A. V. Schally, S. R. Bornstein, Isolation and characterization of adrenocortical progenitors involved in the adaptation to stress. *Proc Natl Acad Sci U S A* **115**, 12997-13002 (2018).
33. R. Lyraki, A. Schedl, Adrenal cortex renewal in health and disease. *Nat Rev Endocrinol* **17**, 421-434 (2021).
34. J. O. Scheys, J. H. Heaton, G. D. Hammer, Evidence of adrenal failure in aging Dax1-deficient mice. *Endocrinology* **152**, 3430-3439 (2011).
35. P. S. Babu, D. L. Bavers, F. Beuschlein, S. Shah, B. Jeffs, J. L. Jameson, G. D. Hammer, Interaction between Dax-1 and steroidogenic factor-1 in vivo: increased adrenal responsiveness to ACTH in the absence of Dax-1. *Endocrinology* **143**, 665-673 (2002).
36. J. C. Achermann, J. J. Meeks, J. L. Jameson, Phenotypic spectrum of mutations in DAX-1 and SF-1. *Mol Cell Endocrinol* **185**, 17-25 (2001).
37. D. S. Lala, D. A. Rice, K. L. Parker, Steroidogenic factor I, a key regulator of steroidogenic enzyme expression, is the mouse homolog of fushi tarazu-factor I. *Mol Endocrinol* **6**, 1249-1258 (1992).
38. S. Honda, K. Morohashi, M. Nomura, H. Takeya, M. Kitajima, T. Omura, Ad4BP regulating steroidogenic P-450 gene is a member of steroid hormone receptor superfamily. *J Biol Chem* **268**, 7494-7502 (1993).
39. B. M. Gummow, J. O. Scheys, V. R. Cancelli, G. D. Hammer, Reciprocal regulation of a glucocorticoid receptor-steroidogenic factor-1 transcription complex on the Dax-1 promoter by glucocorticoids and adrenocorticotropic hormone in the adrenal cortex. *Mol Endocrinol* **20**, 2711-2723 (2006).
40. H. Mizusaki, K. Kawabe, T. Mukai, E. Ariyoshi, M. Kasahara, H. Yoshioka, A. Swain, K. Morohashi, Dax-1 (dosage-sensitive sex reversal-adrenal hypoplasia congenita critical region on the X chromosome, gene 1) gene transcription is regulated by wnt4 in the female developing gonad. *Mol Endocrinol* **17**, 507-519 (2003).
41. A. C. Kim, A. L. Reuter, M. Zubair, T. Else, K. Serecky, N. C. Bingham, G. G. Lavery, K. L. Parker, G. D. Hammer, Targeted disruption of beta-catenin in Sf1-expressing cells impairs development and maintenance of the adrenal cortex. *Development* **135**, 2593-2602 (2008).
42. E. Pignatti, S. Leng, Y. Yuchi, K. S. Borges, N. A. Guagliardo, M. S. Shah, G. Ruiz-Babot, D. Kariyawasam, M. M. Taketo, J. Miao, P. Q. Barrett, D. L. Carlone, D. T. Breault, Beta-Catenin Causes Adrenal Hyperplasia by Blocking Zonal Transdifferentiation. *Cell Rep* **31**, 107524 (2020).
43. S. Ching, E. Vilain, Targeted disruption of Sonic Hedgehog in the mouse adrenal leads to adrenocortical hypoplasia. *Genesis* **47**, 628-637 (2009).
44. L. Guasti, W. C. Candy Sze, T. McKay, R. Grose, P. J. King, FGF signalling through Fgfr2 isoform IIIb regulates adrenal cortex development. *Mol Cell Endocrinol* **371**, 182-188 (2013).
45. Y. Kim, N. Bingham, R. Sekido, K. L. Parker, R. Lovell-Badge, B. Capel, Fibroblast growth factor receptor 2 regulates proliferation and Sertoli differentiation during male sex determination. *Proc Natl Acad Sci U S A* **104**, 16558-16563 (2007).
46. R. J. Fern, M. S. Hahm, H. K. Lu, L. P. Liu, F. S. Gorelick, P. Q. Barrett, Ca2+/calmodulin-dependent protein kinase II activation and regulation of adrenal glomerulosa Ca2+ signaling. *Am J Physiol* **269**, F751-760 (1995).

47. P. Q. Barrett, H. K. Lu, R. Colbran, A. Czernik, J. J. Pancrazio, Stimulation of unitary T-type Ca(2+) channel currents by calmodulin-dependent protein kinase II. *Am J Physiol Cell Physiol* **279**, C1694-1703 (2000).
48. C. Hu, C. G. Rusin, Z. Tan, N. A. Guagliardo, P. Q. Barrett, Zona glomerulosa cells of the mouse adrenal cortex are intrinsic electrical oscillators. *J. Clin. Invest.* **122**, 2046-2053 (2012).
49. J. A. Enyeart, S. J. Danthi, J. J. Enyeart, TREK-1 K+ channels couple angiotensin II receptors to membrane depolarization and aldosterone secretion in bovine adrenal glomerulosa cells. *Am J Physiol Endocrinol Metab* **287**, E1154-1165 (2004).
50. N. A. Guagliardo, J. Yao, C. Hu, E. M. Schertz, D. A. Tyson, R. M. Carey, D. A. Bayliss, P. Q. Barrett, TASK-3 channel deletion in mice recapitulates low-renin essential hypertension. *Hypertension* **59**, 999-1005 (2012).
51. H. Hibino, A. Inanobe, K. Furutani, S. Murakami, I. Findlay, Y. Kurachi, Inwardly rectifying potassium channels: their structure, function, and physiological roles. *Physiol Rev* **90**, 291-366 (2010).
52. E. Seidel, J. Schewe, U. I. Scholl, Genetic causes of primary aldosteronism. *Exp Mol Med* **51**, 1-12 (2019).
53. W. L. Miller, R. J. Auchus, The molecular biology, biochemistry, and physiology of human steroidogenesis and its disorders. *Endocr Rev* **32**, 81-151 (2011).
54. C. de Joussineau, I. Sahut-Barnola, I. Levy, E. Saloustros, P. Val, C. A. Stratakis, A. Martinez, The cAMP pathway and the control of adrenocortical development and growth. *Mol Cell Endocrinol* **351**, 28-36 (2012).
55. J. W. Conn, Presidential address. I. Painting background. II. Primary aldosteronism, a new clinical syndrome. *J Lab Clin Med* **45**, 3-17 (1955).
56. S. Patel, A. Rauf, H. Khan, T. Abu-Izneid, Renin-angiotensin-aldosterone (RAAS): The ubiquitous system for homeostasis and pathologies. *Biomed Pharmacother* **94**, 317-325 (2017).
57. M. Parasiliti-Caprino, C. Lopez, N. Prencipe, B. Lucatello, F. Settanni, G. Giraudo, D. Rossato, G. Mengozzi, E. Ghigo, A. Benso, M. Maccario, Prevalence of primary aldosteronism and association with cardiovascular complications in patients with resistant and refractory hypertension. *J Hypertens* **38**, 1841-1848 (2020).
58. B. Strauch, T. Zelinka, M. Hampf, R. Bernhardt, J. Widimsky, Jr., Prevalence of primary hyperaldosteronism in moderate to severe hypertension in the Central Europe region. *J Hum Hypertens* **17**, 349-352 (2003).
59. S. Monticone, F. D'Ascenzo, C. Moretti, T. A. Williams, F. Veglio, F. Gaita, P. Mulatero, Cardiovascular events and target organ damage in primary aldosteronism compared with essential hypertension: a systematic review and meta-analysis. *Lancet Diabetes Endocrinol* **6**, 41-50 (2018).
60. S. Monticone, J. Burrello, D. Tizzani, C. Bertello, A. Viola, F. Buffolo, L. Gabetti, G. Mengozzi, T. A. Williams, F. Rabbia, F. Veglio, P. Mulatero, Prevalence and Clinical Manifestations of Primary Aldosteronism Encountered in Primary Care Practice. *J Am Coll Cardiol* **69**, 1811-1820 (2017).
61. G. P. Rossi, G. Bernini, C. Caliumi, G. Desideri, B. Fabris, C. Ferri, C. Ganzaroli, G. Giacchetti, C. Letizia, M. Maccario, F. Mallamaci, M. Mannelli, M. J. Mattarello, A. Moretti, G. Palumbo, G. Parenti, E. Porteri, A. Semplicini, D. Rizzoni, E. Rossi, M. Boscaro, A. C. Pessina, F. Mantero, P. S. Investigators, A prospective study of the prevalence of primary aldosteronism in 1,125 hypertensive patients. *J Am Coll Cardiol* **48**, 2293-2300 (2006).

62. W. F. Young, Jr., Diagnosis and treatment of primary aldosteronism: practical clinical perspectives. *J Intern Med* **285**, 126-148 (2019).
63. G. P. Rossi, Primary Aldosteronism: JACC State-of-the-Art Review. *J Am Coll Cardiol* **74**, 2799-2811 (2019).
64. J. W. Funder, R. M. Carey, F. Mantero, M. H. Murad, M. Reincke, H. Shibata, M. Stowasser, W. F. Young, Jr., The Management of Primary Aldosteronism: Case Detection, Diagnosis, and Treatment: An Endocrine Society Clinical Practice Guideline. *J Clin Endocrinol Metab* **101**, 1889-1916 (2016).
65. T. A. Williams, J. W. M. Lenders, P. Mulatero, J. Burrello, M. Rottenkolber, C. Adolf, F. Satoh, L. Amar, M. Quinkler, J. Deinum, F. Beuschlein, K. K. Kitamoto, U. Pham, R. Morimoto, H. Umakoshi, A. Prejbisz, T. Kocjan, M. Naruse, M. Stowasser, T. Nishikawa, W. F. Young, Jr., C. E. Gomez-Sanchez, J. W. Funder, M. Reincke, i. Primary Aldosteronism Surgery Outcome, Outcomes after adrenalectomy for unilateral primary aldosteronism: an international consensus on outcome measures and analysis of remission rates in an international cohort. *Lancet Diabetes Endocrinol* **5**, 689-699 (2017).
66. G. L. Hundemer, G. C. Curhan, N. Yozamp, M. Wang, A. Vaidya, Cardiometabolic outcomes and mortality in medically treated primary aldosteronism: a retrospective cohort study. *Lancet Diabetes Endocrinol* **6**, 51-59 (2018).
67. A. Vaidya, G. L. Hundemer, K. Nanba, W. W. Parksook, J. M. Brown, Primary Aldosteronism: State-of-the-Art Review. *Am J Hypertens* **35**, 967-988 (2022).
68. N. Yozamp, A. Vaidya, The Prevalence of Primary Aldosteronism and Evolving Approaches for Treatment. *Curr Opin Endocr Metab Res* **8**, 30-39 (2019).
69. M. Choi, U. I. Scholl, P. Yue, P. Bjorklund, B. Zhao, C. Nelson-Williams, W. Ji, Y. Cho, A. Patel, C. J. Men, E. Lolis, M. V. Wisgerhof, D. S. Geller, S. Mane, P. Hellman, G. Westin, G. Akerstrom, W. Wang, T. Carling, R. P. Lifton, K+ channel mutations in adrenal aldosterone-producing adenomas and hereditary hypertension. *Science* **331**, 768-772 (2011).
70. U. I. Scholl, C. Nelson-Williams, P. Yue, R. Grekin, R. J. Wyatt, M. J. Dillon, R. Couch, L. K. Hammer, F. L. Harley, A. Farhi, W. H. Wang, R. P. Lifton, Hypertension with or without adrenal hyperplasia due to different inherited mutations in the potassium channel KCNJ5. *Proc Natl Acad Sci U S A* **109**, 2533-2538 (2012).
71. U. I. Scholl, G. Goh, G. Stolting, R. C. de Oliveira, M. Choi, J. D. Overton, A. L. Fonseca, R. Korah, L. F. Starker, J. W. Kunstman, M. L. Prasad, E. A. Hartung, N. Mauras, M. R. Benson, T. Brady, J. R. Shapiro, E. Loring, C. Nelson-Williams, S. K. Libutti, S. Mane, P. Hellman, G. Westin, G. Akerstrom, P. Bjorklund, T. Carling, C. Fahlke, P. Hidalgo, R. P. Lifton, Somatic and germline CACNA1D calcium channel mutations in aldosterone-producing adenomas and primary aldosteronism. *Nat Genet* **45**, 1050-1054 (2013).
72. E. A. Azizan, H. Poulsen, P. Tuluc, J. Zhou, M. V. Clausen, A. Lieb, C. Maniero, S. Garg, E. G. Bochukova, W. Zhao, L. H. Shaikh, C. A. Brighton, A. E. Teo, A. P. Davenport, T. Dekkers, B. Tops, B. Kusters, J. Ceral, G. S. Yeo, S. G. Neogi, I. McFarlane, N. Rosenfeld, F. Marass, J. Hadfield, W. Margas, K. Chaggar, M. Solar, J. Deinum, A. C. Dolphin, I. S. Farooqi, J. Striessnig, P. Nissen, M. J. Brown, Somatic mutations in ATP1A1 and CACNA1D underlie a common subtype of adrenal hypertension. *Nat Genet* **45**, 1055-1060 (2013).
73. U. I. Scholl, G. Stolting, C. Nelson-Williams, A. A. Vichot, M. Choi, E. Loring, M. L. Prasad, G. Goh, T. Carling, C. C. Juhlin, I. Quack, L. C. Rump, A. Thiel, M.

Lande, B. G. Frazier, M. Rasoulpour, D. L. Bowlin, C. B. Sethna, H. Trachtman, C. Fahlke, R. P. Lifton, Recurrent gain of function mutation in calcium channel CACNA1H causes early-onset hypertension with primary aldosteronism. *Elife* **4**, e06315 (2015).
74. K. Nanba, A. R. Blinder, J. Rege, N. G. Hattangady, T. Else, C. J. Liu, S. A. Tomlins, P. Vats, C. Kumar-Sinha, T. J. Giordano, W. E. Rainey, Somatic CACNA1H Mutation As a Cause of Aldosterone-Producing Adenoma. *Hypertension* **75**, 645-649 (2020).
75. U. I. Scholl, G. Stolting, J. Schewe, A. Thiel, H. Tan, C. Nelson-Williams, A. A. Vichot, S. C. Jin, E. Loring, V. Untiet, T. Yoo, J. Choi, S. Xu, A. Wu, M. Kirchner, P. Mertins, L. C. Rump, A. M. Onder, C. Gamble, D. McKenney, R. W. Lash, D. P. Jones, G. Chune, P. Gagliardi, M. Choi, R. Gordon, M. Stowasser, C. Fahlke, R. P. Lifton, CLCN2 chloride channel mutations in familial hyperaldosteronism type II. *Nat Genet* **50**, 349-354 (2018).
76. R. K. Dutta, T. Arnesen, A. Heie, M. Walz, P. Alesina, P. Soderkvist, O. Gimm, A somatic mutation in CLCN2 identified in a sporadic aldosterone-producing adenoma. *Eur J Endocrinol* **181**, K37-K41 (2019).
77. F. Beuschlein, S. Boulkroun, A. Osswald, T. Wieland, H. N. Nielsen, U. D. Lichtenauer, D. Penton, V. R. Schack, L. Amar, E. Fischer, A. Walther, P. Tauber, T. Schwarzmayr, S. Diener, E. Graf, B. Allolio, B. Samson-Couterie, A. Benecke, M. Quinkler, F. Fallo, P. F. Plouin, F. Mantero, T. Meitinger, P. Mulatero, X. Jeunemaitre, R. Warth, B. Vilsen, M. C. Zennaro, T. M. Strom, M. Reincke, Somatic mutations in ATP1A1 and ATP2B3 lead to aldosterone-producing adenomas and secondary hypertension. *Nat Genet* **45**, 440-444, 444e441-442 (2013).
78. X. Wu, E. A. B. Azizan, E. Goodchild, S. Garg, M. Hagiyama, C. P. Cabrera, F. L. Fernandes-Rosa, S. Boulkroun, J. L. Kuan, Z. Tiang, A. David, M. Murakami, C. A. Mein, E. Wozniak, W. Zhao, A. Marker, F. Buss, R. S. Saleeb, J. Salsbury, Y. Tezuka, F. Satoh, K. Oki, A. M. Udager, D. L. Cohen, H. Wachtel, P. J. King, W. M. Drake, M. Gurnell, J. Ceral, A. Ryska, M. Mustangin, Y. P. Wong, G. C. Tan, M. Solar, M. Reincke, W. E. Rainey, R. S. Foo, Y. Takaoka, S. A. Murray, M. C. Zennaro, F. Beuschlein, A. Ito, M. J. Brown, Somatic mutations of CADM1 in aldosterone-producing adenomas and gap junction-dependent regulation of aldosterone production. *Nat Genet* **55**, 1009-1021 (2023).
79. R. Juilee, N. Kazutaka, B. Sascha, K. Carla, R. B. Amy, V. Pankaj, K.-S. Chandan, M. L. Antonio, E. Tobias, Y. Yuto, S. Fumitoshi, S. Hironobu, J. G. Thomas, W. Tracy Ann, R. Martin, F. T. Adina, M. U. Aaron, W. Richard, E. R. William, Zinc transporter somatic gene mutations cause primary aldosteronism. *bioRxiv*, 2022.2007.2025.501443 (2022).
80. M. Tadjine, A. Lampron, L. Ouadi, I. Bourdeau, Frequent mutations of beta-catenin gene in sporadic secreting adrenocortical adenomas. *Clin Endocrinol (Oxf)* **68**, 264-270 (2008).
81. J. Zhou, E. A. B. Azizan, C. P. Cabrera, F. L. Fernandes-Rosa, S. Boulkroun, G. Argentesi, E. Cottrell, L. Amar, X. Wu, S. O'Toole, E. Goodchild, A. Marker, R. Senanayake, S. Garg, T. Akerstrom, S. Backman, S. Jordan, S. Polubothu, D. M. Berney, A. Gluck, K. E. Lines, R. V. Thakker, A. Tuthill, C. Joyce, J. P. Kaski, F. E. Karet Frankl, L. A. Metherell, A. E. D. Teo, M. Gurnell, L. Parvanta, W. M. Drake, E. Wozniak, D. Klinzing, J. L. Kuan, Z. Tiang, C. E. Gomez Sanchez, P. Hellman, R. S. Y. Foo, C. A. Mein, V. A. Kinsler, P. Bjorklund, H. L. Storr, M. C. Zennaro, M. J. Brown, Somatic mutations of GNA11 and GNAQ

in CTNNB1-mutant aldosterone-producing adenomas presenting in puberty, pregnancy or menopause. *Nat Genet* **53**, 1360-1372 (2021).
82. Y. Nakajima, T. Okamura, K. Horiguchi, T. Gohko, T. Miyamoto, T. Satoh, A. Ozawa, S. Ishii, E. Yamada, K. Hashimoto, S. Okada, D. Takata, J. Horiguchi, M. Yamada, GNAS mutations in adrenal aldosterone-producing adenomas. *Endocr J* **63**, 199-204 (2016).
83. Y. Rhayem, L. G. Perez-Rivas, A. Dietz, K. Bathon, C. Gebhard, A. Riester, B. Mauracher, C. Gomez-Sanchez, G. Eisenhofer, T. Schwarzmayr, D. Calebiro, T. M. Strom, M. Reincke, F. Beuschlein, PRKACA Somatic Mutations Are Rare Findings in Aldosterone-Producing Adenomas. *J. Clin. Endocrinol. Metab.* **101**, 3010-3017 (2016).
84. R. P. Lifton, R. G. Dluhy, M. Powers, G. M. Rich, S. Cook, S. Ulick, J. M. Lalouel, A chimaeric 11 beta-hydroxylase/aldosterone synthase gene causes glucocorticoid-remediable aldosteronism and human hypertension. *Nature* **355**, 262-265 (1992).
85. F. L. Fernandes-Rosa, T. A. Williams, A. Riester, O. Steichen, F. Beuschlein, S. Boulkroun, T. M. Strom, S. Monticone, L. Amar, T. Meatchi, F. Mantero, M. V. Cicala, M. Quinkler, F. Fallo, B. Allolio, G. Bernini, M. Maccario, G. Giacchetti, X. Jeunemaitre, P. Mulatero, M. Reincke, M. C. Zennaro, Genetic spectrum and clinical correlates of somatic mutations in aldosterone-producing adenoma. *Hypertension* **64**, 354-361 (2014).
86. R. Taguchi, M. Yamada, Y. Nakajima, T. Satoh, K. Hashimoto, N. Shibusawa, A. Ozawa, S. Okada, N. Rokutanda, D. Takata, Y. Koibuchi, J. Horiguchi, T. Oyama, I. Takeyoshi, M. Mori, Expression and mutations of KCNJ5 mRNA in Japanese patients with aldosterone-producing adenomas. *J Clin Endocrinol Metab* **97**, 1311-1319 (2012).
87. B. Wang, X. Li, X. Zhang, X. Ma, L. Chen, Y. Zhang, X. Lyu, Y. Tang, Q. Huang, Y. Gao, Y. Fan, J. Ouyang, Prevalence and characterization of somatic mutations in Chinese aldosterone-producing adenoma patients. *Medicine (Baltimore)* **94**, e708 (2015).
88. E. A. Azizan, M. Murthy, M. Stowasser, R. Gordon, B. Kowalski, S. Xu, M. J. Brown, K. M. O'Shaughnessy, Somatic mutations affecting the selectivity filter of KCNJ5 are frequent in 2 large unselected collections of adrenal aldosteronomas. *Hypertension* **59**, 587-591 (2012).
89. L. Lenzini, G. Rossitto, G. Maiolino, C. Letizia, J. W. Funder, G. P. Rossi, A Meta-Analysis of Somatic KCNJ5 K(+) Channel Mutations In 1636 Patients With an Aldosterone-Producing Adenoma. *J Clin Endocrinol Metab* **100**, E1089-1095 (2015).
90. A. Spat, L. Hunyady, Control of aldosterone secretion: a model for convergence in cellular signaling pathways. *Physiol Rev* **84**, 489-539 (2004).
91. A. M. Lerario, K. Nanba, A. R. Blinder, S. Suematsu, M. Omura, T. Nishikawa, T. J. Giordano, W. E. Rainey, T. Else, Genetics of aldosterone-producing adenomas with pathogenic KCNJ5 variants. *Endocr Relat Cancer* **26**, 463-470 (2019).
92. A. Tamura, K. Nishimoto, T. Seki, Y. Matsuzawa, J. Saito, M. Omura, C. E. Gomez-Sanchez, K. Makita, S. Matsui, N. Moriya, A. Inoue, M. Nagata, H. Sasano, Y. Nakamura, Y. Yamazaki, Y. Kabe, K. Mukai, T. Kosaka, M. Oya, S. Suematsu, T. Nishikawa, Somatic KCNJ5 mutation occurring early in adrenal development may cause a novel form of juvenile primary aldosteronism. *Mol Cell Endocrinol* **441**, 134-139 (2017).

93. P. Tauber, D. Penton, J. Stindl, E. Humberg, I. Tegtmeier, C. Sterner, F. Beuschlein, M. Reincke, J. Barhanin, S. Bandulik, R. Warth, Pharmacology and pathophysiology of mutated KCNJ5 found in adrenal aldosterone-producing adenomas. *Endocrinology* **155**, 1353-1362 (2014).
94. U. I. Scholl, L. Abriola, C. Zhang, E. N. Reimer, M. Plummer, B. I. Kazmierczak, J. Zhang, D. Hoyer, J. S. Merkel, W. Wang, R. P. Lifton, Macrolides selectively inhibit mutant KCNJ5 potassium channels that cause aldosterone-producing adenoma. *J Clin Invest* **127**, 2739-2750 (2017).
95. B. Caroccia, S. Prisco, T. M. Seccia, M. Piazza, G. Maiolino, G. P. Rossi, Macrolides Blunt Aldosterone Biosynthesis: A Proof-of-Concept Study in KCNJ5 Mutated Adenoma Cells Ex Vivo. *Hypertension* **70**, 1238-1242 (2017).
96. G. Maiolino, G. Ceolotto, M. Battistel, G. Barbiero, M. Cesari, L. Amar, B. Caroccia, R. Padrini, M. Azizi, G. P. Rossi, Macrolides for KCNJ5-mutated aldosterone-producing adenoma (MAPA): design of a study for personalized diagnosis of primary aldosteronism. *Blood Press* **27**, 200-205 (2018).
97. K. Nanba, K. Omata, T. Else, P. C. C. Beck, A. T. Nanba, A. F. Turcu, B. S. Miller, T. J. Giordano, S. A. Tomlins, W. E. Rainey, Targeted Molecular Characterization of Aldosterone-Producing Adenomas in White Americans. *J Clin Endocrinol Metab* **103**, 3869-3876 (2018).
98. K. Nanba, K. Omata, C. E. Gomez-Sanchez, C. A. Stratakis, A. P. Demidowich, M. Suzuki, L. D. R. Thompson, D. L. Cohen, J. M. Luther, L. Gellert, A. Vaidya, J. A. Barletta, T. Else, T. J. Giordano, S. A. Tomlins, W. E. Rainey, Genetic Characteristics of Aldosterone-Producing Adenomas in Blacks. *Hypertension* **73**, 885-892 (2019).
99. K. De Sousa, S. Boulkroun, S. Baron, K. Nanba, M. Wack, W. E. Rainey, A. Rocha, I. Giscos-Douriez, T. Meatchi, L. Amar, S. Travers, F. L. Fernandes-Rosa, M. C. Zennaro, Genetic, Cellular, and Molecular Heterogeneity in Adrenals With Aldosterone-Producing Adenoma. *Hypertension* **75**, 1034-1044 (2020).
100. G. Daniil, F. L. Fernandes-Rosa, J. Chemin, I. Blesneac, J. Beltrand, M. Polak, X. Jeunemaitre, S. Boulkroun, L. Amar, T. M. Strom, P. Lory, M. C. Zennaro, CACNA1H Mutations Are Associated With Different Forms of Primary Aldosteronism. *EBioMedicine* **13**, 225-236 (2016).
101. U. I. Scholl, J. M. Healy, A. Thiel, A. L. Fonseca, T. C. Brown, J. W. Kunstman, M. J. Horne, D. Dietrich, J. Riemer, S. Kucukkoylu, E. N. Reimer, A. C. Reis, G. Goh, G. Kristiansen, A. Mahajan, R. Korah, R. P. Lifton, M. L. Prasad, T. Carling, Novel somatic mutations in primary hyperaldosteronism are related to the clinical, radiological and pathological phenotype. *Clin Endocrinol (Oxf)* **83**, 779-789 (2015).
102. T. Akerstrom, R. Maharjan, H. Sven Willenberg, K. Cupisti, J. Ip, A. Moser, P. Stalberg, B. Robinson, K. Alexander Iwen, H. Dralle, M. K. Walz, H. Lehnert, S. Sidhu, C. Gomez-Sanchez, P. Hellman, P. Bjorklund, Activating mutations in CTNNB1 in aldosterone producing adenomas. *Sci Rep* **6**, 19546 (2016).
103. M. Tetti, S. Gong, F. Veglio, M. Reincke, T. A. Williams, Primary aldosteronism: Pathophysiological mechanisms of cell death and proliferation. *Front Endocrinol (Lausanne)* **13**, 934326 (2022).
104. A. Berthon, C. Drelon, B. Ragazzon, S. Boulkroun, F. Tissier, L. Amar, B. Samson-Couterie, M. C. Zennaro, P. F. Plouin, S. Skah, M. Plateroti, H. Lefebvre, I. Sahut-Barnola, M. Batisse-Lignier, G. Assie, A. M. Lefrancois-Martinez, J. Bertherat, A. Martinez, P. Val, WNT/beta-catenin signalling is

activated in aldosterone-producing adenomas and controls aldosterone production. *Hum Mol Genet* **23**, 889-905 (2014).
105. A. Berthon, I. Sahut-Barnola, S. Lambert-Langlais, C. de Joussineau, C. Damon-Soubeyrand, E. Louiset, M. M. Taketo, F. Tissier, J. Bertherat, A. M. Lefrancois-Martinez, A. Martinez, P. Val, Constitutive beta-catenin activation induces adrenal hyperplasia and promotes adrenal cancer development. *Hum Mol Genet* **19**, 1561-1576 (2010).
106. C. E. Gomez-Sanchez, E. P. Gomez-Sanchez, Mutations of the potassium channel KCNJ5 causing aldosterone-producing adenomas: one or two hits? *Hypertension* **59**, 196-197 (2012).
107. M. C. Zennaro, S. Boulkroun, F. Fernandes-Rosa, Genetic Causes of Functional Adrenocortical Adenomas. *Endocr Rev* **38**, 516-537 (2017).
108. A. X. Chen, K. Nishimoto, K. Nanba, W. E. Rainey, Potassium channels related to primary aldosteronism: Expression similarities and differences between human and rat adrenals. *Mol Cell Endocrinol* **417**, 141-148 (2015).
109. I. Hardege, L. Long, R. Al Maskari, N. Figg, K. M. O'Shaughnessy, Targeted disruption of the Kcnj5 gene in the female mouse lowers aldosterone levels. *Clin Sci (Lond)* **132**, 145-156 (2018).
110. U. Lichtenauer, P. L. Schmid, A. Oßwald, I. Renner-Müller, M. Reincke, R. Warth, E. Wolf, F. Beuschlein, Establishment of an in vivo model for KCNJ5 dependent hyperaldosteronism. *Exp Clin Endocrinol Diabetes* **123**, P09_25 (2015).
111. D. Heitzmann, R. Derand, S. Jungbauer, S. Bandulik, C. Sterner, F. Schweda, A. El Wakil, E. Lalli, N. Guy, R. Mengual, M. Reichold, I. Tegtmeier, S. Bendahhou, C. E. Gomez-Sanchez, M. I. Aller, W. Wisden, A. Weber, F. Lesage, R. Warth, J. Barhanin, Invalidation of TASK1 potassium channels disrupts adrenal gland zonation and mineralocorticoid homeostasis. *EMBO J* **27**, 179-187 (2008).
112. D. Penton, S. Bandulik, F. Schweda, S. Haubs, P. Tauber, M. Reichold, L. D. Cong, A. El Wakil, T. Budde, F. Lesage, E. Lalli, M. C. Zennaro, R. Warth, J. Barhanin, Task3 potassium channel gene invalidation causes low renin and salt-sensitive arterial hypertension. *Endocrinology* **153**, 4740-4748 (2012).
113. S. Bandulik, P. Tauber, D. Penton, F. Schweda, I. Tegtmeier, C. Sterner, E. Lalli, F. Lesage, M. Hartmann, J. Barhanin, R. Warth, Severe hyperaldosteronism in neonatal Task3 potassium channel knockout mice is associated with activation of the intraadrenal renin-angiotensin system. *Endocrinology* **154**, 2712-2722 (2013).
114. L. A. Davies, C. Hu, N. A. Guagliardo, N. Sen, X. Chen, E. M. Talley, R. M. Carey, D. A. Bayliss, P. Q. Barrett, TASK channel deletion in mice causes primary hyperaldosteronism. *Proc Natl Acad Sci U S A* **105**, 2203-2208 (2008).
115. N. A. Guagliardo, J. Yao, E. J. Stipes, S. Cechova, T. H. Le, D. A. Bayliss, D. T. Breault, P. Q. Barrett, Adrenal Tissue-Specific Deletion of TASK Channels Causes Aldosterone-Driven Angiotensin II-Independent Hypertension. *Hypertension* **73**, 407-414 (2019).
116. L. J. Lenk. (TiHo eLib, 2022).
117. K. Oki, M. W. Plonczynski, M. Luis Lam, E. P. Gomez-Sanchez, C. E. Gomez-Sanchez, Potassium channel mutant KCNJ5 T158A expression in HAC-15 cells increases aldosterone synthesis. *Endocrinology* **153**, 1774-1782 (2012).
118. Y. Yang, C. E. Gomez-Sanchez, D. Jaquin, E. T. Aristizabal Prada, L. S. Meyer, T. Knosel, H. Schneider, F. Beuschlein, M. Reincke, T. A. Williams, Primary

Aldosteronism: KCNJ5 Mutations and Adrenocortical Cell Growth. *Hypertension* **74**, 809-816 (2019).
119. M. J. Evans, M. H. Kaufman, Establishment in culture of pluripotential cells from mouse embryos. *Nature* **292**, 154-156 (1981).
120. G. R. Martin, Isolation of a pluripotent cell line from early mouse embryos cultured in medium conditioned by teratocarcinoma stem cells. *Proc Natl Acad Sci U S A* **78**, 7634-7638 (1981).
121. J. A. Thomson, J. Itskovitz-Eldor, S. S. Shapiro, M. A. Waknitz, J. J. Swiergiel, V. S. Marshall, J. M. Jones, Embryonic stem cell lines derived from human blastocysts. *Science* **282**, 1145-1147 (1998).
122. K. Takahashi, S. Yamanaka, Induction of pluripotent stem cells from mouse embryonic and adult fibroblast cultures by defined factors. *Cell* **126**, 663-676 (2006).
123. K. Takahashi, K. Tanabe, M. Ohnuki, M. Narita, T. Ichisaka, K. Tomoda, S. Yamanaka, Induction of pluripotent stem cells from adult human fibroblasts by defined factors. *Cell* **131**, 861-872 (2007).
124. Y. Shi, H. Inoue, J. C. Wu, S. Yamanaka, Induced pluripotent stem cell technology: a decade of progress. *Nat Rev Drug Discov* **16**, 115-130 (2017).
125. R. G. Rowe, G. Q. Daley, Induced pluripotent stem cells in disease modelling and drug discovery. *Nat Rev Genet* **20**, 377-388 (2019).
126. X. Lian, C. Hsiao, G. Wilson, K. Zhu, L. B. Hazeltine, S. M. Azarin, K. K. Raval, J. Zhang, T. J. Kamp, S. P. Palecek, Robust cardiomyocyte differentiation from human pluripotent stem cells via temporal modulation of canonical Wnt signaling. *Proc Natl Acad Sci U S A* **109**, E1848-1857 (2012).
127. T. Takebe, K. Sekine, M. Enomura, H. Koike, M. Kimura, T. Ogaeri, R. R. Zhang, Y. Ueno, Y. W. Zheng, N. Koike, S. Aoyama, Y. Adachi, H. Taniguchi, Vascularized and functional human liver from an iPSC-derived organ bud transplant. *Nature* **499**, 481-484 (2013).
128. R. Morizane, J. V. Bonventre, Generation of nephron progenitor cells and kidney organoids from human pluripotent stem cells. *Nat Protoc* **12**, 195-207 (2017).
129. B. Y. Hu, J. P. Weick, J. Yu, L. X. Ma, X. Q. Zhang, J. A. Thomson, S. C. Zhang, Neural differentiation of human induced pluripotent stem cells follows developmental principles but with variable potency. *Proc Natl Acad Sci U S A* **107**, 4335-4340 (2010).
130. T. Yazawa, S. Kawabe, Y. Inaoka, R. Okada, T. Mizutani, Y. Imamichi, Y. Ju, Y. Yamazaki, Y. Usami, M. Kuribayashi, A. Umezawa, K. Miyamoto, Differentiation of mesenchymal stem cells and embryonic stem cells into steroidogenic cells using steroidogenic factor-1 and liver receptor homolog-1. *Mol Cell Endocrinol* **336**, 127-132 (2011).
131. T. Sonoyama, M. Sone, K. Honda, D. Taura, K. Kojima, M. Inuzuka, N. Kanamoto, N. Tamura, K. Nakao, Differentiation of human embryonic stem cells and human induced pluripotent stem cells into steroid-producing cells. *Endocrinology* **153**, 4336-4345 (2012).
132. L. Li, Y. Li, C. Sottas, M. Culty, J. Fan, Y. Hu, G. Cheung, H. E. Chemes, V. Papadopoulos, Directing differentiation of human induced pluripotent stem cells toward androgen-producing Leydig cells rather than adrenal cells. *Proc Natl Acad Sci U S A* **116**, 23274-23283 (2019).
133. T. Yazawa, T. Mizutani, K. Yamada, H. Kawata, T. Sekiguchi, M. Yoshino, T. Kajitani, Z. Shou, A. Umezawa, K. Miyamoto, Differentiation of adult stem cells

derived from bone marrow stroma into Leydig or adrenocortical cells. *Endocrinology* **147**, 4104-4111 (2006).
134. S. Gondo, T. Okabe, T. Tanaka, H. Morinaga, M. Nomura, R. Takayanagi, H. Nawata, T. Yanase, Adipose tissue-derived and bone marrow-derived mesenchymal cells develop into different lineage of steroidogenic cells by forced expression of steroidogenic factor 1. *Endocrinology* **149**, 4717-4725 (2008).
135. G. Ruiz-Babot, M. Balyura, I. Hadjidemetriou, S. J. Ajodha, D. R. Taylor, L. Ghataore, N. F. Taylor, U. Schubert, C. G. Ziegler, H. L. Storr, M. R. Druce, E. F. Gevers, W. M. Drake, U. Srirangalingam, G. S. Conway, P. J. King, L. A. Metherell, S. R. Bornstein, L. Guasti, Modeling Congenital Adrenal Hyperplasia and Testing Interventions for Adrenal Insufficiency Using Donor-Specific Reprogrammed Cells. *Cell Rep* **22**, 1236-1249 (2018).
136. T. Yazawa, Y. Inaoka, R. Okada, T. Mizutani, Y. Yamazaki, Y. Usami, M. Kuribayashi, M. Orisaka, A. Umezawa, K. Miyamoto, PPAR-gamma coactivator-1alpha regulates progesterone production in ovarian granulosa cells with SF-1 and LRH-1. *Mol Endocrinol* **24**, 485-496 (2010).
137. T. Yazawa, Y. Imamichi, K. Miyamoto, M. R. Khan, J. Uwada, A. Umezawa, T. Taniguchi, Induction of steroidogenic cells from adult stem cells and pluripotent stem cells [Review]. *Endocr J* **63**, 943-951 (2016).
138. T. Yazawa, M. Uesaka, Y. Inaoka, T. Mizutani, T. Sekiguchi, T. Kajitani, T. Kitano, A. Umezawa, K. Miyamoto, Cyp11b1 is induced in the murine gonad by luteinizing hormone/human chorionic gonadotropin and involved in the production of 11-ketotestosterone, a major fish androgen: conservation and evolution of the androgen metabolic pathway. *Endocrinology* **149**, 1786-1792 (2008).
139. T. Yazawa, Y. Inanoka, T. Mizutani, M. Kuribayashi, A. Umezawa, K. Miyamoto, Liver receptor homolog-1 regulates the transcription of steroidogenic enzymes and induces the differentiation of mesenchymal stem cells into steroidogenic cells. *Endocrinology* **150**, 3885-3893 (2009).
140. T. Mizutani, T. Yazawa, Y. Ju, Y. Imamichi, M. Uesaka, Y. Inaoka, K. Matsuura, Y. Kamiki, M. Oki, A. Umezawa, K. Miyamoto, Identification of a novel distal control region upstream of the human steroidogenic acute regulatory protein (StAR) gene that participates in SF-1-dependent chromatin architecture. *J Biol Chem* **285**, 28240-28251 (2010).
141. K. Matsuo, M. Sone, K. Honda-Kohmo, T. Toyohara, T. Sonoyama, D. Taura, K. Kojima, Y. Fukuda, Y. Ohno, M. Inoue, A. Ohta, K. Osafune, K. Nakao, N. Inagaki, Significance of dopamine D1 receptor signalling for steroidogenic differentiation of human induced pluripotent stem cells. *Sci Rep* **7**, 15120 (2017).
142. K. Yanagibashi, M. Haniu, J. E. Shively, W. H. Shen, P. Hall, The synthesis of aldosterone by the adrenal cortex. Two zones (fasciculata and glomerulosa) possess one enzyme for 11 beta-, 18-hydroxylation, and aldehyde synthesis. *J Biol Chem* **261**, 3556-3562 (1986).
143. A. F. Gazdar, H. K. Oie, C. H. Shackleton, T. R. Chen, T. J. Triche, C. E. Myers, G. P. Chrousos, M. F. Brennan, C. A. Stein, R. V. La Rocca, Establishment and characterization of a human adrenocortical carcinoma cell line that expresses multiple pathways of steroid biosynthesis. *Cancer Res* **50**, 5488-5496 (1990).

144. U. D. Lichtenauer, I. Shapiro, A. Osswald, S. Meurer, A. Kulle, M. Reincke, F. Riepe, F. Beuschlein, Characterization of NCI-H295R cells as an in vitro model of hyperaldosteronism. *Horm Metab Res* **45**, 124-129 (2013).
145. F. Tissier, C. Cavard, L. Groussin, K. Perlemoine, G. Fumey, A. M. Hagnere, F. Rene-Corail, E. Jullian, C. Gicquel, X. Bertagna, M. C. Vacher-Lavenu, C. Perret, J. Bertherat, Mutations of beta-catenin in adrenocortical tumors: activation of the Wnt signaling pathway is a frequent event in both benign and malignant adrenocortical tumors. *Cancer Res* **65**, 7622-7627 (2005).
146. T. Wang, W. E. Rainey, Human adrenocortical carcinoma cell lines. *Mol Cell Endocrinol* **351**, 58-65 (2012).
147. E. Samandari, P. Kempna, J. M. Nuoffer, G. Hofer, P. E. Mullis, C. E. Fluck, Human adrenal corticocarcinoma NCI-H295R cells produce more androgens than NCI-H295A cells and differ in 3beta-hydroxysteroid dehydrogenase type 2 and 17,20 lyase activities. *J Endocrinol* **195**, 459-472 (2007).
148. L. H. Maynard, O. Humbert, C. W. Peterson, H. P. Kiem, Genome editing in large animal models. *Mol Ther* **29**, 3140-3152 (2021).
149. D. R. Rodriguez-Rodriguez, R. Ramirez-Solis, M. A. Garza-Elizondo, M. L. Garza-Rodriguez, H. A. Barrera-Saldana, Genome editing: A perspective on the application of CRISPR/Cas9 to study human diseases (Review). *Int J Mol Med* **43**, 1559-1574 (2019).
150. S. I. Mae, A. Shono, F. Shiota, T. Yasuno, M. Kajiwara, N. Gotoda-Nishimura, S. Arai, A. Sato-Otubo, T. Toyoda, K. Takahashi, N. Nakayama, C. A. Cowan, T. Aoi, S. Ogawa, A. P. McMahon, S. Yamanaka, K. Osafune, Monitoring and robust induction of nephrogenic intermediate mesoderm from human pluripotent stem cells. *Nat Commun* **4**, 1367 (2013).
151. A. Q. Lam, B. S. Freedman, R. Morizane, P. H. Lerou, M. T. Valerius, J. V. Bonventre, Rapid and efficient differentiation of human pluripotent stem cells into intermediate mesoderm that forms tubules expressing kidney proximal tubular markers. *J Am Soc Nephrol* **25**, 1211-1225 (2014).
152. F. A. Ran, P. D. Hsu, J. Wright, V. Agarwala, D. A. Scott, F. Zhang, Genome engineering using the CRISPR-Cas9 system. *Nat Protoc* **8**, 2281-2308 (2013).
153. L. Lam, W. W. Chiu, J. S. Davidson, Overestimation of Aldosterone by Immunoassay in Renal Impairment. *Clin Chem* **62**, 890-891 (2016).
154. R. Morizane, A. Q. Lam, B. S. Freedman, S. Kishi, M. T. Valerius, J. V. Bonventre, Nephron organoids derived from human pluripotent stem cells model kidney development and injury. *Nat Biotechnol* **33**, 1193-1200 (2015).
155. N. Kumar, J. Richter, J. Cutts, K. T. Bush, C. Trujillo, S. K. Nigam, T. Gaasterland, D. Brafman, K. Willert, Generation of an expandable intermediate mesoderm restricted progenitor cell line from human pluripotent stem cells. *Elife* **4**, (2015).
156. R. C. Lindsley, J. G. Gill, M. Kyba, T. L. Murphy, K. M. Murphy, Canonical Wnt signaling is required for development of embryonic stem cell-derived mesoderm. *Development* **133**, 3787-3796 (2006).
157. H. Lickert, B. Cox, C. Wehrle, M. M. Taketo, R. Kemler, J. Rossant, Dissecting Wnt/beta-catenin signaling during gastrulation using RNA interference in mouse embryos. *Development* **132**, 2599-2609 (2005).
158. J. Rossant, P. P. Tam, Emerging asymmetry and embryonic patterning in early mouse development. *Dev Cell* **7**, 155-164 (2004).
159. P. Gadue, T. L. Huber, P. J. Paddison, G. M. Keller, Wnt and TGF-beta signaling are required for the induction of an in vitro model of primitive streak

formation using embryonic stem cells. *Proc Natl Acad Sci U S A* **103**, 16806-16811 (2006).
160. T. Sumi, N. Tsuneyoshi, N. Nakatsuji, H. Suemori, Defining early lineage specification of human embryonic stem cells by the orchestrated balance of canonical Wnt/beta-catenin, Activin/Nodal and BMP signaling. *Development* **135**, 2969-2979 (2008).
161. R. G. James, C. N. Kamei, Q. Wang, R. Jiang, T. M. Schultheiss, Odd-skipped related 1 is required for development of the metanephric kidney and regulates formation and differentiation of kidney precursor cells. *Development* **133**, 2995-3004 (2006).
162. J. W. Mugford, P. Sipila, J. A. McMahon, A. P. McMahon, Osr1 expression demarcates a multi-potent population of intermediate mesoderm that undergoes progressive restriction to an Osr1-dependent nephron progenitor compartment within the mammalian kidney. *Dev Biol* **324**, 88-98 (2008).
163. A. Guhr, S. Kobold, S. Seltmann, A. E. M. Seiler Wulczyn, A. Kurtz, P. Loser, Recent Trends in Research with Human Pluripotent Stem Cells: Impact of Research and Use of Cell Lines in Experimental Research and Clinical Trials. *Stem Cell Reports* **11**, 485-496 (2018).
164. N. G. Hattangady, L. O. Olala, W. B. Bollag, W. E. Rainey, Acute and chronic regulation of aldosterone production. *Mol. Cell. Endocrinol.* **350**, 151-162 (2012).
165. C. Ruggiero, E. Lalli, Impact of ACTH Signaling on Transcriptional Regulation of Steroidogenic Genes. *Front Endocrinol (Lausanne)* **7**, 24 (2016).
166. E. M. Walczak, R. Kuick, I. Finco, N. Bohin, S. M. Hrycaj, D. M. Wellik, G. D. Hammer, Wnt signaling inhibits adrenal steroidogenesis by cell-autonomous and non-cell-autonomous mechanisms. *Mol Endocrinol* **28**, 1471-1486 (2014).
167. I. Hadjidemetriou, K. Mariniello, G. Ruiz-Babot, J. Pittaway, A. Mancini, D. Mariannis, C. E. Gomez-Sanchez, L. Parvanta, W. M. Drake, T. T. Chung, T. E. Abdel-Aziz, A. DiMarco, F. F. Palazzo, M. E. Wierman, K. Kiseljak-Vassiliades, P. J. King, L. Guasti, DLK1/PREF1 marks a novel cell population in the human adrenal cortex. *J Steroid Biochem Mol Biol* **193**, 105422 (2019).
168. A. DeLaurier, R. Schweitzer, M. Logan, Pitx1 determines the morphology of muscle, tendon, and bones of the hindlimb. *Dev Biol* **299**, 22-34 (2006).
169. C. Niehrs, Function and biological roles of the Dickkopf family of Wnt modulators. *Oncogene* **25**, 7469-7481 (2006).
170. X. Zhang, N. Zhong, X. Li, M. B. Chen, TRIB3 promotes lung cancer progression by activating beta-catenin signaling. *Eur J Pharmacol* **863**, 172697 (2019).
171. C. J. Groger, M. Grubinger, T. Waldhor, K. Vierlinger, W. Mikulits, Meta-analysis of gene expression signatures defining the epithelial to mesenchymal transition during cancer progression. *PLoS One* **7**, e51136 (2012).
172. J. P. Lopez, E. Brivio, A. Santambrogio, C. De Donno, A. Kos, M. Peters, N. Rost, D. Czamara, T. M. Bruckl, S. Roeh, M. L. Pohlmann, C. Engelhardt, A. Ressle, R. Stoffel, A. Tontsch, J. M. Villamizar, M. Reincke, A. Riester, S. Sbiera, M. Fassnacht, H. S. Mayberg, W. E. Craighead, B. W. Dunlop, C. B. Nemeroff, M. V. Schmidt, E. B. Binder, F. J. Theis, F. Beuschlein, C. L. Andoniadou, A. Chen, Single-cell molecular profiling of all three components of the HPA axis reveals adrenal ABCB1 as a regulator of stress adaptation. *Sci Adv* **7**, (2021).

173. R. Verardo, S. Piazza, E. Klaric, Y. Ciani, G. Bussadori, S. Marzinotto, L. Mariuzzi, D. Cesselli, A. P. Beltrami, M. Mano, M. Itoh, H. Kawaji, T. Lassmann, P. Carninci, Y. Hayashizaki, A. R. Forrest, C. Fantom, C. A. Beltrami, C. Schneider, Specific mesothelial signature marks the heterogeneity of mesenchymal stem cells from high-grade serous ovarian cancer. *Stem Cells* **32**, 2998-3011 (2014).
174. A. Scialdone, Y. Tanaka, W. Jawaid, V. Moignard, N. K. Wilson, I. C. Macaulay, J. C. Marioni, B. Gottgens, Resolving early mesoderm diversification through single-cell expression profiling. *Nature* **535**, 289-293 (2016).
175. E. S. Hanemaaijer, T. Margaritis, K. Sanders, F. L. Bos, T. Candelli, H. Al-Saati, M. M. van Noesel, F. A. G. Meyer-Wentrup, M. van de Wetering, F. C. P. Holstege, H. Clevers, Single-cell atlas of developing murine adrenal gland reveals relation of Schwann cell precursor signature to neuroblastoma phenotype. *Proc Natl Acad Sci U S A* **118**, (2021).
176. A. Sebastian, N. R. Hum, K. A. Martin, S. F. Gilmore, I. Peran, S. W. Byers, E. K. Wheeler, M. A. Coleman, G. G. Loots, Single-Cell Transcriptomic Analysis of Tumor-Derived Fibroblasts and Normal Tissue-Resident Fibroblasts Reveals Fibroblast Heterogeneity in Breast Cancer. *Cancers (Basel)* **12**, (2020).
177. Y. Zhou, J. Williams, P. M. Smallwood, J. Nathans, Sox7, Sox17, and Sox18 Cooperatively Regulate Vascular Development in the Mouse Retina. *PLoS One* **10**, e0143650 (2015).
178. D. Paquet, D. Kwart, A. Chen, A. Sproul, S. Jacob, S. Teo, K. M. Olsen, A. Gregg, S. Noggle, M. Tessier-Lavigne, Efficient introduction of specific homozygous and heterozygous mutations using CRISPR/Cas9. *Nature* **533**, 125-129 (2016).
179. A. E. Taylor, B. Keevil, I. T. Huhtaniemi, Mass spectrometry and immunoassay: how to measure steroid hormones today and tomorrow. *Eur J Endocrinol* **173**, D1-12 (2015).
180. A. N. Hoofnagle, M. H. Wener, The fundamental flaws of immunoassays and potential solutions using tandem mass spectrometry. *J Immunol Methods* **347**, 3-11 (2009).
181. K. Ghazal, S. Brabant, D. Prie, M. L. Piketty, Hormone Immunoassay Interference: A 2021 Update. *Ann Lab Med* **42**, 3-23 (2022).
182. J. C. Jones, G. D. Carter, G. A. MacGregor, Interference by polar metabolites in a direct radioimmunoassay for plasma aldosterone. *Ann Clin Biochem* **18**, 54-59 (1981).
183. T. Bledsoe, G. W. Liddle, A. Riondel, D. P. Island, D. Bloomfield, B. Sinclair-Smith, Comparative fates of intravenously and orally administered aldosterone: evidence for extrahepatic formation of acid-hydrolyzable conjugate in man. *J Clin Invest* **45**, 264-269 (1966).
184. T. M. Seccia, B. Caroccia, E. P. Gomez-Sanchez, P. E. Vanderriele, C. E. Gomez-Sanchez, G. P. Rossi, Review of Markers of Zona Glomerulosa and Aldosterone-Producing Adenoma Cells. *Hypertension* **70**, 867-874 (2017).
185. K. J. Basham, S. Rodriguez, A. F. Turcu, A. M. Lerario, C. Y. Logan, M. R. Rysztak, C. E. Gomez-Sanchez, D. T. Breault, B. K. Koo, H. Clevers, R. Nusse, P. Val, G. D. Hammer, A ZNRF3-dependent Wnt/beta-catenin signaling gradient is required for adrenal homeostasis. *Genes Dev* **33**, 209-220 (2019).
186. A. Menard, N. Abou Nader, A. Levasseur, G. St-Jean, M. L. G. Le Roy, D. Boerboom, M. O. Benoit-Biancamano, A. Boyer, Targeted Disruption of Lats1

and Lats2 in Mice Impairs Adrenal Cortex Development and Alters Adrenocortical Cell Fate. *Endocrinology* **161**, (2020).
187. K. Matsuzaki, K. Kimura, K. Kurokawa, T. Miyazaki, Identification of aldosterone metabolites formed by A6 cells. *J Steroid Biochem Mol Biol* **38**, 657-662 (1991).
188. U. I. Scholl, Genetics of Primary Aldosteronism. *Hypertension* **79**, 887-897 (2022).
189. L. Aragao-Santiago, C. E. Gomez-Sanchez, P. Mulatero, A. Spyroglou, M. Reincke, T. A. Williams, Mouse Models of Primary Aldosteronism: From Physiology to Pathophysiology. *Endocrinology* **158**, 4129-4138 (2017).
190. J. Schewe, E. Seidel, S. Forslund, L. Marko, J. Peters, D. N. Muller, C. Fahlke, G. Stolting, U. Scholl, Elevated aldosterone and blood pressure in a mouse model of familial hyperaldosteronism with ClC-2 mutation. *Nat. Commun.* **10**, 5155 (2019).
191. E. Seidel, J. Schewe, J. Zhang, H. A. Dinh, S. K. Forslund, L. Marko, N. Hellmig, J. Peters, D. N. Muller, R. P. Lifton, T. Nottoli, G. Stolting, U. I. Scholl, Enhanced Ca(2+) signaling, mild primary aldosteronism, and hypertension in a familial hyperaldosteronism mouse model (Cacna1h (M1560V/+)). *Proc. Natl. Acad. Sci. U. S. A.* **118**, (2021).
192. T. Wang, J. G. Rowland, J. Parmar, M. Nesterova, T. Seki, W. E. Rainey, Comparison of aldosterone production among human adrenocortical cell lines. *Horm Metab Res* **44**, 245-250 (2012).
193. F. L. Fernandes-Rosa, S. Boulkroun, M. C. Zennaro, Genetic and Genomic Mechanisms of Primary Aldosteronism. *Trends Mol. Med.* **26**, 819-832 (2020).
194. S. Boulkroun, F. L. Fernandes-Rosa, M. C. Zennaro, Molecular and Cellular Mechanisms of Aldosterone Producing Adenoma Development. *Front Endocrinol (Lausanne)* **6**, 95 (2015).
195. R. L. Rushworth, D. J. Torpy, H. Falhammar, Adrenal Crisis. Reply. *N Engl J Med* **381**, 2182-2183 (2019).
196. S. R. Bornstein, B. Allolio, W. Arlt, A. Barthel, A. Don-Wauchope, G. D. Hammer, E. S. Husebye, D. P. Merke, M. H. Murad, C. A. Stratakis, D. J. Torpy, Diagnosis and Treatment of Primary Adrenal Insufficiency: An Endocrine Society Clinical Practice Guideline. *J Clin Endocrinol Metab* **101**, 364-389 (2016).
197. J. Suzuki, F. Otsuka, K. Inagaki, M. Takeda, T. Ogura, H. Makino, Novel action of activin and bone morphogenetic protein in regulating aldosterone production by human adrenocortical cells. *Endocrinology* **145**, 639-649 (2004).
198. J. Rege, H. K. Nishimoto, K. Nishimoto, R. J. Rodgers, R. J. Auchus, W. E. Rainey, Bone Morphogenetic Protein-4 (BMP4): A Paracrine Regulator of Human Adrenal C19 Steroid Synthesis. *Endocrinology* **156**, 2530-2540 (2015).
199. A. Penhoat, W. E. Rainey, I. Viard, J. M. Saez, Regulation of adrenal cell-differentiated functions by growth factors. *Horm Res* **42**, 39-43 (1994).
200. B. Caroccia, A. Fassina, T. M. Seccia, C. Recarti, L. Petrelli, A. S. Belloni, M. R. Pelizzo, G. P. Rossi, Isolation of human adrenocortical aldosterone-producing cells by a novel immunomagnetic beads method. *Endocrinology* **151**, 1375-1380 (2010).
201. M. A. Lancaster, M. Renner, C. A. Martin, D. Wenzel, L. S. Bicknell, M. E. Hurles, T. Homfray, J. M. Penninger, A. P. Jackson, J. A. Knoblich, Cerebral organoids model human brain development and microcephaly. *Nature* **501**, 373-379 (2013).

202. K. W. McCracken, E. M. Cata, C. M. Crawford, K. L. Sinagoga, M. Schumacher, B. E. Rockich, Y. H. Tsai, C. N. Mayhew, J. R. Spence, Y. Zavros, J. M. Wells, Modelling human development and disease in pluripotent stem-cell-derived gastric organoids. *Nature* **516**, 400-404 (2014).
203. M. Takasato, P. X. Er, H. S. Chiu, B. Maier, G. J. Baillie, C. Ferguson, R. G. Parton, E. J. Wolvetang, M. S. Roost, S. M. Chuva de Sousa Lopes, M. H. Little, Kidney organoids from human iPS cells contain multiple lineages and model human nephrogenesis. *Nature* **526**, 564-568 (2015).
204. A. Haidan, S. R. Bornstein, A. Glasow, K. Uhlmann, C. Lubke, M. Ehrhart-Bornstein, Basal steroidogenic activity of adrenocortical cells is increased 10-fold by coculture with chromaffin cells. *Endocrinology* **139**, 772-780 (1998).
205. S. Kanton, S. P. Pasca, Human assembloids. *Development* **149**, (2022).

Statutory Declaration / Eidesstattliche Versicherung

„Ich, Kieu Nhi Tran Vo, versichere an Eides statt durch meine eigenhändige Unterschrift, dass ich die vorgelegte Dissertation mit dem Thema: Untersuchung einer *KCNJ5*-Mutation beim Primären Hyperaldosteronismus in einem adrenokortikalen Zellmodell aus humanen induzierten pluripotenten Stammzellen (Human Induced Pluripotent Stem Cell-derived Adrenocortical Cell Model Reveals the Pathophysiology of *KCNJ5* Mutation in Primary Aldosteronism) selbstständig und ohne nicht offengelegte Hilfe Dritter verfasst und keine anderen als die angegebenen Quellen und Hilfsmittel genutzt habe.

Alle Stellen, die wörtlich oder dem Sinne nach auf Publikationen oder Vorträgen anderer Autoren/innen beruhen, sind als solche in korrekter Zitierung kenntlich gemacht. Die Abschnitte zu Methodik (insbesondere praktische Arbeiten, Laborbestimmungen, statistische Aufarbeitung) und Resultaten (insbesondere Abbildungen, Graphiken und Tabellen) werden von mir verantwortet.

Ich versichere ferner, dass ich die in Zusammenarbeit mit anderen Personen generierten Daten, Datenauswertungen und Schlussfolgerungen korrekt gekennzeichnet und meinen eigenen Beitrag sowie die Beiträge anderer Personen korrekt kenntlich gemacht habe (siehe Anteilserklärung). Texte oder Textteile, die gemeinsam mit anderen erstellt oder verwendet wurden, habe ich korrekt kenntlich gemacht.

Meine Anteile an etwaigen Publikationen zu dieser Dissertation entsprechen denen, die in der untenstehenden gemeinsamen Erklärung mit dem/der Erstbetreuer/in, angegeben sind. Für sämtliche im Rahmen der Dissertation entstandenen Publikationen wurden die Richtlinien des ICMJE (International Committee of Medical Journal Editors; www.icmje.og) zur Autorenschaft eingehalten. Ich erkläre ferner, dass ich mich zur Einhaltung der Satzung der Charité – Universitätsmedizin Berlin zur Sicherung Guter Wissenschaftlicher Praxis verpflichte.

Weiterhin versichere ich, dass ich diese Dissertation weder in gleicher noch in ähnlicher Form bereits an einer anderen Fakultät eingereicht habe.

Die Bedeutung dieser eidesstattlichen Versicherung und die strafrechtlichen Folgen einer unwahren eidesstattlichen Versicherung (§§156, 161 des Strafgesetzbuches) sind mir bekannt und bewusst.“

_____ _____

Datum Unterschrift

My curriculum vitae does not appear in the electronic version of my paper for reasons of data protection.

My curriculum vitae does not appear in the electronic version of my paper for reasons of data protection.

Acknowledgment

First and foremost, I would like to express my sincere gratitude to my supervisor, Prof. Ute Scholl, for her invaluable guidance, support, and encouragement throughout this study. Without her, this project would not have done well.

To the following people, whom I have met and learned from, I thank:

Dr. Valeria Fernandez Vallone, thank you for your great support and the best mentorship that I shall never forget. You are not only a mentor with whom I can share my difficulties at work, but also a friend who always listens to me through the up and down of my journey.

Dr. Gabriel Stoeting, who was always willing to share his knowledge and advice, and bear with my questions.

Iana, thank you for being the best fellow I could ever wish for and for everything else inside and outside the lab. I sincerely treasure the time we spent together.

Lab members and friends, Nicole, Eric, Marina, An, Janek and Luise, for all the advice, conversations, and encouragement.

I would like to thank Dr. Harald Stachelscheid, as my second supervisor, for his tremendous support and thoughtful comments on this project.

I would like to acknowledge the Einstein Center for Regenerative Therapies (ECRT) for Young Scientist Kickbox and Consumable funding; the BIH Stem Cell Core Facility; Caroline Braeuning of the Flow Cytometry technology platform (BIMSB/MDC), Genomics platform (BIMSB/MDC) for technical assistance.

I wish to thank our collaborators for their contribution and valuable advice: Dr. Benedikt Obermayer-Wasserscheidt (Core Unit Bioinformatics-BIH), Prof. Sebastian Bachmann (Charité), Dr. Manfred Rauh (Universitätsklinikum Erlangen), Prof. Graeme Eisenhofer (Technische Universität Dresden).

Finally, my most special thanks to my family and friend, Linh, for always being the source of my strength.

Certificate of the accredited statistician

CHARITÉ

CharitéCentrum für Human- und Gesundheitswissenschaften

Charité | Campus Charité Mitte | 10117 Berlin

Institut für Biometrie und klinische Epidemiologie (iBikE)

Direktor: Prof. Dr. Frank Konietschke

Postanschrift:
Charitéplatz 1 | 10117 Berlin
Besucheranschrift:
Reinhardtstr. 58 | 10117 Berlin

Tel. +49 (0)30 450 562171
frank.konietschke@charite.de
https://biometrie.charite.de/

Name, Vorname: Tran Vo, Kieu Nhi

Emailadresse: kieu-nhi.tran-vo@bih-charite.de

Matrikelnummer: 227404

PromotionsbetreuerIn: Univ.-Prof. Dr. Ute Scholl

Promotionsinstitution / Klinik: BIH - Center of Functional Genomics

Bescheinigung

Hiermit bescheinige ich, dass *Frau Kieu Nhi Tran Vo* innerhalb der Service Unit Biometrie des Instituts für Biometrie und klinische Epidemiologie (iBikE) bei mir eine statistische Beratung zu einem Promotionsvorhaben wahrgenommen hat. Folgende Beratungstermine wurden wahrgenommen:

- *Termin 1: 28.04.2023*

Folgende wesentliche Ratschläge hinsichtlich einer sinnvollen Auswertung und Interpretation der Daten wurden während der Beratung erteilt:

- Aufgrund der kleinen Fallzahl sollten keine statistischen Tests durchgeführt werden, sondern nur eine Deskription der Daten vorgenommen werden.
- Auch bei der Deskription der Daten immer angeben, dass es sich hierbei um eine kleine Stichprobe handelt und die Aussagekraft dadurch reduziert ist.
- Kreuztabellen und Liniendiagramme zum Berichten erstellen.

Diese Bescheinigung garantiert nicht die richtige Umsetzung der in der Beratung gemachten Vorschläge, die korrekte Durchführung der empfohlenen statistischen Verfahren und die richtige Darstellung und Interpretation der Ergebnisse. Die Verantwortung hierfür obliegt allein dem Promovierenden. Das Institut für Biometrie und klinische Epidemiologie übernimmt hierfür keine Haftung.

Datum: 28.04.2023 Name des Beraters/ der Beraterin: Simrit Rattan

Unterschrift BeraterIn, Institutsstempel

CHARITÉ
UNIVERSITÄTSMEDIZIN BERLIN
Institut für Biometrie und
Klinische Epidemiologie
Campus Charité Mitte
Charitéplatz 1 | D-10117 Berlin
Sitz: Reinhardtstr. 58

Simrit Rattan
Digital unterschrieben von Simrit Rattan
Datum: 2023.04.28 12:18:34 +02'00'